Roles of the Histone Deacetylases Rpd3 and Hst1 in the Regulation of NAD^+ Metabolism

By

BENJAMIN RONALD GROTH

DISSERTATION

Submitted in partial satisfaction of the requirements for the degree of

DOCTOR OF PHILOSOPHY

in

Microbiology

in the

OFFICE OF GRADUATE STUDIES

of the

UNIVERSITY OF CALIFORNIA

DAVIS

Approved:

Su-Ju Lin, Chair

Rebecca Parales

David Wilson

Committee in Charge

2022

ABSTRACT

Nicotinamide adenine dinucleotide (NAD^+) is an enzymatic cofactor with a large variety of crucial roles in metabolism and signaling. Perturbations to NAD^+ metabolism are associated with a diverse set of diseases, ranging from cancer to neurological damage. As a result, NAD^+ metabolism is an eminent topic of interest. However, the complex network of factors interacting with NAD^+ metabolism is not completely elaborated. To clarify and investigate the regulation of NAD^+ metabolism, genetic screens were developed to quantitate altered release of NAD^+ precursors in yeast strains of interest. This allowed for the observation that deletion of the histone deacetylase (HDAC) *RPD3* causes stark reduction in release of the intermediate of *de novo* NAD^+ biosynthesis, QA (quinolinic acid). It was found that that Rpd3 interacts in an antagonistic fashion with the class III HDAC Hst1, a repressor of the *de novo*-mediating *BNA* genes. The two HDACs are responsible for the production of differential chromatin modifications at the *BNA2* promoter. Moreover, Rpd3 and Hst1, along with the transcription activator Pho2, link the regulation of *de novo* NAD^+ biosynthesis with regulation of genes in the phosphate (Pi) sensing *PHO* pathway. Pi sensing was shown to interact in a variety of complex ways with *de novo* NAD^+ metabolism and NR salvage, establishing a considerable degree of coordination between these pathways. Altogether, these results highlight a critical role for Rpd3 as a positive regulator of *de novo* NAD^+ metabolism.

TABLE OF CONTENTS

LIST OF ABBREVIATIONS

3-HA: 3-hydroxyanthranilic acid
3-HK: 3-hydroxykynurenine
AICAR: 5′-phosphoribosyl-4-carboxamide- 5-aminoimidazole
ADP: adenosine diphosphate
ATP: adenosine triphosphate
HDAC: histone deacetylase
KA: kynurenic acid
KYN: kynurenine
NA: nicotinic acid
NaAD: nicotinic acid adenine dinucleotide
NAD^+: nicotinamide adenine dinucleotide (oxidized)
NADH: nicotinamide adenine dinucleotide (reduced)
$NADP^+$: nicotinamide adenine dinucleotide phosphate (oxidized)
NAM: nicotinamide
NaMN: nicotinic acid mononucleotide
NFK: N-formyl kynurenine
NMN: nicotinamide mononucleotide
NR: nicotinamide riboside
PARP: poly-ADP-ribose polymerase
Pi: phosphate
PRPP: phosphoribosyl pyrophosphate
QA: quinolinic acid
TRP: tryptophan
ZMP: 5′-phosphoribosyl-5-amino-4-imidazole carboxamide monophosphate

LIST OF YEAST STRAINS

LAB ARCHIVE #	GENOTYPE	REFERENCE
BY4742	*Wild-type MATα his3Δ1 leu2Δ1 ura3Δ*	Open Biosystems
LSC 2162-2	*BY4742 rpd3Δ::kanMX*	Chapter 2, 3
LSC 434-1	*BY4742 hst1Δ::kanMX*	Chapter 2, 3
LSC 2550-1	*BY4742 hst1Δ rpd3Δ::kanMX*	Chapter 2, 3
LSC 2118-1	*BY4742 bna4Δ npt1Δ nrk1Δ::kanMX*	Chapter 2, 3
LSC 2300-3	*BY4742 bna1Δ npt1Δ nrk1Δ::kanMX*	Chapter 2, 3
LSC 1934	*BY4742 bna6Δ nrk1Δ nrt1Δ:kanMX*	Chapter 2, 3
LSC 1123-1	*BY4742 bna6Δ pho5Δ npt1Δ:kanMX*	Chapter 2, 3
LSC 2712-4	*BY4742 BNA1-HA::HIS3*	Chapter 2
LSC 2716-2	*BY4742 BNA1-HA::HIS3 rpd3Δ::hygB*	Chapter 2
LSC 2715-6	*BY4742 BNA1-HA::HIS3 hst1Δ::kanMX*	Chapter 2
LSC 2725-1	*BY4742 BNA1-HA::HIS3 rpd3Δ::hygB hst1Δ::kanMX*	Chapter 2
LSC 2710-10	*BY4742 BNA2-HA::HIS3*	Chapter 2
LSC 2718-12	*BY4742 BNA2-HA::HIS3 rpd3Δ::hygB*	Chapter 2
LSC 2717-1	*BY4742 BNA2-HA::HIS3 hst1Δ::kanMX*	Chapter 2
LSC 2726-1	*BY4742 BNA2-HA::HIS3 rpd3Δ::hygB hst1Δ::kanMX*	Chapter 2
LSC 2714-1	*BY4742 BNA5-HA::HIS3*	Chapter 2
LSC 2722-4	*BY4742 BNA5-HA::HIS3 rpd3Δ::hygB*	Chapter 2
LSC 2721-11	*BY4742 BNA5-HA::HIS3 hst1Δ::kanMX*	Chapter 2
LSC 2728-1	*BY4742 BNA5-HA::HIS3 rpd3Δ::hygB hst1Δ::kanMX*	Chapter 2
LSC 2664-1	*BY4742 pPP35-BNA2*	Chapter 2
LSC 2665-1	*BY4742 pPP35-BNA2 rpd3Δ::kanMX*	Chapter 2
LSC 2670-1	*BY4742 pPP35-BNA2 , pPP81-BNA6 rpd3Δ::kanMX*	Chapter 2
LSC 2629-1	*BY4742 pPP81-BNA6*	Chapter 2
LSC 2630-1	*BY4742 pPP81-BNA6 rpd3Δ::kanMX*	Chapter 2
LSC 2646-2	*BY4742 RPD3-HA::kanMX gal80Δ*	Chapter 2
LSC 2653-1	*BY4742 RPD3-HA::kanMX gal80Δ hst1Δ::hygB*	Chapter 2
LSC 2650-1	*BY4742 HST1-HA::kanMX*	Chapter 2
LSC 2652-2	*BY4742 HST1-HA::kanMX rpd3Δ::hygB*	Chapter 2
LSC 2700-1	*BY4742 rco1Δ::kanMX*	Chapter 3
LSC 2701-6	*BY4742 rxt2Δ::kanMX*	Chapter 3
LSC 2688-2	*BY4742 ade16Δade17Δ::kanMX*	Chapter 3
LSC 2689-3	*BY4742 ade16Δade17Δ::kanMX hst1Δ::hygB*	Chapter 3
LSC 2641-1	*BY4742 bas1Δ::kanMX*	Chapter 3

LSC 2642-5	*BY4742 bas1Δ::kanMX hst1Δ::hygB*	Chapter 3
LSC 2690-4	*BY4742 ade16Δ ade17Δ::kanMX rpd3Δ::hygB*	Chapter 3
LSC 1250-1	*BY4742 pho84Δ::kanMX*	Chapter 3
LSC 2748-2	*BY4742 hst1Δ::hygB pho84Δ::kanMX*	Chapter 3

LIST OF PLASMIDS

LAB ARCHIVE #	PLASMID NAME	Reference
SJLP 132	p*UG6*	(1)
SJLP 133	p*SH47*	(1)
SJLP 56	p*AG32*	(2)
SJLP 309	p*FA6a-3HA-His3MX6*	(3)
SJLP 459	p*PP35*	(4)
SJLP 462	p*PP35-BNA2*	(3)
SJLP 1	p*PP81*	(4)
SJLP 146	p*PP81-BNA6*	(5)
SJLP 8	p*FA6a-3HA-kanMX6*	(6)
SJLP 308	p*FA6a-kanMX6-PGAL1-3HA*	(6)

LIST OF PRIMERS

LAB ARCHIVE #	NAME	SEQUENCE	Purpose	Chapter
SJLO 2530	5’ RPD3-Kan	CATACAAAACATTCGTGGCTACAACTCGATATCCGTGCAG ATGGCATAGGCCACTAGTGGATC	rpd3Δ::kanMX	2, 3
SJLO 2531	3’ RPD3-Kan	TATTTATATTCGTATATACTTCCAACTCTTTTTTTCAATAGC AGCTGAAGCTTCGTACGC	rpd3Δ::kanMX	2, 3
SJLO 86	5’ Kan confirmation	GGATGTATGGGCTAAATG	kanMX deletion confirmation	2, 3
SJLO 2533	DOWN RPD3 confirmation	TGTATGAACGGAACGCATC	rpd3Δ::kanMX confirmation w/ 86	2, 3
SJLO 263	5’ HST1-kan	CTATGTTGTGATAACCCTCGTTGGTAGTGATACGAACACTG CATAGGCCACTAGTGGATC	hst1Δ::kanMX	2, 3
SJLO 264	3’ HST1-kan	ATACATGAATGAAATGCTCGAATATATGCAATAGCAGCGG CAGCTGAAGCTTCGTACGC	hst1Δ::kanMX	2, 3
SJLO 266	DOWN HST1 confirmation	AATTGAGATTGAATATTC	hst1Δ::kanMX confirmation w/ 86	2, 3
SJLO 1956	BNA1-a-F	CCAACTCCCGAATGGTTCTA	BNA1 qPCR	2, 3
SJLO 1957	BNA1-a-R	ATCAGCAAACCGAACAGGAC	BNA1 qPCR	2, 3
SJLO 1958	BNA2-a-F	GGGTGTTTGGACTTGGAAAA	BNA2 qPCR	2, 3
SJLO 1959	BNA2-a-R	CACCGCTTCTAATGGCTCTC	BNA2 qPCR	2, 3
SJLO 1962	BNA4-a-F	CGTTACATCCAAGCGGTTTT	BNA4 qPCR	2, 3
SJLO 1963	BNA4-a-R	TTGCTTTCCAGCCCTTTCTA	BNA4 qPCR	2, 3
SJLO 1964	BNA5-a-F	CATTGGGATTCAGGCAATCT	BNA5 qPCR	2, 3
SJLO 1965	BNA5-a-R	GCTTCCAACAGTTCCGTCAT	BNA5 qPCR	2, 3
SJLO 2028	BNA6-a-F	AGTGAAGATGAAGCCACAGAG	BNA6 qPCR	2, 3
SJLO 2029	BNA6-a-R	GCCTCCACTACATTCCAAGAG	BNA6 qPCR	2, 3
SJLO 2621	TAF10-a-F	AGCAGATGTACGAGTGAAACG	TAF10 qPCR	2, 3
SJLO 2622	TAF10-a-R	CCTGGAATATTCGTAGGCATCC	TAF10 qPCR	2, 3

SJLO 3015	BNA1 HA 5’	GACATGTTTCCATTGCAAGACGTTAAACTACGCACGCCCTC AATCTAATCGGATCCCCGGGTTAATTAA	BNA1-HA::HIS3	2
SJLO 3016	BNA1 HA 3’	AAGAGAGCTATAAAAGTACAACTAACAACTCTTCTAATAC GAATTCGAGCTCGTTTAAAC	BNA1-HA::HIS3	2
SJLO 2503	tADH1 HIS confirmation	AAAGCAACCTGACCTACAGG	BNA1-HA tag confirmation	2
SJLO 3014	BNA1 HA confirmation 5’	TGTTGTGGAACAAGATAG	BNA1-HA tag confirmation	2
SJLO 3003	BNA2 HA 5’	GACTGTCGCCACTGCGGACATTAAAAATGAAGATAAAAAT CGGATCCCCGGGTTAATTAA	BNA2-HA::HIS3	2
SJLO 3009	BNA2 HA 3’	ACAACTGAAAAGCTTTAAGTTGCGAGGCTTCTGCATCAAC GAATTCGAGCTCGTTTAAAC	BNA2-HA::HIS3	2
SJLO 3005	BNA2 HA confirmation 5’	GTTACCAAGTACATTATT	BNA2-HA tag confirmation	2
SJLO 3021	BNA5 HA 5’	AGATGTATACATTGCGGTGAATGCACTAAATGAGGCGATG GATAAGTTGCGGATCCCCGGGTTAATTAA	BNA5-HA::HIS3	2
SJLO 3022	BNA5 HA 3’	ATATCCAAAAGAAGATGAAGGCGATGCGGTCACTCTAGGA GAATTCGAGCTCGTTTAAAC	BNA5-HA::HIS3	2
SJLO 3020	BNA5 HA confirmation 5’	GTCACTTTACTTCGATTCT	BNA5-HA tag confirmation	2
SJLO 1123	NotI-BNA2 5’	ACTGGCGGCCGCATGAACAACACTTCCATAACCGGA	Cloning into pPP35	2
SJLO 1124	NheI-BNA2-3’	ATCGGCTAGCTCAATTTTTATCTTCATTTTTAATGTC	Cloning into pPP35	2
SJLO 2931	RPD3-HA (N-terminal) 5’	ACCATAAAGGTTCATAAAACAATTGCGCCATACAAAACAT GAATTCGAGCTCGTTTAAAC	Rpd3-HA::kanMX	2
SJLO 2932	RPD3-HA (N-terminal) 3’	TGACCGTGATCGGATCAAAAGGTGTTGCTTCATATACCATG CACTGAGCAGCGTAATCTG	Rpd3-HA::kanMX	2

SJLO 2941	RPD3-HA N-terminal confirmation	AGTTCCCAACGTCTGCAT	Rpd3-HA::kanMX	2
SJLO 2836	5’ HST1-Hph	CGAACACTTCTCTTCTTTTTTGTTGTTTTTGTGAGAAAAAAAAATCTAAATGAACATACGTACGCTGCAGGTCGAC	hst1Δ::hygB	2, 3
SJLO 2837	3’ HST1-Hph	CCCCTTCTGTGTTTTCTTCTTTTTTTTTTTTTTTTTTTTTTGGAATTTACTGTTATCGATGAATTCGAGCTCG	hst1Δ::hygB	2, 3
SJLO 2683	5’ hph confirmation	ACATCATCTGCCCAGATGCG	hygB deletion confirmation	2, 3
SJLO 2946	HST1-HA 5’	TAGATAAAGGTACGTATAAGATTAAGAAACAGCCACGAAAGAAACAACAGCGGATCCCCGGGTTAATTAA	HST1-HA::kanMX	2
SJLO 2947	HST1-HA 3’	TGCAATAGCAGCGGTATACTTATTTTTACTCCCCCTTCTGTGTTTTCTTCGAATTCGAGCTCGTTTAAAC	HST1-HA::kanMX	2
SJLO 2948	HST1-HA confirmation	GATTTCGAAGTTGAAGTT	HST1-HA::kanMX	2
SJLO 2866	5’ RPD3-Hph	GCGCCATACAAAACATTCGTGGCTACAACTCGATATCCGTGCAGATGGTACGTACGCTGCAGGTCGAC	rpd3Δ::hygB	2, 3
SJLO 2867	3’ RPD3-Hph	TTCACATTATTTATATTCGTATATACTTCCAACTCTTTTTTTCAATAGATCGATGAATTCGAGCTCG	rpd3Δ::hygB	2, 3
SJLO 2540	BNA2 promoter set1 FWD	ACCAACCGGTCAACAA	ChIP at BNA2 promoter (site 1)	2
SJLO 2541	BNA2 promoter set1 REV	GAGAATCCAACTGGAACCTACC	ChIP at BNA2 promoter (site 1)	2
SJLO 2542	BNA2 promoter set2 FWD	CTTGCAGATCACTCTGTTCTTTG	ChIP at BNA2 promoter (site 2)	2
SJLO 2543	BNA2 promoter set2 REV	CAACCATCGTTAGCCAATCAG	ChIP at BNA2 promoter (site 2)	2

SJLO 2544	BNA2 promoter set3 FWD	CAGAGTCTCAGCTGCTGCTTG	ChIP at BNA2 promoter (site 3)	2
SJLO 2545	BNA2 promoter set3 REV	GATAGCCCTGTCACCAGTATCG	ChIP at BNA2 promoter (site 3)	2
SJLO 2546	BNA2 promoter set4 FWD	CCGCAATTCGTCGTAAACTG	ChIP at BNA2 promoter (site 4)	2
SJLO 2547	BNA2 promoter set4 REV	ACGACAATTAAGCAGCACAAG	ChIP at BNA2 promoter (site 4)	2
SJLO 2548	BNA2 promoter set5 FWD	CTGTCACACACATCAGATGTCC	ChIP at BNA2 promoter (site 5)	2
SJLO 2549	BNA2 promoter set5 REV	ATATCGGCGTTGACTCTTTCTT	ChIP at BNA2 promoter (site 5)	2
SJLO 2016	NPT1-a-F	TTCTGGAGACCCAGTTGAGTA	NPT1 qPCR	2
SJLO 2017	NPT1-a-R	CTTTAGCTGCATGGGAGTAAGT	NPT1 qPCR	2
SJLO 1982	NMA1-a-F	GAAGATGATGACGCGGATTT	NMA1 qPCR	2
SJLO 1983	NMA1-a-R	AGGTTCTTGCTTGACGAACG	NMA1 qPCR	2
SJLO 1984	NMA2-a-F	ACTCAAGCAACCGAATGGAC	NMA2 qPCR	2
SJLO 1985	NMA2-a-R	GTACCCCCAAATTCCCAGTC	NMA2 qPCR	2
SJLO 1970	TNA1-a-F	CCACCTTGTAGGAACGCAAT	TNA1 qPCR	2
SJLO 1971	TNA1-a-R	AAGCAGTTCCGAGCGAAATA	TNA1 qPCR	2
SJLO 1974	PNC1-a-F	CCAGACATATTTCGTTCGCA	PNC1 qPCR	2
SJLO 1975	PNC1-a-R	CCAATTGACTACCCCAGGTG	PNC1 qPCR	2
SJLO 1990	NRT1-a-F	TTCGTTTACTGGGGGCTATG	NRT1 qPCR	2
SJLO 1991	NRT1-a-R	AAGCACGGATTTCTTCCTCA	NRT1 qPCR	2
SJLO 1988	NRK1-a-F	TGGATCCGCCGTATTATTTC	NRK1 qPCR	2
SJLO 1989	NRK1-a-R	TTCGCAATTGGAGTGTCATC	NRK1 qPCR	2
SJLO 1994	POF1-a-F	TACGCCAGTGACATCCTTGA	POF1 qPCR	2

SJLO 1995	POF1-a-R	CCACTTGCCCATTCTTCAGT	POF1 qPCR	2
SJLO 2018	FUN26-a-F	GAAGGTGAGGAACTCCAACTAAA	FUN26 qPCR	2
SJLO 2019	FUN26-a-R	GTAGGTGGCAGACGCAAATA	FUN26 qPCR	2
SJLO 2004	ISN1-a-F	TCTTGGTGTTCGTTCATTGC	ISN1 qPCR	2
SJLO 2005	ISN1-a-R	TGAGGGGATGCTATCCAGAG	ISN1 qPCR	2
SJLO 2006	SDT1-a-F	ACAGATACGCTGGTCTGCAA	SDT1 qPCR	2
SJLO 2007	SDT1-a-R	TGTTTTCATGCCCAATTTGA	SDT1 qPCR	2
SJLO 2026	URH1-a-F	CACAAGGCCATAGCTACTTACA	URH1 qPCR	2
SJLO 2027	URH1-a-R	CCCGATTCAAATCCTTGCATATC	URH1 qPCR	2
SJLO 2000	PNP1-a-F	GTTCCCGAAGTCATTGTTGC	PNP1 qPCR	2
SJLO 2001	PNP1-a-R	ACTTCAGCGTGAGTCGCTTT	PNP1 qPCR	2
SJLO 2086	PHO5-a-F	TACTCTTTCCCTGGCGACTA	PHO5 qPCR	3
SJLO 2087	PHO5-a-R	GGGTATCTTTCACCATGTCTACC	PHO5 qPCR	3
SJLO 2070	PHO8-a-F	CATCACAGACCTTGTGGTACAG	PHO8 qPCR	3
SJLO 2071	PHO8-a-R	GGAGTGGCATCTGTGATTCTT	PHO8 qPCR	3
SJLO 2991	5’ RCO1-Kan	GCAACAAGCACGAGAGGAAGGAAGAAGAATACCAAGTAG CATAGGCCACTAGTGGATC	rco1Δ::kanMX	3
SJLO 2992	3’ RCO1-Kan	GTGTGTATATATGTAAGGAAGGTGTTCACGTTCCTGATCAG CTGAAGCTTCGTACGC	rco1Δ::kanMX	3
SJLO 2995	DOWN RCO1 confirmation	GACGACGAAGAAGGTGATGG	rco1Δ::kanMX	3
SJLO 2993	5’ RXT2-Kan	CGTTGCTTGATGACAGCATCTCCTGCAAAAAAGAGGTGCA TAGGCCACTAGTGGATC	rxt2Δ::kanMX	3
SJLO 2994	3’ RXT2-Kan	GACAGATGATGAAACAGACCCGAACTTCGTAAAAGTCATC AGCTGAAGCTTCGTACGC	rxt2Δ::kanMX	3
SJLO 2996	DOWN RXT2 confirmation	GAGATCAACGCTTTCCCAGAC	rxt2Δ::kanMX	3
SJLO 2979	ADE16-Kan 5’	CAATACCCCATTCCAAACAAAGAATCCAAATATACCGCAT AGGCCACTAGTGGATC	ade16Δade17Δ::kanMX	3
SJLO 2980	ADE16-Kan 3’	CACTTGTATTCAGCTATATATGTTGTTTCTGTTCTTCTCCAG CTGAAGCTTCGTACGC	ade16Δade17Δ::kanMX	3

SJLO 2981	DOWN ADE16 confirmation	CGGTCATCTTTGTTGTTCGTCC	ade16Δade17Δ::kanMX	3
SJLO 2982	ADE17-Kan 5’	GTAGTTTTGCTAGCTTGGACATCAAAGCACATATCACCATGCATAGGCCACTAGTGGATC	ade16Δade17Δ::kanMX	3
SJLO 2983	ADE17-Kan 3’	GAGGAGGAAAGAATAAACTATACATCGATTTGCCGTCATTCAGCTGAAGCTTCGTACGC	ade16Δade17Δ::kanMX	3
SJLO 2984	DOWN ADE17 confirmation	GGTACTGTAAGGTTCATCCTG	ade16Δade17Δ::kanMX	3
SJLO 2938	5’ BAS1-Kan	GCTCTTTTTTTTTTATCGCAGAATACATTTTATCGAGGCATAGGCCACTAGTGGATC	bas1Δ::kanMX	3
SJLO 2939	3’ BAS1-Kan	CAATTGAAAGATTTGTGTTTTTTTTCGGCCTTGCCTTCCAGCTGAAGCTTCGTACGC	bas1Δ::kanMX	3
SJLO 2940	DOWN BAS1 confirmation	CCCTTTGTGTTTGTGGGC	bas1Δ::kanMX	3
SJLO 1502	5’ PHO84-Kan	TTCACTTCTAAATTTTATCTTTCCTCATCTCGTAGATCACGCATAGGCCACTAGTGGATC	pho84Δ::kanMX	3
SJLO 1503	3’ PHO84-Kan	ATTTGTTCTAGTTTACAAGTTTTAGTGCATCTTTGAGGCTCAGCTGAAGCTTCGTACGC	pho84Δ::kanMX	3
SJLO 1504	DOWN PHO84 confirmation	CAGAGAGATGTGAGGAAA	pho84Δ::kanMX	3

CHAPTER 1: An Introduction to NAD^+ Metabolism

Portions of this chapter were previously published in Frontiers in Molecular Biosciences (7)*

*Groth et al, *Front Mol Biosci* **8**, 686412 (2021), open access

Discovery of nicotinamide adenine dinucleotide and historical context - Over a century of work has been applied to the elucidation of the role and significance of NAD^+. NAD^+ was first identified by Arthur Harden and William John Young, who noted that the addition of boiled yeast extract significantly augmented glucose fermentation by yeast cells (8). The non-heat-sensitive factor responsible for this effect was described as a "coferment" (9) and later characterized as "cozymase" (10). Later, this co-enzyme was further characterized as mediating an early step of fermentation, and it was later determined that this "cozymase" was a redox cofactor, a nucleotide, and also a participant in the oxidation of acetaldehyde to alcohol (11). It was later discovered that "cozymase" contains nicotinamide, is reduced via the addition of hydride ions, and is composed of two bases, two pentose sugars, two phosphates (12). The chemical mechanism of NAD^+ as a redox cofactor was demonstrated to proceed via the addition of hydride and reduction of a double bond in the nicotinamide moiety of NAD^+ (13).The fundamental role and structure of NAD^+ as a glycolytic electron carrier was hereby established. NAD^+ and its reduced form NADH are essential redox cofactors with wide-ranging and significant roles in the cell. NAD^+ is well known as an electron carrier in core metabolic pathways, as in glycolysis, oxidative phosphorylation, and beta-oxidation of fatty acids. NAD^+ also serves as a co-substrate in several non-redox reactions, such as sirtuin-mediated protein deacetylation, which regulates the activity of many target proteins including histones. Sirtuins are Sir2 family proteins (class III histone deacetylases, HDACs) the activity of which depends on NAD^+ (14-16). In addition, NAD^+ is also consumed by the poly-ADP-ribose polymerases (PARPs). In humans, the PARP enzymes were identified as DNA-dependent catalysts of ADP-ribosylation (17). It was later discovered that NAD^+ served as the substrate for this ADP-ribosylation reaction (18). PARP-dependent ADP-ribosylation of proteins is initiated in response

to DNA damage, specifically for the purpose of ADP-ribosylation during base excision repair of single-strand breaks (19). NAD^+ is also consumed by CD38, a cell surface NAD^+ glycohydrolase (an ectonucleotidase) Although its biological function is not completely understood, CD38 activation has been shown to cause NAD^+ decline in several cell/tissue types and CD38 inhibition is able to restore NAD^+ (20,21). Consequently, NAD^+ has a multifarious and highly important influence on cellular health, affecting an extensive suite of processes, including: DNA repair, central metabolism, circadian rhythms, meiosis and lifespan (22-28). Owing to its centrality in cellular homeostasis, defects in NAD^+ metabolism are often associated with a variety of disease states, seen in diabetes, neurological disorders, and various cancers (23-27,29-42). Administration of NAD^+ precursors such as nicotinamide mononucleotide (NMN), nicotinamide (NAM), nicotinic acid riboside (NaR), nicotinamide riboside (NR), and dihydronicotinamide riboside (NRH) has been shown to increase NAD^+ levels and ameliorate associated deficiencies in various model systems and in humans (24,26,28-32,34,35,37,43-57). However, the molecular mechanisms underlying the beneficial effects of NAD^+ precursor treatments are not completely understood. For this reason and due to the key role performed by NAD^+ in the maintenance of cellular health, it is of vital importance to understand how the cell synthesizes and regulates its NAD^+ pool.

Pathways of NAD^+ biosynthesis - NAD^+ biosynthesis pathways are largely conserved from bacteria to humans with a few species-specific differences. Overall, the cellular NAD^+ pool is maintained by three major pathways: 1) *de novo* synthesis; 2) salvage from NA-NAM; and 3) salvage from NR. These pathways converge at several different points and consume cellular pools of ATP (adenosine triphosphate), phosphoribosyl pyrophosphate (PRPP), and glutamine (58,59). Specific NAD^+ intermediates also contribute to other biosynthesis pathways or have

signaling functions, and have diverse biological activities in humans (22,38,58-63). Therefore, cells must maintain these metabolites in a controlled manner to promote their fitness and survival in response to various growth conditions.

Under NA abundant conditions, such as in most yeast growth media, NA/NAM salvage is the preferred NAD^+ biosynthesis route (64). The first step in the elaboration of the NA/NAM salvage pathway was made in 1938, when Conrad Elvehjem identified "black tongue factor", effective in the prevention of canine pellagra symptoms, as NAM and NA (65) and later demonstrated the dependence of NAD^+ biosynthesis on Niacin (66). NAD^+ biosynthesis from the NAM derivative NMN was first demonstrated by the addition of NMN and ATP to yeast lysate (67), although in budding yeast this occurs as part of the NR salvage pathway (68). Later, the steps of the NA/NAM salvage pathway were worked out in erythrocytes by Jack Preiss and Philip Handler, after whom the pathway is sometimes identified as the "Preiss-Handler pathway." NA may be converted to NAD^+ via NaMN and NaAD (69,70). In budding yeast, the pathway proceeds from NAM to NA via deamidation by Pnc1 (71), from NA to NaMN via phosphoribosylation carried out by Npt1 (16), then from NaMN to NaAD via adenylation by Nma1 and Nma2 (72,73); lastly, NaAD is converted into NAD^+ by Qns1 (74). NAM is produced from many NAD^+ consuming reactions including sirtuin mediated protein deacetylation (14-16). Humans lack a functional homolog for Pnc1; instead, NAM may be converted into NMN by NamPRT, which then becomes NAD^+ via NMNAT (29). Interestingly, recent studies show that microbiota in the gut may assist the conversion of NAM to NA by bacterial nicotinamidases (75), which suggests NAM salvage to NA may also take place in humans with the aid of gut bacteria.

NR was later identified as another precursor for NAD^+ (76). Salvage of NAD^+ from NR may proceed by two routes, the first being its conversion into NAM via Urh1, Meu2, and Pnp1 (45), corresponding to entrance into the NA/NAM salvage pathway. The second relies on phosphorylation of NR to NMN by Nrk1 (76), followed by conversion into NAD+ by adenylation by Pof1 and Nma1/Nma2 (68). The NR salvage branch may confer flexibility in part due to compartmentalization of enzymes and precursors in this pathway (5,22,58). Moreover, yeast cells release and re-uptake small NAD^+ precursors such as NA, NAM, QA and NR (68,77,78). Specific transporters Tna1 (for NA and QA) (79,80) and Nrt1 (for NR) (81) are responsible for the uptake of NAD^+ precursors whereas the mechanisms of precursor release remain unclear. It has been suggested that vesicular trafficking may also play a role in the movement of NAD^+ metabolites (22,58,77).

Lastly, the *de novo* pathway of NAD^+ biosynthesis, also known as the kynurenine (KYN) pathway of tryptophan (TRP) degradation, in budding yeast is facilitated by the *BNA* (*B*iosynthesis of *N*icotinic *A*cid) genes under aerobic conditions (82). *De novo* metabolism in budding yeast and higher eukaryotes begins with conversion of TRP into NFK (83). This step is mediated by Bna2 in budding yeast (82). This is followed by the conversion of NFK to KYN via Bna7 (84), KYN to 3-HK via Bna5, then 3-HK to 3-HA via Bna4 (82). 3-HA is then converted into 2-amino-3-carboxymuconic semialdehyde by Bna1, followed by spontaneous cyclization to QA (85). Finally, Bna6, alternately referred to as Qpt1, transfers the phosphoribosyl moiety from PRPP to QA, resulting in the formation of NaMN, at which point the *de novo* pathway merges with NA/NAM salvage (82,86).

Budding yeast may serve as a tractable and comparatively simpler model for the study of *de novo* metabolism in humans, which is largely conserved between the two species (87). *De*

novo metabolites have a complex and vast connection with immunity, inflammation, infection, nutrient sensing, and a wide variety of other pathways in the human cell (7). Study of the *de novo* pathway is therefore a crucial part of understanding each of these relations.

Activation of IDO1 and *de novo* pathway during inflammation - As briefly discussed above, *de novo* pathway metabolites play important roles in immune regulation. The synthesis of *de novo* pathway metabolites is also tightly controlled by the immune system (36,61,88-90). Here, we further discuss the interconnections of the *de novo* pathway activity, inflammation, immunity, and NAD^+ metabolism.

The first and rate-limiting step in the *de novo* pathway is the conversion of TRP to N-formylkynurenine (NFK), which is then converted to KYN and later other *de novo* metabolites (91,92). This NAD^+ synthesis-associated TRP catabolism is initiated by tryptophan 2,3-dioxygenase (TDO) and/or indoleamine 2,3-dioxygenase (IDO). Among the many cell types that express *de novo* pathway enzymes, TDO is expressed highly in liver. There are two isoforms of IDO (IDO1 and IDO2) in mammals. *IDO1* is broadly expressed in various type of tissues whereas *IDO2* has a restricted pattern of expression (61,90). The activity of IDO1, is stimulated by a variety of pro-inflammatory signals, chief among which is interferon-γ (IFN-γ). Mechanistically, IFN-γ downregulates the production of the adapter molecule DAP12, an event strongly associated with raised IDO1 activity in dendritic cells, leading to the endogenous production of KYN (93). IDO1 may also be activated to a comparatively lesser degree by a variety of pro-inflammatory cytokines and factors including lipopolysaccharide (LPS), tumor necrosis factor (TNF), platelet activating factor (PAF), and other interferons (94-101). It has been reported that TNF-α and IFN-γ cooperate synergistically in the promotion of IDO1 activity (102). On the other hand, IDO1 expression is reduced by anti-inflammatory cytokines such as

interleukin 4 (IL-4) and interleukin 13 (IL-13) (103,104). Kupffer cells were also seen to upregulate IDO1 in response to the administration of IFN-γ, leading to raised KYN levels (105). In addition, intracellular QA levels increase dramatically in response to immune stimulation in macrophages, microglia, dendritic cells, and other cells of the immune system. For example, injecting the hippocampus of rats with LPS results in a marked increase of QA levels in all compartments of the spleen that persists for several days. Injection of LPS also resulted in the recruitment of a large number of macrophages and microglia to the brain, where, surprisingly, very few cells displayed raised QA levels. This suggests that the brain balances the production of immunosuppressive *de novo* metabolites and the restoration of depleted NAD^+ levels with the neurotoxic QA (106). As precursors for NAD^+, it is likely that a portion of QA and KYN metabolites are directed towards replenishing cellular NAD^+ levels in response to inflammation and infection. Detailed mechanisms await to be further studied.

NAD^+-consuming enzymes also play an important role in inflammation. The NAD^+-dependent sirtuin proteins may serve as an example. One major feature of the inflammatory response is high energy consumption, which results in changes of the NAD^+/NADH redox ratio. It has been shown that the sirtuins sense the changes of intracellular NAD^+/NADH ratio to regulate inflammatory response (107-109). It has also been shown that NAMPT, the rate-limiting enzyme for NAD^+ synthesis from NAM, is readily induced in neutrophils and macrophages by infections or pro-inflammatory cytokines and mediators (110). A switch of NAD^+ synthesis from NAMPT-dependent salvage to IDO1-dependent *de novo* synthesis was observed in sustained immune tolerance. Mechanistically, it was suggested that activation of *de novo* NAD^+ synthesis supplemented the nuclear NAD^+ pool, which prolonged SIRT1 mediated repression of inflammatory gene (111). CD38 is a major NAD^+-consuming enzyme responsible for the age-

related NAD^+ decline (20,21). It has been shown that CD38 expression increases during aging in mouse metabolic tissues such as the white adipose tissue (WAT) and liver. Recent studies showed that inflammation increases CD38-mediated NAD^+ degradation activity, which decreases NAD^+. The increase in CD38 in metabolic tissues during aging is likely mediated by accumulation of pro-inflammatory M1-like macrophages that also express CD38 (41,42).

In immune cells, as in most non-liver tissues, TRP catabolism is initiated by IDO. This enzyme is ubiquitously expressed and has affinity for substrates other than TRP, including 5-hydroxytryptophan and serotonin (61). IDO1-mediated TRP catabolism in the host microenvironment occupied by parasites, viruses, and bacteria has been seen as a way to curb their proliferation (112). However, immune cells can also contribute to TRP degradation during nonpathogenic inflammation, indicating that IDO1 has a broader spectrum of activity on immune cell regulation (113). Since an unrestrained immune response is detrimental to cells, IDO1 expression is highly regulated in the immune system. IDO1 expression is stimulated by pathogens- and host-derived signals including pro-inflammatory cytokines (e.g. IFN-γ) and endotoxins (e.g. LPS), which can also be inhibited by anti-inflammatory cytokines (114-116). IDO1-dependent TRP degradation promotes an immunosuppressive environment by the production of TRP metabolites with immune activity, as well as by triggering an amino acid-sensing signal in cells due to TRP depletion (61). Therefore, this pathway has emerged as a rate-limiting step for metabolic immune regulation.

Immune activation and suppression by the *de novo* pathway metabolites - Control of TRP metabolism by IDO in dendritic cells (DCs) has been suggested to be a regulator of innate and adaptive immune responses (88). *De novo* metabolites suppress the activity of various immune cells including dendritic cells and macrophages in mice (88). Antigen tolerance is mediated by

IDO1 activity in T cells (117) as well as in dendritic cells (118). It has been shown that both KYN metabolites and IDO1 can initiate tolerogenesis by dendritic cells and that IDO-mediated KYN production in DC leads to the proliferation of regulatory T cells (Tregs) (88,93,119). Positive feedback also occurs wherein IDO1 activity in DCs promotes the emergence of regulatory T cell phenotypes in CD4+ T cells, which itself then stimulates further IDO1 activity in DCs (120,121). It is suggested that these effects are mediated at least partly by KYN activation of aryl hydrocarbon receptor (AhR), a ligand-activated transcription factor expressed in cells of both innate and adaptive immune systems (122). Several *de novo* pathway metabolites, including KYN, 3-HK, and 3-hydroxyanthranilic acid (3-HA), promote apoptosis and consequently may serve to combat the proliferation of infectious pathogens (123). 3-HA also promotes the production of transforming growth factor b (TGF-β), which further drives T cells toward regulatory phenotypes (95,120). 3-HA also appears to suppress glial cytokine expression during inflammation, while it increases the expression of the antioxidant and anti-inflammatory enzyme, hemeoxygenase-1 (124).

The stimulation of *de novo* pathway activity during inflammation also depletes cellular TRP stores and thereby reduces the amount available for conversion to other metabolites such as serotonin and melatonin (62). Infections, stress, and dietary intake all contribute to the usage of TRP in *de novo* metabolism, limiting its availability for serotonin biosynthesis (120). As a neurotransmitter, serotonin is involved in the regulation of the central nervous system, the cardiovascular system, and many other processes in the body (125), while melatonin affects a range of phenotypes including oxidative stress response, mitochondrial metabolism (126), and circadian rhythms (127). Moreover, a recent study in yeast showed that overexpression of *BNA2* (*BNA2*-oe) increased flux through the TRP-producing shikimate/aromatic amino acid biosynthesis

pathways, leading to reduced lipid droplet formation in aging cells due to depletion of necessary precursors (128). Interestingly this study also showed that *BNA2*-oe-induced life span extension and reduced lipid droplet formation is independent of NAD^+ production.

Physiological roles of the *de novo* pathway metabolites - Aberrations in *de novo* pathway metabolites are found in a variety of diseases and are often related to inflammation and oxidative stress in the affected tissues. Dysregulation of these metabolites has been implicated in neurodegenerative and neurological disorders, as well as in psychiatric diseases such as depression and schizophrenia (36,61,88-90). For example, QA, KA, and 3-HK, have all been shown to be related in some capacity to neurological health (109,129). QA is neurotoxic, an agonist of the NMDA receptor, which ordinarily binds glutamate. High levels of QA result in hyperactivation of this receptor and excitotoxicity, as well as glutamate toxicity due to excessive glutamate release from astrocytes and inhibited glutamine synthetase function (100). QA in complex with Fe^{3+} also results in oxidative damage to lipids (100,130,131). Elevated QA levels have previously been identified in cases of HIV-associated neurological damage (132), Alzheimer's disease (133), multiple sclerosis (134,135). Conversely, KA is generally neuroprotective, tending to decline in Huntington's disease (136). The effect of KA opposes that of QA in acting as an antagonist of the NMDA receptor and other glutamate receptors, as well as of the α-7 nicotinic acetylcholine receptor (137). However, raised KA levels are also associated with neurological dysfunction, seen in a variety of cases ranging from Alzheimer's disease (138) to Down's syndrome (139). Increased 3-HK levels are associated with Alzheimer's disease (140) and, like QA, 3-HK's neurotoxic effects are associated with free radical generation (141). Indeed, elevated levels of both 3-HK and QA are a feature of Huntington's disease as well (142-144). 3-HK and 3-HA, however, have also been shown to reduce the cytokine-induced destruction of

neurons (124). It is therefore important for cells to effectively regulate flux through the *de novo* pathway and balance the levels of each intermediate produced.

Alterations in the *de novo* pathway metabolism have far-ranging effects on many other aspects of host health as well. The *de novo* pathway has, for instance, a significant influence on the liver. Activation of lipid oxidation and mitochondrial proliferation in the livers of rats resulted in increased serum levels of TRP, downstream *de novo* metabolites, and NAM, altogether indicating that mitochondrial activity in hepatocytes is strongly correlated with *de novo* biosynthesis of NAD^+. It was also seen however that this resulted in reduced levels of IDO1 expression, while the KYN/TRP ratio was negatively correlated with mitochondrial function (145); this suggests other forms of TRP metabolism may also play a role. Further, heightened hepatic and adipose tissue expression of IDO1 is observed in obese individuals (146). Moreover, liver has a central role in modulating systemic TRP levels because hepatocytes are the only cell types that contain all the components for any branch of *de novo* metabolism (147).

IDO1 expression is limited to particular cell types, among which are a variety of immune cells described in the beginning of this section, as well as the smooth muscle cells of the cardiovascular system (99). A second IDO isoform, IDO2, is expressed in the human liver, spleen, kidney, and brain, though not in the heart (99,148). IDO2 appears to be constitutively expressed and does not respond to inflammatory signals in the manner of IDO1 (149). The reliance of the heart and vasculature on IDO1 may make the influence of the immune system on cardiovascular *de novo* metabolism activity particularly significant. IDO1 is also expressed in tumors and lymph nodes, which help create an immunosuppressive microenvironment both by depleting TRP and by accumulating immunosuppressive *de novo* metabolites. It has been suggested that IDO1 expression produced *de novo* metabolites contribute to the escape of the immune response by

binding to and activating AhR, a primary receptor of *de novo* metabolites (150,151). High levels of IDO have also been detected in many types of tumors associated with poor response. Owing to its role in immunosuppression, IDO has also been proposed to be a target of cancer therapy (152,153)

Impact of infection on *de novo* pathway metabolites - It has been increasingly seen that *de novo* pathway metabolite homeostasis is disrupted during infection. As noted previously, there is a well-established association between host immunity and flux through the KYN pathway, while several pathogens themselves and their mechanisms of infection have also been shown to induce alterations in *de novo* pathway metabolism. Most studies centered on the toxicity, protective effects, and/or immunosuppressive effects of the *de novo* pathway metabolites. It is unclear whether NAD^+ levels were also significantly altered in the host cells by specific pathogens in some of these studies.

Toxoplasma gondii appears to reduce traffic through the *de novo* pathway by the phosphorylation-mediated degradation of IDO1. The mechanism appears to involve AKT-mediated phosphorylation signaling cascade. After infection by *T. gondii,* IDO1 levels decline, presumably resulting in reduced levels of KYN. It appears that supplementation with KYN and the KYN analog teriflunomide hinders the establishment of *T. gondii* infection, as does the production of free radicals (154). As noted previously, the *de novo* pathway intermediates 3-HK and QA are known to stimulate free radical production. This leaves the question of whether and in what manner *de novo* pathway activity may be protective against toxoplasmosis, which, like perturbations of *de novo* pathway metabolism, is often associated with neurological disorders (155). 3-HK has been shown to stimulate apoptosis by the production of oxidative stress, the crosslinking of proteins, and the inhibition of the respiratory electron transport chain (156).

Majumdar et al. hypothesize that the activation of apoptotic pathways by *de novo* metabolites is one factor responsible for host resistance to *T. gondii* infection (154).

Infection by Borna disease virus (BDV) also results in dysfunctional *de novo* pathway metabolism. BDV, like *T. gondii*, is well known to cause neurological damage. Formisano, et al. investigated the BDV-alone vs. immune-mediated consequences of infection by examining both adult and neonatal rats (157). The authors identified a modest increase in IDO1 expression in the cerebellum and hippocampus of neonatal rats during infection, while immune competent adult rats show a marked increase of IDO1 expression in the cerebellum and hemispheres of the brain. Expression of KATII, the main enzyme of neural KYN biosynthesis, is increased in the brain tissue of neonatal, but not adult rats. Levels of KYN monooxygenase (KMO), which produces 3-HK from KYN, in both adult and neonatal rats are elevated compared to mock-infected animals. Neonatal rats exhibit raised levels of QA in the hippocampus and striatum, with no changes of KYN levels in brain tissue (157). This may hint at a possible consequence of BDV-altered *de novo* metabolism being the production of excess neurotoxic QA. In any event, an immune-independent role of BDV in the manipulation of *de novo* pathway metabolism is clear. In addition, both adult and neonatal rats experience adverse neurological effects from BDV infection. It is therefore likely that at least part of the means by which BDV harms neurological health may occur by way of direct influence on *de novo* pathway metabolism, with different effects observed depending on immune mobilization.

Aberrations of *de novo* pathway activity also appear to be associated with infection by the SARS-CoV-2 coronavirus responsible for COVID-19. Raised serum levels of KYN and KA were noted in COVID-19 patients which, interestingly, correlated with serum levels of interleukin-6 (IL-6), a hallmark of SARS-CoV-2 infection. This relationship may be explained in part by the

pro-inflammatory character of several *de novo* metabolites, or by the stimulation of certain *de novo* pathway enzymes (e.g. IDO1 activity promoted by IFN-γ) by inflammation. This is concomitant with reduced levels of TRP and its other metabolites, such as serotonin, suggesting that cellular TRP stores are shunted through the *de novo* pathway in SARS-CoV-2 infected cells, which may be related to the "cytokine storm" seen in severe cases (158).

The *de novo* pathway also appears to play a key role in human immunodeficiency virus (HIV) pathogenesis. An HIV-infected group of Subsaharan Africans showed altered *de novo* pathway metabolism relative to a non-infected control group, displaying reduced TRP levels, raised KYN and NAM levels and, most notably, an approximately 20-fold increase of QA (159). Increases of cellular QA concentration, though less significant, have also been associated with HIV infection elsewhere, with the distinction that the groups surveyed were drawn from developed countries (132,160,161). QA, being a potent neurotoxin, may in part explain the neurological damage associated with the progression of HIV infection (162). Raised KYN concentration is also negatively correlated with CD4 levels (159,163). The KYN/TRP ratio in HIV-infected women is increased relative to healthy volunteers, rises with age, and is negatively correlated with platelet count (163). In contrast to its protective effect against neurological problems, a high KYN/TRP ratio appears to be associated with aging and the progression of HIV, though of course this is confounded by a likely concomitant rise of QA. Altogether, this suggests a mechanism by which HIV promotes flux through the *de novo* pathway, thereby increasing the cellular levels of these *de novo* metabolites.

Hepatitis C virus (HCV) is also known to dysregulate *de novo* pathway metabolism during infection. In patients coinfected with HIV and HCV, levels of KYN, an immunosuppressant, are significantly elevated, together with the KYN/TRP ratio. Raised KYN levels are also positively

correlated with fibrosis of the liver and with insulin levels under these conditions. After successful HCV treatment with IFN-γ/ribavirin, KYN levels remained elevated (164). Another group confirmed that HIV/HCV coinfection raises the KYN/TRP ratio relative to other surveyed groups (non-infected, HIV monoinfected) and that this ratio is positively correlated with liver stiffness (163). HCV patients with and without cirrhosis also display increased levels of IDO1 activity, which appear to stabilize after treatment (165).

Further, a link has been established between the development of several severe viral pathologies of the central nervous system and dysregulated *de novo* metabolism. The development of subacute sclerosing panencephalitis (SSPE) after measles infection was associated with significantly raised QA levels in cerebrospinal fluid. Patients with bacterial and viral meningitis displayed even more drastic phenotypes, with QA levels raised by approximately an order of magnitude compared to uninfected control patients. SSPE patients, however, did not show significantly altered KYN/TRP ratios (166). Moreover, infection of mice with hamster neurotropic measles virus leads to the development of encephalitis as well as a marked increase in levels of QA and 3-HK (but again, not KYN) in the hippocampus (167).

A significant number of infectious fungi have also been noted to alter host IDO activity, both positively and negatively, suggesting a nexus between these infectious agents, KYN/TRP metabolism, and the host immune response (168). Interestingly, it has recently been discovered that loss of the native IDO genes of the fungus, *Aspergillus fumigatus*, redirects TRP catabolism into a pathway mediated by the aromatic aminotransferase AroH, which generates indole acetate and indolepyruvate (168). Mice were also shown to be more vulnerable to infection by *A. fumigatus* fungi lacking IDO, while mice without IDO1 displayed a similarly increased susceptibility to infection. The authors also noted raised inflammation after infection with fungi

lacking IDO genes vs. wild-type controls, which was hypothesized to be due to production of AhR ligands by way of the indole pathway. Indeed, deletion of AroH/I reduces the virulence of *A. fumigatus.* Altogether, this suggests a state of homeostasis evinced between the host and fungus, downregulating immune signaling and inflammation through *de novo* pathway activity (169).

Regulation of *de novo* NAD^+ metabolism - The foregoing discussion has attempted to identify the reciprocal connections between various signaling pathways and the production of *de novo* pathway metabolites, with a particular focus on their modulation by infection, whether due to inflammatory stress produced by infection or hijacking of host signaling by pathogens. It now remains to trace a general network of the signals known to affect *de novo* pathway activity and associated *de novo* NAD^+ metabolism. Several NAD^+ homeostasis regulatory factors have been identified in yeast, which include transcriptional control, feedback inhibition, nutrient sensing, and enzyme or metabolite compartmentalization (5,59,68,77,78,170-175). In this section, we discuss stress and nutrient signaling pathways that have been suggested to modulate *de novo* NAD^+ metabolism in yeast and in higher eukaryotes. Some of these factors may serve as potential targets of infectious pathogens and immune stimulation.

In budding yeast, activity of *de novo* NAD^+ metabolism is also known to be sensitive to levels of micronutrients such as certain metal ions. Both copper depletion and copper stress in particular were seen to elevate *BNA* gene expression above levels observed under standard conditions (78,176). In the latter case this is likely mediated by the copper-sensing transcription factor Mac1, here serving as a co-repressor, which is inhibited in the presence of excess copper (177). The causal influences underlying increased *BNA* expression under copper depleted conditions are more elusive and likely do not depend on Mac1 given its propensity for activity under copper limiting conditions. However, iron transport in *S. cerevisiae* depends on cellular

copper levels, which results in reduced intracellular iron levels in the absence of copper (178,179). This may therefore indicate a potential link between iron homeostasis and *de novo* NAD^+ metabolism as well. In fact, it has been observed that deletion of *CCC2*, an intracellular copper transporting ATPase, leads to raised *BNA2* and *BNA4* expression under low copper conditions and reduced levels under high copper conditions. Deletion of another copper chaperone protein, *ATX1*, produces opposite results, wherein *BNA* induction occurs in copper-rich conditions but is repressed under copper-limited conditions (176). Both Atx1 and Ccc2 are required for the mode of copper transport that later facilitates iron transport. Atx1 is a copper chaperone that passes copper from Ctr1, its membrane transporter, to Ccc2, where it is later inserted into Fet3 in order to enable high affinity iron transport (180). Wild type cells conversely show induced *BNA* expression under both conditions (78). This is especially interesting in light of the requirement of iron for the catalytic activity of 3-hydroxyanthranilate-3,4-dioxygenase (HAAO; human homolog of Bna1) (181) and the marked stimulation of Bna1 activity by iron supplementation (182), together with the generation of oxidative stress by QA in the presence of iron (183), the latter of which in particular may make the down-regulation of *de novo* activity in the presence of iron (corresponding to up-regulation in its absence) a significant factor for cell function. Both copper and iron are capable of producing oxidative stress (179), making the homeostasis of these two metals, considered together with oxidative *de novo* pathway intermediates like the 3-HK or the aforementioned QA, an important factor to regulate. The connection between *de novo* and metal ion homeostasis is therefore significant and may be an additional factor contributing to the dysregulation of *de novo* metabolism in disease states.

De novo NAD^+ biosynthesis is also shown to be stimulated by adenine limitation (59). This occurs due to flux through the *de novo* adenine biosynthetic pathways resulting in raised levels of

the intermediate 5-aminoimidazole-4-carboxamide ribonucleotide (AICAR). AICAR then promotes Bas1-Pho2 complex formation, which serves as a transcriptional activator for the BNA genes of *de novo* NAD^+ biosynthesis (59). This links *de novo* NAD^+ production not only to purine metabolism, but possibly to phosphate sensing as well, as AICAR also promotes the formation of the Pho2-Pho4 complex (184), a transcriptional activator of *PHO* pathway targets, which are expressed under phosphate depleted conditions. The sharing of Pho2 between these two complexes is a particularly interesting point which may have implications for the sensitivity of *de novo* NAD^+ metabolism to cellular phosphate levels.

The *de novo* pathway is inactive under anoxic conditions, due to the oxygen dependence of the reactions mediated by Bna2, Bna4, and Bna1 (82,185). It is also known that heme is necessary for the activity of mammalian IDO. Heme appears to be a limiting factor for *de novo* NAD^+ biosynthesis, as heme titration by apo-myoglobin significantly reduces IDO1 activity (186). IDO1 binding to heme is also influenced by iron, with iron supplementation significantly raising IDO1 activity (187). Moreover, the oxidation state of iron is also an important factor in IDO1-heme interaction, with IDO1 showing approximately 10-fold greater affinity for heme in the presence of ferrous (Fe^{2+}) vs. ferric (Fe^{3+}) iron (186). This may possibly lead to downregulation of *de novo* metabolism under conditions of oxidative stress, a strategy that would prevent the further production of oxidative *de novo* intermediates such as 3-HK and QA. IDO2 may also negatively regulate *de novo* metabolism activity in some contexts due to competition with IDO1 for heme (188). Like IDO1 (186), Bna2 may also require heme for its function due to the high degree of homology between the two enzymes and the ability of IDO1 to complement Bna2 function in budding yeast (189). This would indicate a close link between *de novo* metabolism and mitochondrial respiration, both of which require oxygen and, putatively, heme. Indeed, Bna4

localizes to the mitochondrial outer membrane and links *de novo* NAD^+ metabolism with mitochondrial function (190). Deletion of KMO (yeast Bna4) was seen to suppress polyQ-mediated cytotoxicity (191). It appears that this is dependent upon the accumulation of *de novo* intermediates downstream of Bna4, namely 3-HK and QA (191). Bna4 inhibition reduces the levels of these compounds as well as cytotoxicity and production of ROS (192). Moreover, in mouse models of Alzheimer's and Huntington's diseases, the inhibition of KMO (Bna4 in yeast) was confirmed to protect against neurodegeneration (144,193).

A genetic screen also revealed that Bna4 is a flavoprotein, binding to flavin adenine dinucleotide (FAD^+) (194). This may link the biosynthesis of FAD^+ and NAD^+ and make *de novo* NAD^+ biosynthesis sensitive to cellular FAD^+ levels, consequently integrating the factors involved in the regulation of FAD^+ metabolism with the regulation of NAD^+ metabolism. Interestingly, NAD^+ and FAD^+ metabolism have elsewhere been seen to be connected; it is known that NAD^+ inhibits the activity of FAD pyrophosphatase and prevents FAD degradation (195). Pyridoxal 5-phosphate (PLP) is also known to be required as a cofactor for kynureninase (Bna5) (82,185) and kynurenine oxoglutarate transaminase (KYN aminotransferase, Bna3) (84,185). Although the latter is not strictly part of the *de novo* pathway, it converts KYN to KA and may therefore influence the levels of *de novo* intermediates and flux through the pathway. This could potentially connect *de novo* metabolism with factors involved in pyridoxal biosynthesis, which requires intermediates of glycolysis and the pentose phosphate pathway, along with ammonia (196). Pyridoxal kinase, involved in pyridoxal salvage by phosphorylating it to PLP (along with the respective phosphorylation of pyridoxine and pyridoxamine), is inhibited by a variety of common compounds, among which are caffeine, theobromine (197), dopamine (198), and various pharmaceuticals (196). The requirement of PLP as a cofactor of kynureninase (Kynu) (199) and

KYN aminotransferase (KAT) (200) is conserved in human. The pathways enumerated above may therefore indicate some avenues by which a ramifying network of signals is connected with the regulation of *de novo* NAD^+ metabolism.

Histone deacetylases and epigenetic regulation of *de novo* NAD^+ metabolism - In budding yeast, *de novo* NAD^+ biosynthesis activity is normally repressed under NAD^+ replete conditions wherein NA/NAM salvage activity is high. Silencing of the *de novo* pathway *BNA* genes is mediated by the NAD^+-dependent sirtuin Hst1 and associated co-repressor complexes. During NAD^+ depletion, the *BNA* genes are de-repressed due to loss of Hst1 activity leading to NAD^+ synthesis from the *de novo* branch (78,170). Hst1 has also been shown to interact with Mac1, which is not recruited to the *BNA2* promoter in the absence of Hst1 (78). In addition, the eponymous yeast sirtuin Sir2 has been seen to negatively regulate *BNA1* (201). This establishes a role for sirtuins in mediating epigenetic regulation of the *de novo* pathway.

The sirtuins of budding yeast are additionally known as class III HDACs, distinguished by their requirement for NAD^+ to mediate their catalytic activities (25). Sir2 (*S*ilent *I*nformation *R*egulator *2*), the namesake of this class of HDACs, was first discovered as a repressor of the silent mating type loci (202,203). In addition, Sir2 is known foremost as a repressor of rDNA loci (204) and telomeric regions (205,206). First among the class III HDACs, Sir2 was later discovered to require NAD^+ in order to carry out HDAC activity (15). and to be non-competitively inhibited by NAM (207-209). As a fellow sirtuin, Hst1 exhibits many of the same properties as Sir2. It requires NAD^+ for its catalytic function (210) and is inhibited by NAM (173). Indeed, of all other budding yeast sirtuins it shows the greatest level of amino acid identity with Sir2 (211,212) and there is evidence that Hst1 may sometimes overtake the role of Sir2 in its absence (210,213). Hst1 interacts with Sum1 as part of the Hst1-Sum1-Rft1 complex

(210,214,215). Sum1 specifically is responsible for recruiting Hst1 to chromatin (214), while Rft1 is required for interaction between Sum1 and Hst1 (215). In addition to its role as a regulator of *de novo* NAD^+ metabolism (78,170), Hst1 has also been seen to regulate meiosis (214), telomere maintenance, and central metabolism (216). Among the known histone targets of Hst1 are H3K4 (217), H4K5, and H4K12 (218), and it may also deacetylate H4K16 in the absence of Sir2 (210,213).

Class I includes Rpd3-like HDACs, while class II is composed of the Hda1-like HDACs (219). These two HDACs were the earliest identified in budding yeast (220). Rpd3 is a global deacetylase (221) and is found in two distinct forms: the Rpd3L complex and the Rpd3S complex (220,222,223). The core Rpd3 proteins, shared between the two complexes, are the catalytic Rpd3 subunit itself, the Sin3 scaffolding protein (224), and Ume1 (223). Unique to Rpd3L are the following: Pho23, Sap30, Sds3, Cti6, Rxt2, Rxt3, Dep1, Ume6, and Ash1 (222). Rpd3L is typically active in the promoter region of its target genes (225,226) and may be recruited to a wide variety of targets by several means: by sequence-specific binding of Ume6 (222,227), by sequence-specific binding of Ash1 (222,228), or by recognition of Set1-dependent di- (229) and trimethylation of H3K4 (230,231). Rpd3L has further been seen to interact with Whi5, Stb2, and SBF during recruitment (232). On the other hand, the Rco1 and Eaf3 subunits are unique to Rpd3S (223). Rpd3S is typically active within the open reading frame of target genes (223,226) and may be recruited by the binding of Eaf3 and Rco1 to methylated H3K36, carried out by Set2 (233).

HDACs most often act as repressors of gene expression by removing acetyl modifications from the core histone proteins (234,235), although Rpd3 in particular has also been associated with the activation of gene expression (201,221,236,237). Indeed, both Rpd3L and Rpd3S may

serve as either positive or negative regulators dependent on context (238,239). Rpd3 is known to affect an extensive suite of processes in the cell, including hypoxia response (240), heat stress response (238), and meiosis (241). With HDACs being epigenetic regulators, having a correspondingly wide range of targets, HDACs have received a good deal of attention related to the study and treatment of disease (242-244). Consequently, understanding the mechanisms and roles of HDAC activity is a crucial part of unravelling the contributing factors to cellular health and disease states.

In this work, we establish a role for Rpd3 as a positive regulator of *de novo* NAD^+ metabolism in budding yeast and, specifically, as an antagonist of Hst1 activity. A "cross-feeding" screen developed by our lab has identified *rpd3*Δ cells as having significantly reduced QA levels, while *hst1*Δ cells display an opposite phenotype of starkly increased QA release. We found that Rpd3 and Hst1 antagonistically regulate the majority of the *BNA* genes of *de novo* NAD^+ metabolism and that they provide a link between all branches of NAD^+ biosynthesis in budding yeast, as well as connecting them with cellular phosphate sensing. This work will help to elucidate the complex network of reciprocal signaling in which *de novo* NAD^+ metabolism participates as well as to further develop the regulatory model described above, ultimately providing greater understanding of the causes and treatment of disorders involving dysregulated NAD^+ metabolism.

CHAPTER 2: The Histone Deacetylases Rpd3 and Hst1 Antagonistically Regulate *de novo* NAD^+ Metabolism in the Budding Yeast *Saccharomyces cerevisiae*

This research was originally published in Journal of Biological Chemistry (3)*

*Groth et al, *J Biol Chem* **298**, 102410 (2022), open access

ABSTRACT

NAD^+ is a cellular redox cofactor involved in many essential processes. The regulation of NAD^+ metabolism and the signaling networks reciprocally interacting with NAD^+-producing metabolic pathways are not yet fully understood. The NAD^+-dependent histone deacetylase (HDAC) Hst1 has been shown to inhibit *de novo* NAD^+ synthesis by repressing biosynthesis of nicotinic acid (*BNA*) gene expression. Here, we alternatively identify HDAC Rpd3 as a positive regulator of *de novo* NAD^+ metabolism in the budding yeast *Saccharomyces cerevisiae*. We reveal that deletion of *RPD3* causes marked decreases in the production of *de novo* pathway metabolites, in direct contrast to deletion of *HST1*. We determined the *BNA* expression profiles of *rpd3*Δ and *hst1Δ* cells to be similarly opposed, suggesting the two HDACs may regulate the *BNA* genes in an antagonistic fashion. Our ChIP analysis revealed Rpd3 and Hst1 mutually influence each other's binding distribution at the *BNA2* promoter. We demonstrate Hst1 to be the main deacetylase active at the *BNA2* promoter, with *hst1Δ* cells displaying increased acetylation of the N-terminal tail lysine residues of histone H4, H4K5 and H4K12. Conversely, we show that deletion of *RPD3* reduces the acetylation of these residues in a Hst1-dependent manner. This suggests Rpd3 may function to oppose spreading of Hst1-dependent heterochromatin and represents a unique form of antagonism between HDACs in regulating gene expression. Moreover, we found that Rpd3 and Hst1 also co-regulate additional targets involved in other branches of NAD^+ metabolism. These findings help elucidate the complex interconnections involved in effecting the regulation of NAD^+ metabolism.

INTRODUCTION

Nicotinamide adenine dinucleotide (NAD^+) is a metabolite with crucial roles in a variety of cellular processes. It is involved in the oxidative steps of glycolysis and in mitochondrial energy

production as a redox cofactor, in epigenetic regulation as a co-substrate for class III histone deacetylases (HDACs), also known as sirtuins (14-16), and in DNA repair as a substrate for poly-ADP-ribose polymerases (PARPs) (19). As such, defects of NAD^+ metabolism are associated with a broad range of disorders, such as diabetes, Alzheimer's disease, and various cancers (23-27,29-42).

NAD^+ may be produced by three major pathways: 1) *de novo* biosynthesis from L-tryptophan (TRP), 2) salvage of nicotinic acid (NA) and nicotinamide (NAM), and 3) salvage of nicotinamide riboside (NR) (Fig. 2-1*A*) (Chapter 2, Figure 1*A*). These pathways are largely conserved, with a few species-specific differences, and consume cellular pools of ATP, phosphoribosyl pyrophosphate (PRPP), and glutamine (58,59). The *de novo* pathway is also known as the kynurenine (KYN) pathway of TRP degradation. In yeast, this pathway is characterized by the synthesis of quinolinic acid (QA) from TRP by five enzymatic reactions mediated by the Bna (biosynthesis of nicotinic acid) proteins (Bna2, Bna7, Bna4, Bna5, Bna1) and a spontaneous cyclization (82). Bna6 then converts QA into nicotinic acid mononucleotide (NaMN), which is also produced by the NA-NAM salvage branch (Fig. 1*A*). Under standard NA-abundant growth conditions, NA-NAM salvage is the preferred NAD^+ biosynthesis route (64). NAM may come from NAD^+ consuming reactions including sirtuin mediated protein deacetylation (14-16). NAM can be converted to NA by a nicotinamidase Pnc1 (71), leading to NaMN production by Npt1 (Fig. 1*A*). Although human cells do not have Pnc1-like nicotinamidases, recent studies suggest NAM salvage to NA may also take place in humans with the aid of gut bacterial nicotinamidases (75). In the NR salvage branch, NR can enter the NA-NAM salvage branch when converted to NAM by nucleotidases Urh1 and Pnp1 (45,245). NR can also be converted to nicotinamide mononucleotide (NMN) by the NR kinase, Nrk1 (76). NMN adenylyltransferases (NMNATs;

Nma1, Nma2, and Pof1 in yeast) are responsible for the conversion of NMN to NAD^+ (68,72,246). Nma1 and Nma2 also convert NaMN to nicotinic acid adenine dinucleotide (NaAD) (72,246), which is converted to NAD^+ by the glutamine-dependent NAD^+ synthetase Qns1 (74). Under NAD^+ repleted conditions, the *de novo* pathway *BNA* genes are repressed by the NAD^+-dependent sirtuin Hst1 (78,170). Conversely, NAD^+ depletion results in decreased Hst1 activity leading to transcription activation of the *BNA* genes. Yeast cells also release and re-uptake small NAD^+ precursors such as NA, NAM, QA and NR (Fig. 2-1*A*) (68,77,78,80,174). The mechanisms of precursor release remain unclear, and it has been suggested that vesicular trafficking may play a role (22,58,77). Transport of NAD^+ precursors into yeast cells is mediated by specific transporters Tna1 (for NA and QA) (79,80) and Nrt1 (for NR) (81).

Supplementation of precursors in each pathway has been shown to produce positive outcomes in some disease models (26,39). However, given the complexity of NAD^+ metabolism and its interaction with other signaling networks, it is often necessary to understand the pathways affected in each particular disease state in order to derive the greatest advantage from treatment and determine the most useful precursor for each case. This represents one major benefit that may be won by a detailed study of the molecular mechanisms governing the regulation of each level of NAD^+ metabolism. In addition to being crucial for the maintenance of cellular NAD^+ pools, the intermediates of these pathways often have multifarious other roles (7,22,32). For instance, intermediates of *de novo* metabolism have been associated with both beneficial and adverse influences on neurological health (36,61,89), and have also been shown to interact with immune signaling (36,61,88-90). Indeed, *de novo* metabolism, despite being a relatively minor contributor to the NAD^+ pool compared to salvage of NA, NAM, and NR, is increasingly recognized as an

important element of NAD^+ metabolism with a variety of far-ranging influences on cellular health (46,61).

The regulation of the *de novo* pathway of NAD^+ biosynthesis is still incompletely understood. Previous studies in yeast have shown the sirtuin Hst1 (170) and the copper-sensing transcription factor Mac1 (78) to be negative regulators of *de novo* metabolism, while a complex of Bas1 and Pho2 transcriptionally activates *de novo* metabolism under conditions of adenine depletion (59). In addition, a fragment of the Huntingtin protein was shown to activate production of several *de novo* intermediates, an effect which is ameliorated by the inhibition of the class I histone deacetylase Rpd3 (192). Deletion of *RPD3* has also been shown to reduce expression of *BNA1* (201). In this study, we identified Rpd3 as a positive regulator of the majority of the *BNA* genes of *de novo* NAD^+ biosynthesis, the deletion of which results in markedly diminished production of several *de novo* pathway metabolites. In addition, we characterized the interaction of Rpd3 with the NAD^+-dependent Hst1 in the regulation of *de novo* NAD^+ metabolism. This work helps to elaborate the mechanism by which *BNA* expression is regulated and to clarify the connection of *de novo* NAD^+ metabolism to other branches of metabolism and signaling in the cell.

RESULTS

The histone deacetylase Rpd3 is a positive regulator of QA production - The signaling pathways that regulate NAD^+ metabolism remain unclear in part due to the dynamic nature and complexity of NAD^+ synthesis pathways. Making use of the tendency of yeast cells to constantly release and retrieve small NAD^+ precursors (68,77,80,174), we developed genetic screens to identify and study novel NAD^+ homeostasis factors. The *rpd3*Δ mutant was identified in a screen for mutants that showed altered QA release using a "cross-feeding" assay as described previously (78). As illustrated in Fig. 2-1*B*, a lawn of QA-dependent "recipient cells" (*bna4*Δ*npt1*Δ*nrk1*Δ) are

first spread onto an agar plate. These cells cannot grow because they are dependent on exogenous QA for NAD^+ synthesis, while standard growth medium does not contain QA. Next, "feeder cells" (strains of interest) are spotted onto the lawn of "recipient cells". In this manner, the "feeder cells" release QA to support the growth of "recipient cells" by cross-feeding. This assay determines relative levels of total QA produced and released by "feeder cells" and is considered as a readout for *de novo* pathway activity (Fig. 2-1*B*). The *rpd3*Δ mutant caught our attention because it did not appear to release QA when compared to wild-type cells (WT) (Fig. 2-1*C*). This was surprising, because we previously reported that cells lacking another histone deacetylase, Hst1, exhibited the opposite phenotype (78) (Fig. 2-1*C*). Interestingly, the *hst1Δrpd3Δ* double mutant showed increased QA release, closely matching that seen for the *hst1Δ* single mutant (Fig. 2-1*C*), suggesting Hst1 may function downstream of Rpd3. Next, we examined whether the QA cross-feeding deficiency observed in the *rpd3*Δ mutant (Fig. 2-1*C*) was due to decreased QA production or altered QA transport. To answer this question, we determined the QA content in the cell lysate and growth medium using quantitative liquid assays. Our results showed that the *rpd3*Δ mutant is likely defective in QA production, because it has a significant reduction in both extracellular (Fig. 2-1*D*) and intracellular QA pools (Fig. 2-1*E*). Interestingly, despite releasing a significantly higher amount of QA (Fig. 2-1*C*, 2-1*D*), the *hst1Δ* and *hst1Δrpd3Δ* mutants appeared to have slightly lower intracellular QA levels (Fig. 1*E*). This is in line with our previous report that yeast cells seem to maintain low intracellular QA levels and that excess QA is either released extracellularly or converted to NAD^+ (78). QA accumulation may be detrimental to cells; for example, it has been linked with the production of reactive oxygen species (ROS) (36). However, the factors leading *hst1Δ* and *hst1Δrpd3Δ* cells to store less QA remain unclear.

Cells lacking Rpd3 also show altered NA-NAM salvage, NR salvage, and *de novo* activities - Next we examined whether Rpd3 also plays a role in regulating the other two branches of NAD^+ metabolism, and whether there is an interaction between Rpd3 and Hst1 for this regulation as observed in the regulation of *de novo* QA production. As shown in Fig. 2-2*A*, the *hst1*Δ and *hst1*Δ*rpd3*Δ mutants showed increased NA-NAM release whereas the *rpd3*Δ single mutant did not. This suggests that Rpd3 plays a role in NA/NAM salvage and that Hst1 may function downstream of Rpd3. Note that WT cells did not show visible NA-NAM release (Fig. 2-2*A*), and therefore, it was unclear whether the *rpd3*Δ mutant has reduced or unchanged NA/NAM production. This observation is consistent with a previous report that the majority of NA-NAM is stored intracellularly (77). To address this question, we determined intracellular NA-NAM levels and were able to observe a reduction in NA-NAM levels in *rpd3*Δ cells (Fig. 2-2*B*). Conversely, release of NR is increased in *rpd3*Δ cells in comparison with WT, while little difference is evident in both *hst1Δ* and *hst1Δrpd3Δ* cells (Fig. 2-2*C*). Interestingly, intracellular NR levels were raised not only in *rpd3Δ*, but also in *hst1Δ* cells and, to a remarkably high degree, *hst1Δrpd3Δ* cells (Fig. 2-2*D*). Although the *hst1*Δ and *rpd3*Δ mutants both showed increased NR production (Fig. 2-2*D*), increased NR release was only observed in the *rpd3*Δ but not in the *hst1*Δ mutants (Fig. 2-2*C*). This is likely due to an increase in NR import in the *hst1*Δ mutants since the expression of NR transporter, Nrt1, is increased in these cells (78) (Fig. 2-5*A*). These results also suggest some degree of synergy between Rpd3 and Hst1 in the regulation of the NR salvage pathway.

We next investigated the influence of *rpd3*Δ and *hst1*Δ on cellular NAD^+ pools. As shown in Fig. 2*E*, a moderate, yet significant, reduction in NAD^+ levels was observed in both *rpd3*Δ and *hst1*Δ*rpd3*Δ mutants (Fig. 2-2*E*) when cells were grown in standard synthetic complete media (SC). It has been suggested that NA-NAM salvage is the favored route for NAD^+ synthesis when

NA is present (64) (which is the case for all standard growth media). Therefore, observed NAD^+ defects in *rpd3*Δ cells may be due to deficient NA-NAM salvage (78,170). To directly examine whether the *rpd3*Δ mutant is defective in *de novo* NAD^+ synthesis, cells were cultivated in medium lacking NA (NA-free SC), removing exogenous precursors for the salvage pathways and isolating *de novo* metabolism for analysis. As shown in Fig. 2-2*F*, decreased NAD^+ levels were observed in *rpd3Δ* cells (Fig. 2-2*F*), which was in line with the defects in QA production exhibited by these cells (Fig. 2-1*C*, 2-1*D*). Conversely, NAD^+ levels were raised to a similar degree in both *hst1Δ* and *hst1Δrpd3Δ* cells, in alignment with the increased QA production observed in both strains (Fig. 2-1*D*). This also suggests that the reduced levels of intracellular QA observed in these two strains (Fig. 2-1*E*) may be due to more efficient NAD^+ synthesis.

In order to determine whether the defects seen in QA and NAD^+ production were reflective of a general dysfunction in *de novo* NAD^+ metabolism (Fig. 2-1*A*), we analyzed several intermediates of the pathway present in the cell lysate by mass spectrometry (MS). In accordance with expectations, *rpd3*Δ cells displayed increased TRP levels, while *hst1Δ* and *hst1Δrpd3Δ* cells showed reduced accumulation of TRP (Fig. 2-3*A*). This suggests that *rpd3*Δ cells are deficient for TRP utilization via the *de novo* NAD^+ biosynthesis pathway, while *hst1Δ* and *hst1Δrpd3Δ* cells consume more TRP due to increased *de novo* pathway activity. Indeed, *rpd3*Δ cells showed reduced levels of KYN (Fig. 2-3*B*), 3-HK (Fig. 2-3*C*), and 3-HA (Fig. 2-3*D*). Although *hst1Δ* cells showed reduced levels of KYN, an early intermediate of *de novo* NAD^+ metabolism, both *hst1Δ* and *hst1Δrpd3Δ* cells exhibited increased levels of the downstream intermediates 3-HK and 3-HA, likely due to the rapid flux of *de novo* metabolism expected for cells lacking Hst1 (78). Due to the extremely low concentration of QA stored in the cell (Fig. 2-1*E*) (78), we were unable to detect QA in the cell lysate by MS using same standard conditions. Since most excess QA is released

extracellularly, the QA cross-feeding plate assay appears to be a convenient readout for released QA. Moreover, the plate assay measures QA accumulation in the growth media during the entire time course of recipient cell growth, and therefore, the readout signal may be amplified. MS analysis also confirmed increased intracellular NA accumulation in *hst1Δ* and *hst1Δrpd3Δ* cells (Fig. 2-3*E*), suggested by the cross-feeding studies of NA-NAM (Fig. 2*A* and 2*B*).

Rpd3 is important for optimal activation of the BNA genes in *de novo* metabolism - To further study the role of Rpd3 in NAD^+ metabolism**,** we first asked whether the defects in *de novo* NAD^+ metabolism shown in *rpd3*Δ cells was due to dysregulation of the *BNA* gene expression (Fig. 2-1*A*). As expected, *rpd3Δ* cells showed strongly reduced expression of most of the *BNA* genes involved in *de novo* metabolism (Fig. 2-4*A*). *BNA7* appears to be insensitive to the factors affecting the other *BNA* genes (78), while *BNA3* is not strictly a part of the course of the *de novo* pathway (Fig. 2-1*A*) (87); hence, the two were not investigated. Consistent with previous studies (78,170), *hst1Δ* cells exhibited markedly increased *BNA* expression, while *hst1Δrpd3Δ* cells showed an expression phenotype most closely resembling *hst1Δ*, yet in most cases slightly but significantly below the levels seen in *hst1Δ* alone (Fig. 2-4*A*). The ability of *hst1Δrpd3Δ* to override the expression deficits observed in *rpd3Δ* cells suggests that Hst1 functions downstream of Rpd3 and that Rpd3 promotes transcription possibly by opposing the repressive activity of Hst1 on the *BNA* gene promoters. However, additional factors are likely involved, as *BNA* gene expression in *hst1*Δ*rpd3*Δ cells was not fully restored to level observed in *hst1*Δ cells (Fig. 2-4*A*). We further confirmed that observed *BNA* expression changes were reflective of Bna protein expression. As shown in Fig. 2-4*B,* significant decreases of the three Bna proteins examined (Bna1, Bna2, and Bna5) were observed in *rpd3*Δ cells whereas significant increases of these proteins were observed in *hst1*Δ and *hst1*Δ*rpd3*Δ cells.

Having shown Rpd3 to be a positive regulator of *BNA* expression, we then sought to investigate whether decreased *BNA* expression is ultimately responsible for the low QA and NAD^+ levels in *rpd3Δ* cells. We began with *BNA2*, the rate-limiting enzyme of the *de novo* pathway (78), and inquired whether restoration of this step could replenish the low QA levels seen in *rpd3Δ* cells. We found that overexpression of *BNA2* (from the *ADH1* promoter, so as to decouple it from regulation by Rpd3) was only sufficient to induce a small but significant increase in QA levels, which nevertheless remained far below those seen in WT cells (Fig. 2-4*C* and 2-4*D*). Pairing overexpression of *BNA2* with *BNA6*, which increases QA assimilation into NAD^+ (Fig. 2-1*A*), we found that *BNA6*-oe effectively cleared the small amount of QA accumulated in *rpd3Δ BNA2*-oe cells (Fig. 2-4*D*). We then examined whether this modest increase of QA induced by *BNA2*-oe could restore the NAD^+ levels of *rpd3Δ* cells. As shown in Fig. 2-4*E*, neither *BNA2*-oe alone, nor *BNA2*-oe+*BNA6*-oe was sufficient to stimulate any visible increase in the NAD^+ pool in *rpd3Δ* cells. This indicated that each step of *de novo* metabolism would need to be accounted for in order to achieve full restoration of NAD^+ levels in *rpd3Δ* cells. To test whether this was the case, we attempted to reinstate *de novo* activity by bypassing the earlier steps of the pathway. To achieve this, we cultured cells in NA-free SC supplemented with QA and over-expressed *BNA6* (Fig. 2-4*F, right*), feeding directly into the main pathway of NAD^+ biosynthesis via NaMN (Fig. 2-1*A*). As controls, we also included cells grown in standard SC (Fig. 2-4*F*, *left*) and NA-free SC (Fig. 2-4*F*, *middle*) without QA supplementation. As shown in Fig. 2-4*F* (*right*), neither QA supplementation nor *BNA6*-oe alone was sufficient to raise NAD^+ levels in *rpd3Δ* cells to any significant degree. When paired however, the two adjustments were able to restore NAD^+ levels in *rpd3Δ* back to those observed in WT cells. Interestingly, the NAD^+ levels under these conditions

were still slightly below that of WT cells with *BNA6-oe* and QA supplementation, suggesting other factors downstream of *BNA6* may also be impacted due to *rpd3*Δ.

Rpd3 binding to the *BNA2* promoter is altered by deleting Hst1 and vice versa - Next, we sought to investigate the interaction between Rpd3 and Hst1 at the promoter of the *BNA* genes. Hst1 has been shown to bind to the promoter of *BNA2* (78), which mediates the first and rate-limiting step of *de novo* QA synthesis. Therefore, we determined whether Rpd3 affects the binding activity of Hst1 at the *BNA2* promoter and *vice versa*. To achieve this, we carried out ChIP studies of various *BNA2* promoter fragment using HA-tagged Rpd3 (Rpd3-HA) and Hst1 (Hst1-HA) strains. Fig. 2-5*A* (*top*) shows Rpd3 and Hst1 protein levels used for this study. It appeared that deletion of *HST1* resulted in slightly increased expression of Rpd3-HA, while deletion of *RPD3* resulted in somewhat decreased levels of Hst1-HA (Fig. 2-5*A, top*). However, we did not expect this to have a significant influence on Rpd3 binding to the *BNA2* promoter. As shown in Fig. 2-5*A* (*top*), the Rpd3-HA WT strain showed a normal level of QA release and was still sensitive to the dosage of Hst1, as deleting *HST1* in this strain was able to significantly increase QA release (Fig. 2-5*B, top*). Similarly, deleting *RPD3* in Hst1-HA WT cells also drastically reduced QA release (Fig. 2-5*B. bottom*), suggesting that Hst1-HA remained an efficient repressor and was recruited to the *BNA2* promoter in both WT and *rpd3Δ* backgrounds. Fig. 2-5*A* (*bottom*) illustrates *BNA2* promoter fragments (*BNA2* #1, #2, #3, #4, #5) used in ChIP studies. As shown in Fig. 2-5*C*, the binding activity of Rpd3 was increased near the middle of the *BNA2* promoter (*BNA2* #2, #3) and tapered off toward the -1000 and 0 sites. Interestingly, when Hst1 is absent, Rpd3 appears to move away from the middle of the promoter (*BNA2* #3) and instead occupying the ends (*BNA2* #1, #2, #4 #5) (Fig. 2-5*C*). In particular, we noted the highest increase of Rpd3 occupancy near site #5 (*BNA2* #5), directly proximal to the transcription start site. This is in accordance with expectation,

as Hst1 was previously shown to exhibit the highest binding activity in this region of the *BNA2* promoter (78). Ultimately, when Hst1 is absent, Rpd3 binding distribution on the *BNA2* promoter is altered, with the most significant increase near the transcription start site. This result suggests Hst1 may oppose Rpd3 binding at specific regions of the *BNA2* promoter. Next, we examined whether the absence of Rpd3 would affect Hst1 binding to the *BNA2* promoter. In agreement with previous studies (78), Hst1 binding activity was the highest near the transcription start site (*BNA2* #5) in a pattern ascending from the -1000 to 0 position (Fig. 2-5*D*). Interestingly, when Rpd3 is absent, not only was the ascending binding pattern of Hst1 abolished; the overall Hst1 binding activity was also significantly reduced. This result indicates that Rpd3 indeed affects Hst1 binding distribution at the *BNA2* promoter, but also raises the possibility that Rpd3 may be important for Hst1 binding. However, the latter contradicts the expectation that Rpd3, as a positive regulator of *BNA* expression, would most likely oppose Hst1 binding. It is clear that Hst1 in the *rpd3Δ* background is still highly proficient in silencing *BNA* expression and limiting *de novo* activity (Fig. 2-4*A* and Fig. 2-5*B*) and remains bound at levels significantly above those at the *TAF10* control site (Fig. 2-5*D*). Otherwise, the *rpd3*ΔHst1-*HA* cells would have shown a similar high QA release phenotype as seen in *hst1*Δ cells, which was not the case here (Fig. 2-5*B*). Therefore, it is more likely that the ascending binding pattern of Hst1 is due to higher Rpd3 binding activity toward the middle of the *BNA2* promoter and that in the absence of Rpd3, Hst1 is able to re-distribute more evenly on the *BNA2* promoter. This conclusion supports a model in which Rpd3 may oppose Hst1 binding at specific regions of the *BNA2* promoter, possibly by preventing the over-spreading of silenced chromatin, which is important for proper *BNA* gene expression. The cause of this generally reduced Hst1 binding may also be the reduced NAD^+ levels exhibited by the *rpd3Δ* mutant (Fig. 2-2*E*). As an NAD^+-dependent HDAC, the activity of Hst1 is expected to

decrease under conditions of NAD^+ limitation, which is reflected in the observed reduction in Hst1 binding activity. Supporting this, it has been reported that of all the sirtuins, Hst1 is most sensitive to NAD^+ levels, responding quickly to perturbations to the NAD^+ pool within the range of physiological concentration (170). It is also possible that without the opposing effect of Rpd3, Hst1 does not need to access the *BNA2* promoter frequently in order to maintain silent chromatin.

Rpd3 and Hst1 deacetylate the N-terminal lysine residues of the core histone protein H4 - Having determined how Rpd3 and Hst1 interact in the binding of the *BNA2* promoter, we then sought to determine how each HDAC affects the histone acetylation status of the *BNA2* promoter. In investigating this question, we examined histone acetylation at two of the promoter sites indicated in Fig. 2-5*A* in order to account for any possible local effects of each HDAC. Rpd3 binding peaks at the middle of the promoter near site #3 (Fig. 2-5*C*), while Hst1 binding peaks immediately upstream of the transcription start site at site #5 (Fig. 2-5*D*). Rpd3 has previously been shown to deacetylate a wide variety of lysine residues on the N-terminal tail of core histone proteins, among these being H4K5, H4K8, H4K12, H3K9, H3K14, H3K18, H3K23, H3K27, and H2AK7 (220,247,248). Hst1, on the other hand, has been identified as a deacetylase of H3K4 (217), H4K5, and potentially H4K12 (218). Owing to Rpd3 and Hst1 having H4K5 and H4K12 as shared targets, we chose to focus on histone H4 as a potential site of competition between Rpd3 and Hst1. Our ChIP results showed that Hst1 is the primary deacetylase for H4K5-Ac and H4K12-Ac at the *BNA2* promoter, as the levels of H4K5-Ac and H4K12-Ac were increased in *hst1*Δ cells (at both site #3 and site #5). Deleting *RPD3* slightly yet significantly decreases the level of H4K5-Ac and H4K12-Ac (at site #5, near the transcription start site) (Fig. 2-6*A*, 2-6*B*). This is interesting in light of the fact that deletion of *RPD3* was previously associated with increased acetylation of both of these residues (220). In this case, however, Rpd3 seems to interfere with the deacetylation

of both by an unknown mechanism, while Hst1 appears to be the primary deacetylase for these residues at the *BNA2* promoter. These results suggest that in the absence of Rpd3, another HDAC, likely Hst1, deacetylates H4K5-Ac and H4K12-Ac more efficiently at the *BNA2* promoter. Supporting this, deleting *HST1* in *rpd3*Δ cells restored acetylation to similar levels observed in the *hst1*Δ cells (Fig. 2-6*A*, 2-6*B*).

Interestingly, the acetylation patterns seen for H4K8 differed from that of H4K5 and H4K12 (Fig. 2-6*C*). H4K8-Ac was comparatively difficult to detect at site #3, possibly indicating that it is less abundant than the other acetyl marks. Moreover, H4K8-Ac abundance was increased in *rpd3Δ* cells, in conformity with the previously established role of Rpd3 as a deacetylase of H4K8. On the other hand, any enrichment of H4K8-Ac in *hst1*Δ cells was minor and nonsignificant, unlike acetylation of the other two residues. However, H4K8-Ac levels were strongly increased in *hst1*Δ*rpd3*Δ cells, pointing to the possibility of synergy between the two HDACs in the deacetylation of H4K8. These results suggest that Hst1 is the primary deacetylase of H4K5 and K4K12 at the *BNA2* promoter, while Rpd3 works to limit deacetylation of these residues in this context, in close agreement with the antagonism seen between the two in the regulation of *BNA* expression and *de novo* NAD^+ metabolism. On the other hand, the two HDACs also appear to both deacetylate H4K8 to some degree, suggesting a variety of different interactions between Rpd3 and Hst1 at the *BNA2* promoter, all of which ultimately combine to regulate *BNA2* expression in a specific manner. Ultimately, Hst1 seems to promote repressed chromatin status at the *BNA2* promoter (Fig. 2-6*D*). H4 acetylation (Fig. 2-6*A*, *B*, *C*), Rpd3 binding (Fig. 2-5*C*), and *BNA2* expression are all increased in *hst1*Δ cells (Fig. 2-4*A*). On the other hand, Rpd3 activity is likely associated with de-repressed chromatin status in this context (Fig. 2-6*D*); H4K5 and H4K12 acetylation is somewhat reduced in *rpd3Δ* cells (Fig. 2-6*A*, *B*), while *BNA2* expression is very

strongly decreased (Fig. 2-4*A*). Moreover, the reduced binding of Hst1 to the *BNA2* promoter in *rpd3Δ* cells (Fig. 2-5*D*) may in part be caused by this putative repressed chromatin structure.

***De novo* NAD$^+$ metabolism, NA-NAM salvage, NR salvage, and transport of NAD$^+$ precursors are integrated by Rpd3 and Hst1** - Next, we further examined how Rpd3 and Hst1 may affect other branches of NAD$^+$ metabolism. We tested the expression of genes known to be involved in NA-NAM and NR salvage in WT, *rpd3Δ*, *hst1Δ*, and *hst1Δrpd3Δ* cells by qRT-PCR (Fig. 2-7*A*). As shown in Fig. 2-7*A*, differential expression of NA-NAM salvage genes including *NPT1*, *TNA1* and *PNC1* was observed. A significant decrease in *NPT1* expression was seen in *rpd3Δ* and *hst1Δrpd3Δ* cells (Fig. 2-7*A*). These changes may account for the low NAD$^+$ phenotype of *rpd3Δ* and *hst1Δrpd3Δ* cells in SC media (Fig. 2-2*E*, 2-4*F*) since Npt1 is a major NAD$^+$ biosynthesis enzyme in NA-NAM salvage (Fig. 2-1*A*). Decreased expression of *PNC1* in *rpd3*Δ and *hst1*Δ cells with a further decrease in *hst1*Δ*rpd3*Δ cells suggests that the two HDACs positively and independently regulate *PNC1*. The significant reduction of *PNC1* expression in *hst1Δrpd3Δ* cells correlates with the high levels of NA-NAM accumulation seen in these cells (Fig. 2-2*B*). Interestingly, *rpd3*Δ cells showed a contrasting expression pattern of *URH1* and *PNP1* (Fig. 2-7*B*), both being nucleosidases that convert NR to NAM (Fig. 2-1*A*). Since Urh1 has been suggested to be the primary mediator of this reaction (77), decreased *URH1* expression likely contributes to the increased NR (Fig. 2-2*D*) and reduced NA-NAM (Fig. 2-2*B*) observed in *rpd3*Δ cells. Moreover, increased expression of *ISN1* (Fig. 2-7*B*), a nucleotidase converting NMN to NR, may contribute to increased NR observed in *rpd3*Δ cells (Fig. 2-2*D*). Interestingly, we observed increased expression of *POF1* in *rpd3*Δ and *hst1*Δ cells with a further increase in *hst1*Δ*rpd3*Δ cells. Although Pof1 has been shown to convert NMN to NAD$^+$ (68), its cellular function is not fully understood. In addition, we noted that the two HDACs appear to regulate the QA/NA transport gene *TNA1* and

the NR transport gene *NRT1* in a manner closely resembling the *BNA* genes, with decreased expression observed in *rpd3Δ* cells and increased expression in *hst1Δ* cells (Fig. 2-7*A*). In both cases the *hst1Δrpd3Δ* cells showed a clearly intermediate level of expression most closely matching that of WT. It should be noted, however, that this altered *TNA1* expression is likely not a significant contributor to the *de novo* pathway defects observed in *rpd3*Δ and *hst1*Δ cells, with both strains exhibiting phenotypes opposite those expected in association with aberrant Tna1 activity. We also found that *rpd3Δ*, *hst1Δ*, and *hst1Δrpd3Δ* cells evinced markedly reduced levels of *FUN26* expression, a vacuolar NR transporter (174). Overall, these gene expression results are in line with observed aberrant NAD^+ precursor phenotypes. However, it remains unclear what accounts for the significant increase of NR production seen in *hst1Δrpd3Δ* cells (Fig. 2-2*D*).

DISCUSSION

In this study, we have established a role for Rpd3 as a positive regulator of *de novo* NAD^+ metabolism. In particular, it opposes the negative regulation of the *BNA* genes by another HDAC Hst1 (Fig. 2-4*A* and Fig. 2-6). The *rpd3*Δ and *hst1*Δ mutants show contrasting QA release phenotypes. Interestingly, *hst1*Δ appears to override *rpd3*Δ, and the *hst1*Δ*rpd3*Δ double mutant behaves like the *hst1*Δ single mutant (Fig. 2-1*C*, 2-1*D*), with the exception of intracellular QA levels (Fig. 2-1*E*). Our studies suggest that the high *BNA6* expression in *hst1*Δ and *hst1*Δ*rpd3*Δ cells (Fig. 2-4*A*) may facilitate QA assimilation and therefore reduce intracellular QA accumulation. The same pattern of reduced *de novo* metabolism in *rpd3*Δ cells and increased metabolism in *hst1*Δ cells is seen for several intermediates upstream of QA, namely 3-HK (Fig. 2-3*C*) and 3-HA (Fig. 2-3*D*). Moreover, *rpd3*Δ cells accumulate TRP (Fig. 2-3*A*), likely due to reduced Bna2 activity at the first and rate-limiting step of *de novo* NAD^+ metabolism, while *hst1*Δ and *hst1*Δ*rpd3*Δ cells accumulate less TRP than WT cells, reflecting increased consumption via

de novo metabolism. Rpd3 has also been implicated in recycling of Tat2, a TRP transporter. The growth of a strain defective in Tat2-depedent transport is significantly inhibited under low TRP conditions by deletion of *RPD3* (249). We saw, however, that *rpd3*Δ cells remain proficient for TRP uptake, accumulating the metabolite above levels seen in WT cells (Fig. 2-3*A*). This suggests that reduced assimilation of TRP into NAD^+ via the *de novo* pathway may contribute to the growth defects of *rpd3*Δ cells in low TRP media (249). In addition to defective *de novo* NAD^+ metabolism, cells lacking Rpd3 also show altered NA-NAM and NR salvage activities. Although contrasting NA-NAM release phenotypes are also observed in *rpd3*Δ and *hst1*Δ mutants (Fig. 2-2*A*, 2-2*B*), it appears that different downstream genes are dysregulated in each mutant. The lower NA-NAM levels in the *rpd3*Δ mutant (Fig. 2-2*A*, 2-2*B*) are likely due to overall lower NAD^+ levels (Fig. 2-2*E*, 2-2*F*). It is also possible that reduced *URH1* expression (Fig. 2-7*B*) results in less NR to NAM conversion (58). In *hst1*Δ (including *hst1*Δ*rpd3*Δ) cells, increased intracellular NA-NAM levels (Fig. 2-2*B*) are likely due to increased expression of the NA transporter *TNA1* as well as reduced nicotinamidase *PNC1* expression (Fig. 2-7*A*). On the other hand, the *rpd3*Δ and *hst1*Δ mutants also show contrasting NR release patterns, but this time the *rpd3*Δ mutant releases more NR (Fig. 2-2*C*). The *hst1*Δ mutant appears to release less NR because most NR is accumulated intracellularly (Fig. 2-2*D*) due to high expression of the NR transporter *NRT1* (Fig. 2-7*B*). Increased NR release in the *rpd3*Δ mutant is likely due to decreased *NRT1* expression (Fig. 2-7*B*). Notably, *rpd3*Δ and *hst1*Δ have a synergistic effect on NR production (Fig. 2-2*D*), which has also been seen for the expression of other genes involved in NR salvage including *POF1* (Fig. 2-7*B*). Overall, our results show that Rpd3 and Hst1 opposingly co-regulate the *de novo BNA* genes, yet they seem to affect different target genes in the salvage pathways. Among the genes examined, only the NAD^+

precursor transporters *NRT1* and *TNA1* (Fig. 2-7*A*, 2-7*B*) appear to be regulated by the two HDACs in a manner resembling the *BNA* genes (Fig. 2-4*A*).

Our studies also indicate that observed NAD^+ deficiencies in *rpd3*Δ cells are likely caused by various factors discussed above depending on specific growth conditions. In standard NA-rich growth media, *de novo* pathway is repressed by the NAD^+-dependent Hst1. Therefore, observed low NAD^+ defects in *rpd3*Δ (and *hst1*Δ*rpd3*Δ) cells (Fig. 2-2*E*) likely result from increased NR production in conjunction with a blockage in NR flow to NA-NAM salvage and reduced NA assimilation due to decreased expression of *NPT1* (Fig. 2-7*A*) and *URH1* (Fig. 2-7*B*). The effects of *rpd3*Δ and *hst1*Δ on *de novo* pathway activity are better understood since this pathway can be studied in defined NA-free growth media (Fig. 2-2*F*). Under this condition, observed NAD^+ deficiencies are mainly due to reduced *BNA* expression, and so deleting *hst1*Δ overrides *rpd3*Δ and increases NAD^+ levels (Fig. 2-2*F*). We also show that dysregulation of multiple *BNA* genes contributes to NAD^+ deficiencies in *rpd3*Δ cells, since over-expressing individual rate-limiting *BNA2* gene and the *BNA6* gene was not sufficient to restore NAD^+ levels (Fig. 2-4*E*). However, we were able to restore the levels of NAD^+ in *rpd3*Δ cells by supplementing QA and overexpressing *BNA6* (Fig. 2-4*F*). These studies confirm that Rpd3 is important for optimal *BNA* gene expression and *de novo* NAD^+ synthesis. To understand the mechanisms Rpd3 and Hst1 mediated regulation of *BNA* expression, we carried out ChIP studies to study the binding distributions of Rpd3 and Hst1 on the promoter of the *BNA2* genes (Fig. 2-5*C*, 2-5*D*). The results gathered point toward a model in which Hst1 serves to limit Rpd3's distribution pattern on the *BNA2* promoter. Rpd3 also appears to affect the interaction of Hst1 with the *BNA2* promoter but the effect is less significant, as the overall Hst1 binding activity at the *BNA2* promoter is reduced in *rpd3*Δ cells (Fig. 2-5*C*, 2-5*D*, 2-5*E*). It is possible that Hst1 activity is reduced in *rpd3*Δ cells

due to reduced NAD^+ levels. This is interesting in light of the fact that Hst1 appears to work downstream of Rpd3, with *hst1Δ* sufficient to raise *BNA* expression and QA production to a similar extent in WT and *rpd3Δ* backgrounds. Therefore, we anticipate that additional factors may also play a role in the antagonistic *BNA* gene expression regulation exerted by Rpd3 and Hst1. One possibility is that specific transcription factors and/or chromatin re-modeling factors are recruited to or excluded from the *BNA* promoter by specific chromatin modifications effected by the two HDACs.

Similar instances of antagonism between Rpd3 and other sirtuins have been noted in previous studies, with Rpd3 opposing repression of the silent mating-type loci by Sir2 and thereby promoting transcription (248). Rpd3 has also been shown to limit Sir2 spreading at telomere boundaries (250). While it is typical for HDACs to serve as chromatin silencers (219), Rpd3 has long been noted for seeming to promote transcription of certain genes (221). Interestingly, it was previously noted that the role played by Rpd3 in opposing Sir2 activity was indeed mediated by its catalytic HDAC activity, but that the effect did not depend on any of the known histone targets of Rpd3 (248). Indeed, there are many examples of HDACs acting on non-histone proteins (251,252), making the possible avenues of HDAC-dependent regulation quite extensive. Moreover, restoration of silencing by *RPD3* deletion in a *sir2*-catalytic-dead strain was dependent on Hst3 activity (248), highlighting the complementarity and interactive roles of different HDACs. In the case of *de novo* pathway regulation however, our QA cross-feeding screen (Fig. 2-1*B*) did not indicate the involvement of any other HDACs aside from Rpd3 and Hst1. It appears that some or all *BNA* genes may be regulated in a unique fashion. For example, Sir2 has previously been identified as a negative regulator of *BNA1* expression, with *sir2*Δ cells showing *BNA1* expression increased by approximately 2-fold (201). The positive regulator Bas1-Pho2, for instance, appears

to affect each *BNA* gene to significantly varying degrees (59). We have previously seen as well that *BNA7* is insensitive to many of the factors that regulate other *BNA* genes (78). It does appear that Rpd3 and Hst1 are ubiquitous regulators of *de novo* NAD^+ metabolism, however, this property may not extend to other regulators of the pathway. It will likely be necessary to study each *BNA* gene individually in order to fully elaborate the intricacies of *de novo* pathway regulation.

It has also been shown that treatment with sodium butyrate and other HDAC inhibitors is able to suppress aberrant *de novo* metabolism in Huntingtin-expressing cells in a similar fashion to *ume1Δ* and *rxt3Δ* (192), while treatment with the sirtuin inhibitor NAM produces effects on *BNA* expression similar to those observed in *hst1Δ* (78). These studies suggest that the catalytic activities of each HDAC are required at least to some extent and that the role each plays is not purely structural. In agreement with this notion, both HDACs seemed to have a rather significant effect on the acetylation status of histone H4. In particular, we found that the abundance of H4K5-Ac (Fig. 2-6*A*) and H4K12-Ac (Fig. 2-6*B*) was significantly increased in *hst1Δ* and *hst1*Δ*rpd3*Δ cells, while H4K8-Ac abundance was significantly increased in *rpd3*Δ cells and very greatly raised in *hst1*Δ*rpd3*Δ cells (Fig. 2-6*C*). Altogether, these results seem to implicate Hst1 as the major deacetylase active at the *BNA2* promoter and, together with increased *de novo* activity and *BNA* expression observed in *hst1Δ* cells, point toward a role for Hst1 in establishing a repressive chromatin architecture at the *BNA* promoters. Conversely, Rpd3, with the exception of H4K8-Ac, appears to generally limit deacetylation at the *BNA2* promoter. In combination with decreased *BNA* expression seen in *rpd3*Δ cells, Rpd3 appears to act in the capacity of a positive regulator by limiting Hst1-dependent deacetylation.

Though the specific mechanism of this antagonism between Rpd3 and Hst1 remains to be further investigated, there are several possibilities suggested by these results. Limitation of Hst1-

dependent deacetylation by Rpd3 may proceed by means of competition for the same targets, such as H4K5-Ac and H4K12-Ac, wherein limited deacetylation by Rpd3 prevents recognition and full deacetylation by Hst1. It has previously been reported that certain HDACs may be recruited by a specific acetyl mark. For instance, H4K16-Ac, a target of Sir2, has been shown to promote the binding of Sir2 to chromatin (253). It is also possible that other acetyl marks may be targeted primarily by Rpd3, potentially including H4K8-Ac, reconfiguring the chromatin so as to interfere with Hst1 activity at different marks, the net result of which might be decreased silencing by Hst1. We saw that deletion of *RPD3* unexpectedly decreased Hst1 binding to the *BNA2* promoter (Fig. 2-5*D*); one possible explanation for this is that the repressive heterochromatin structure formed by Hst1 HDAC activity in the absence of Rpd3 might then limit the continued binding of Hst1 itself, with only enough Hst1 binding to maintain the heterochromatin structure. Finally, histone modifications made by Rpd3 may also be involved in the recruitment of additional chromatin remodeling factors or transcription factors to the *BNA2* promoter, which may then interact with Hst1. It has previously been established that the copper-sensing transcription factor Mac1 (78) and the Bas1-Pho2 complex (59) regulate *BNA* expression. How these factors, and possibly others, might interact with Rpd3 and Hst1 is a matter for future study.

It appears ultimately that Hst1 is involved in the formation of heterochromatin at the *BNA2* promoter via deacetylation of the N-terminal lysines of H4, while Rpd3 opposes Hst1 HDAC activity and maintains a less repressed chromatin structure (Fig. 2-6*D*). Whether Rpd3 and Hst1 target additional residues on other histones remains a topic for further study. Rpd3 has been shown to target a very wide group of acetyl-lysine residues across several different histone proteins, including H3K9, H3K14, H3K18, H3K23, H3K27, and H2AK7 (247), while Hst1 is known to deacetylate H3K4 (217) and may also deacetylate H4K16 in the absence of Sir2 and Pde2 (213).

Additionally, it remains to be investigated what effect each acetyl-lysine mark has on *BNA* expression and chromatin structure, and whether Rpd3 and Hst1 do indeed regulate heterochromatin formation in the manner proposed (78,248).

In summary, Rpd3 and Hst1 appear to exert opposing influence on *de novo* NAD^+ metabolism and also integrate the regulation of several disparate branches of NAD^+ metabolism. This set of regulators helps coordinate a variety of interrelated metabolic signals in budding yeast. Further work will be required to explore the detailed mechanistic interactions among these regulators and to establish the means by which they compete and cooperate to influence the cellular pools of NAD^+ and its precursors. Rpd3 and Hst1, having homologs in human HDAC1 and SIRT1, respectively, represent links between the study of the epigenetic regulation of NAD^+ metabolism and various disease states. Aberrant NAD^+ metabolism and associated dysregulation of sirtuin activities have been implicated in a number of human disorders (25-27,38-41). HDAC1 has also been associated with a variety of diseases, and HDAC inhibition generally has received attention as a therapeutic intervention in a variety of contexts (254-256). It is currently unclear whether sirtuins and HDAC1 also regulate NAD^+ metabolism in other organisms by similar mechanisms. It would be interesting to determine what other genes are also co-regulated by Hst1 and Rpd3 in future studies. Notably, many NAD^+ intermediates also have a manifold set of relationships with cellular health. For instance, the intermediates of the *de novo* pathway have diverse interactions with infectious mechanisms, metabolic stress, and immune signaling (7). Altogether, this work contributes to the elaboration of the relations by which NAD^+ metabolism is governed and helps to connect different branches of NAD^+ metabolism among each other.

EXPERIMENTAL PROCEDURES

Yeast strains, growth media, and plasmids - Yeast strain BY4742 *MATα his3Δ1 leu2Δ0 lys2Δ0 ura3Δ0* acquired from Open Biosystems (257) was used as the parental WT strain for this study. Standard growth media including synthetic minimal (SD), synthetic complete (SC), and yeast extract/peptone/dextrose (YPD) rich media were made as described (258). Special NA-free SD and NA-free SC were made by using niacin-free yeast nitrogen base acquired from Sunrise Science Products. Gene deletions were carried out by replacing the coding regions of WT genes with gene-specific PCR products generated using either the p*AG32-hphMX4* (2) or the reusable *loxP-kanMX-loxP* (pUG6) (1) cassettes as templates. Multiple gene deletions employed a galactose-inducible Cre recombinase to remove the *loxP-kanMX-loxP* cassette, followed by another round of gene deletion (1). The HA epitope tag was added to target genes directly in the genome using the *pFA6a-3HA-kanMX6* (for *HST1*) or p*FA6a-kanMX6-PGAL1-3HA* (for *RPD3*) plasmids as template for PCR mediated tagging (6). The *BNA6-oe* and *BNA2-oe* plasmids p*ADH1-BNA6* (5) and p*ADH1-BNA2-URA3* were made in the integrative p*PP81* (*LEU2*) and p*PP35* vectors respectively. After Pac1 digestion, the linearized plasmids were introduced to yeast cells as described (258). The p*ADH1-BNA2-URA3* plasmid was made by cloning the Not1-Nhe1 DNA fragment from the p*ADH1-BNA2* plasmid (78) into p*PP35* cut with Not1 and Nhe1.

QA, NR, and NA-NAM cross-feeding plate assays - These assays employed specific mutants, which depend on QA, NR, or NA-NAM for growth, as "recipient cells", and yeast strains of interest as "feeder cells". First, recipient cells were plated as a lawn on a solid agar plate (~10^4 cells/cm^2). Next, ~2x10^4 cells of each feeder cell strain (2 μl cell suspension made in sterile water at A_{600} of 1) was spotted onto the lawn of recipient cells. Plates were then incubated at 30˚C for 3 days. Since the growth media do not contain the NAD^+ intermediates needed for the growth of recipient cells, the extent of the recipient cell growth indicates the levels of specific NAD^+

intermediates released by feeder cells. QA cross-feeding was carried out on SC or SD using the QA dependent *npt1*Δ*nrk1*Δ*bna4*Δ mutant. NR cross-feeding was carried out on YPD or SC using the NR dependent *npt1*Δ*bna6*Δ*pho5*Δ mutant. NA-NAM cross-feeding was carried out on NA-free SC or NA-free SD using the NA-NAM dependent *bna6*Δ*nrk1*Δ*nrt1*Δ mutant.

Measurement(s) of NAD^+, NADH, QA, NR and NA-NAM - Total intracellular levels of NAD^+ and NADH were determined using enzymatic cycling reactions as described (4). In brief, approximately 1 A_{600} unit (1 A_{600} unit = $1x10^7$ cells/ml) cells grown to early-logarithmic phase in SC (~6 hr growth from A_{600} of 0.1) were collected in duplicate by centrifugation. Acid extraction was performed in one tube to obtain NAD^+, and alkali extraction was performed in the other to obtain NADH for 40 minutes at 60˚C. Amplification of NAD^+ or NADH in the form of malate was carried out using 3 µl or 4 µl of neutralized acid or alkali extracted lysate in 100 µl of cycling reaction for 1 hour at room temperature. The reaction was terminated by heating at 100˚C for 5 minutes. Next, malate produced from the cycling reaction was converted to oxaloacetate and then to aspartate and a-ketoglutarate by the addition of 1 ml malate indicator reagent for 20 minutes at room temperature. The reaction produced a corresponding amount of NADH as readout, which was measured fluorometrically with excitation at 365 nm and emission monitored at 460 nm. Standard curves for determining NAD^+ and NADH concentrations were obtained as follows: NAD^+ and NADH were added into the acid and alkali buffer to a final concentration of 0, 2.5, and 7.5 µM, which were then treated with the same procedure along with other samples. The fluorometer was calibrated each time before use with 0, 5, 10, 20, 30, and 40 µM NADH to ensure that the detection was within a linear range. Levels of NAD^+ intermediates (QA, NR and NA-NAM) were determined by a liquid-based cross-feeding bioassay as previously described (5,77,174) with modifications. To prepare cell extracts for intracellular NAD^+ intermediates

determination, approximately 200 A_{600} unit (for NR and NA-NAM) or 900 A_{600} unit (for QA) donor cells grown to late-logarithmic phase in SC (~16 hr growth from an A_{600} of 0.1) were collected by centrifugation and lysed by bead-beating (Biospec Products) in 400 μl (per 200 A_{600} unit cells) ice-cold 50 mM ammonium acetate solution. The supernatant was collected by centrifugation and the pellet was extracted two more times with 600 µl ice-cold 50 mM ammonium acetate solution, which generates 1600 µl cell lysate. After filter sterilization, 100-200 μl of clear extract (2.5 mL for QA) was used to supplement 8 ml cultures of recipient cells with starting A_{600} of 0.05 in SC. To determine extracellular NAD^+ intermediates levels, 20 ml supernatant of donor cell culture was collected, filter-sterilized, and then 4 ml was added to recipient cell culture in 2x SC to a final volume of 8 ml with total starting A_{600} of 0.05. A control culture of recipient cells in SC without supplementation was included in all experiments. For measuring relative QA levels, *npt1*Δ*nrk1*Δ*bna4*Δ and *npt1*Δ*nrk1*Δ*bna1*Δ mutants were used as recipient cells. The *npt1*Δ*bna6*Δ*pho5*Δ recipient cells were used to measure relative NR levels. To measure relative NA/NAM levels, the *bna6*Δ*nrk1*Δ*nrt1*Δ recipient cells were grown in NA-free SC. After incubation at 30˚C for 24 hours, growth of the recipient cells (A_{600}) was measured and normalized to the cell number of each donor strain. A_{600} readings were then converted to concentrations of QA, NR, and NA/NAM using the standard curves established as previously described (77,174).

Mass spectrometry analysis of metabolite levels - Metabolomic data were acquired at the UC Davis West Coast Metabolomics Center. For each sample, approximately 300 A_{600} unit (for QA) cells grown to late-logarithmic phase in SC (~16 hr growth from an A_{600} of 0.1) were collected by centrifugation. Snap freezing was achieved by dry ice. Frozen cell pellets were kept in Eppendorf tubes and then subject to metabolite extraction and Mass Spectrometry analysis. Cells were extracted following recommendations published before (259). GC-TOF was performed with an

Agilent 6890 gas chromatography instrument with an Rtx-5Sil MS column coupled to a Leco Pegasus IV time of flight mass spectrometer (260). For data processing, ChromaTOF version 4.50.8 was used in conjunction with the BinBase algorithm as previously described (261). Metabolite identifications were performed according to the Metabolomics Standards Initiative by using chromatography-specific databases in conjunction with Mass Bank of North America (http://massbank.us) and NIST 20 mass spectral libraries (262).

Quantitative PCR (qPCR) analysis of gene expression levels - Approximately 40 A_{600} unit cells grown to early-logarithmic phase in SD (6 hr growth from A_{600} of 0.1) were collected by centrifugation. Total RNA was isolated using GeneJET RNA purification Kit (Thermo Scientific) and cDNA was synthesized using QuantiTect Reverse Transcription kit (Qiagen) according to the manufacturer's instructions. For each qPCR reaction, 50 ng of cDNA and 500 nM of each primer were used. qPCR reaction was run on Roche LightCycler 480 using LightCycler 480 SYBR green I Master Mix (Roche) as previously described (68). Average size of the amplicon for each gene was ~ 150 bp. The target mRNA transcript levels were normalized to *TAF10* transcript levels.

Protein Extraction and Western Blot Analysis - Approximately 50 A_{600} unit cells grown in SC to early-logarithmic phase (A_{600} of ~1) were collected by centrifugation. The cell lysate was obtained by bead-beating in lysis buffer: 50 mM Tris-HCl, pH 7.5, 100 mM NaCl, 1% Triton X-100, 5 mM EDTA (pH=8), 1 mM PMSF, and protease inhibitor cocktail (Pierce™). The protein concentration was measured using the Bradford assay (Bio-Rad) and 20-25 µg (Hst1, Bna, PGK) or 40 µg (Rpd3) of total protein was loaded in each lane. After electrophoresis, the protein was transferred to a polyvinylidene fluoride membrane (GE healthcare). Blocking was carried out using OneBlock™ Western-CL Blocking buffer. The membranes were then washed, blotted with either anti-HA rabbit antibody (Cell Signaling 3724S) or anti-PGK mouse antibody (Invitrogen 459250).

Protein was visualized using anti-mouse or anti-rabbit IgG antibody conjugate to horseradish peroxidase (Invitrogen), and the ECL-reagents (Amersham^{TM}, GE). The chemiluminescent image was analyzed using the Amersham Imager 600 (GE) system and software provided by the manufacturer.

Chromatin immunoprecipitation (ChIP) assay - Approximately 500 A_{600} unit cells grown to early-logarithmic phase in SD were cross-linked with 1% formaldehyde for 30 min at room temperature and stopped by adding glycine to a final concentration of 125 mM. Cells were pelleted by centrifugation and washed 2 times with cold Tris-buffered saline (20 mM Tris-HCl, pH7.5, 150 mM NaCl). Cells were lysed by bead-beating in 1 ml of FA-140 lysis buffer (50 mM HEPES, 140 mM NaCl, 1% Triton X-100, 1 mM EDTA, 0.1% sodium deoxycholate, 0.1 mM PMSF, 1x protease inhibitor cocktail (Pierce)) (263). The cell lysate was drawn off the beads and centrifuged at a maximum speed (13,200 rpm) for 30 min at 4°C. The chromatin pellet was resuspended in 1 ml of FA-140 lysis buffer and sonicated on ice 8 times with 20 second pulses using a Branson 450 Sonicator (output control set at 1.5 and duty cycle held at constant) to shear chromatin to an average length of ~ 500 bp. Sonicated chromatin solution was centrifuged twice at 10,000 rpm for 10 min at 4°C. The supernatant was then aliquoted into two tubes (labeled "IP" and "no-Ab"). The IP samples were incubated overnight at 4°C with anti-HA monoclonal antibody (ab1424, Abcam) at a dilution of 1:150. Both IP and no-Ab samples were incubated with 60 µl of ChIP-grade protein G beads (Cell Signaling Technology) for 2 hours at 4°C and then washed as described (263). DNA was then eluted from the beads 2 times with 125 µl of elution buffer (5X TE, 1% SDS). The combined DNA solution and input samples were incubated at 65°C overnight to reverse the cross-linking. The purified DNA samples were analyzed by qPCR. The amount of immunoprecipitated specific promoter DNA was determined relative to no-Ab DNA. For quantitation of histone acetyl-

lysine marks, each mark, along with the H4 protein itself, was precipitated as above using the following antibodies: ab10158, Abcam (H4); 71-290-6, Invitrogen (H4K5-Ac); ab15823, Abcam (H4K8-Ac); ab46983, Abcam (H4K12-Ac). The amount of each mark was determined relative to no-Ab DNA and H4 bound DNA.

FIGURE 2-1

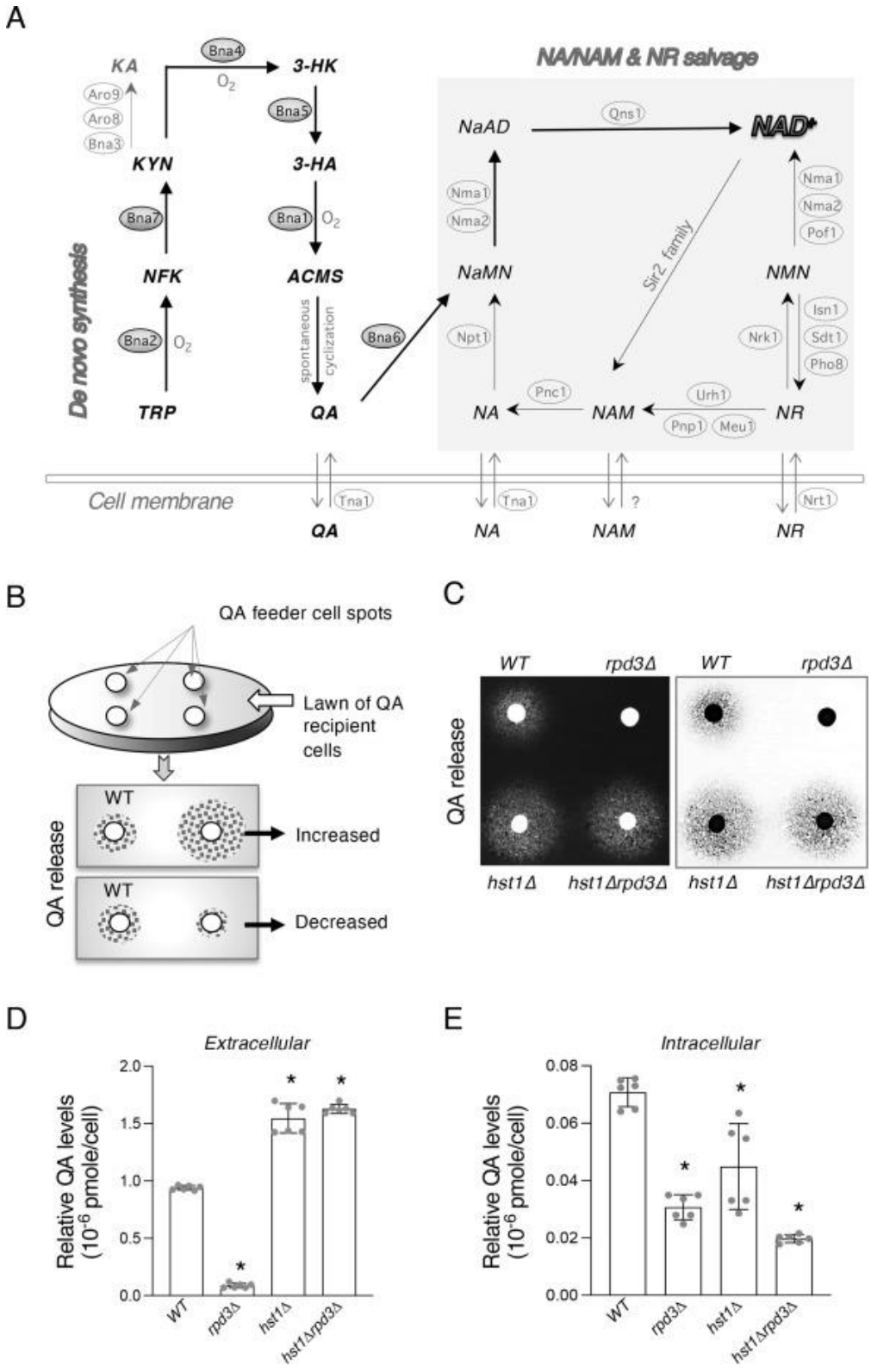
A
KA
Bna4
O2
3-HK
Aro9
Aro8
Bna3
Bna5
KYN
3-HA
Bna7
Bna1
O2
NFK
ACMS
De novo synthesis
Bna2
O2
spontaneous cyclization
Bna6
TRP
QA
NA/NAM & NR salvage
NaAD
Qns1
NAD+
Nma1
Nma2
Pof1
Sir2 family
NaMN
NMN
Isn1
Nrk1
Sdt1
Pho8
Npt1
Pnc1
Urh1
NA
NAM
NR
Pnp1
Meu1
Cell membrane
Tna1
Tna1
?
Nrt1
QA
NA
NAM
NR
B
QA feeder cell spots
Lawn of QA recipient cells
WT
Increased
WT
Decreased
QA release
C
WT
rpd3Δ
WT
rpd3Δ
QA release
hst1Δ
hst1Δrpd3Δ
hst1Δ
hst1Δrpd3Δ
D
Extracellular
Relative QA levels (10-6 pmole/cell)
2.0
1.5
1.0
0.5
0.0
WT
rpd3Δ
hst1Δ
hst1Δrpd3Δ
E
Intracellular
Relative QA levels (10-6 pmole/cell)
0.08
0.06
0.04
0.02
0.00
WT
rpd3Δ
hst1Δ
hst1Δrpd3Δ

FIGURE 2-1. Cells lacking *RPD3* are deficient for *de novo* QA production.
A, model of the NAD^+ biosynthetic pathways in *Saccharomyces cerevisiae*. *De novo* NAD^+ metabolism begins with TRP, which is converted into NaMN by the Bna enzymes (Bna2, -7, -4, -5, -1, -6) (*left*). NaMN is also produced by salvage of NA and NAM, which is further connected with salvage of NR (*right*). NR is metabolized to NMN by Nrk1, which is then converted to NAD^+ by Nma1, Nma2 and Pof1. Abbreviations of NAD^+ intermediates are shown in bold and italicized. NA, nicotinic acid. NAM, nicotinamide. NR, nicotinamide riboside. QA, quinolinic acid. TRP, L-tryptophan. NFK, N-formylkynurenine. KYN, kynurenine. 3-HK, 3-hydroxykynurenine. 3-HA, 3-hydroxyanthranilic acid. ACMS, 2-amino-3-carboximuconate-6-semialdehyde. KA, kynurenic acid. NaMN, nicotinic acid mononucleotide. NaAD, deamido-NAD^+. NMN, nicotinamide mononucleotide. Abbreviations of protein names are shown in ovals. Bna2, tryptophan 2,3-dioxygenase. Bna7, kynurenine formamidase. Bna4, kynurenine 3-monooxygenase. Bna5, kynureninase. Bna1, 3-hydroxyanthranilate 3,4-dioxygenase. Bna6, quinolinic acid phosphoribosyl transferase. Aro9/Aro8 and Bna3, kynurenine aminotransferase. Nma1/2, NaMN/NMN adenylyltransferase (NMNAT). Pof1, NMN adenylyltransferase (NMNAT). Qns1, glutamine-dependent NAD^+ synthetase. Npt1, nicotinic acid phosphoribosyl transferase. Pnc1, nicotinamidase. Sir2 family, NAD^+-dependent protein deacetylases. Urh1, Pnp1 and Meu1, nucleosidases. Nrk1, NR kinase. Isn1 and Sdt1, nucleotidases. Pho8 and Pho5, phosphatases. Tna1, NA and QA transporter. Nrt1, NR transporter.
B, illustration of the QA cross-feeding assay used to determine relative levels of QA release in strains of interest. Spots of haploid single-deletion feeder cells were applied to a lawn of QA-dependent recipient cells (*bna4Δnrk1Δnpt1Δ*) and allow to grow for 2-3 days at 30˚C. The density of recipient cell growth around the feeder cell spots correlates with the amount of QA released by the feeder cells.
C, deletion of *RPD3* (*rpd3Δ)* decreases QA cross-feeding activities, while deletion of *HST1* (*hst1Δ*) as well as *HST1* and *RPD3* together (*hst1Δrpd3Δ*) increases QA cross-feeding activities. Feeder cell spots along with recipient cells were grown on SC plates at 30˚C for 2 days. For clarity, inverse image is also shown (*right*).
D, extracellular QA levels determined in the growth media. Deletion of *RPD3* decreases QA release, while deletion of *HST1* as well as *HST1* and *RPD3* together increases QA release.
E, intracellular QA levels determined in the cell lysates. Deletion of *RPD3* decreases intracellular stores of QA.

For *D* and *E*, the graphs are based on data of two independent experiments. Error bars represent data from two biological replicates per strain each with three technical replicates (total n=6 per strain). The p values are calculated using student's t test (*, p<0.05).

FIGURE 2-2

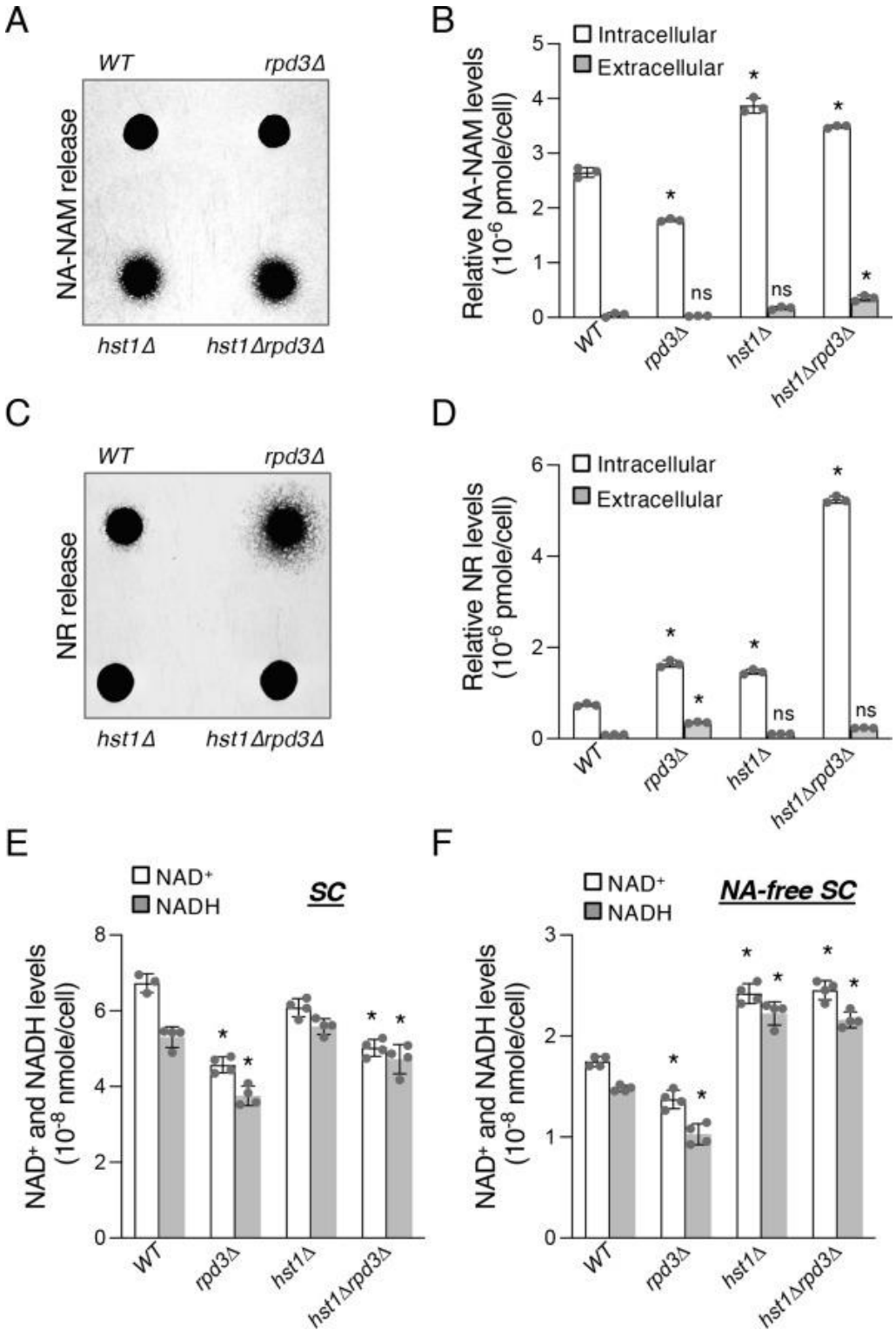
A
WT
rpd3Δ
NA-NAM release
hst1Δ
hst1Δrpd3Δ
B
Intracellular
Extracellular
Relative NA-NAM levels (10-6 pmole/cell)
ns
WT
rpd3Δ
hst1Δ
hst1Δrpd3Δ
C
WT
rpd3Δ
NR release
hst1Δ
hst1Δrpd3Δ
D
Intracellular
Extracellular
Relative NR levels (10-6 pmole/cell)
ns
WT
rpd3Δ
hst1Δ
hst1Δrpd3Δ
E
NAD+
NADH
SC
NAD+ and NADH levels (10-8 nmole/cell)
WT
rpd3Δ
hst1Δ
hst1Δrpd3Δ
F
NAD+
NADH
NA-free SC
NAD+ and NADH levels (10-8 nmole/cell)
WT
rpd3Δ
hst1Δ
hst1Δrpd3Δ

FIGURE 2-2. Determination of NAD^+ salvage pathway intermediates and NAD^+ levels in cells lacking *RPD3* and *HST1*.

***A**, hst1Δ* and *hst1Δrpd3Δ* cells show increased NA-NAM cross-feeding activities. Feeder cells spots along with NA-NAM dependent recipient cells (*bna6Δnkr1Δnrt1Δ*) were grown on NA-free SC plate at 30˚C for 3 days.

***B**,* quantification of NA-NAM production by measuring *the* extracellular (released) and intracellular (stored) levels of NA-NAM. *rpd3Δ* cells show decreased release and intracellular storage of NA-NAM*, while hst1Δ* and *hst1Δrpd3Δ* cells show increased release and storage of NA-NAM.

***C**, rpd3Δ* cells show increased NR cross-feeding activities whereas *hst1Δ* and *hst1Δrpd3Δ* cells show decreased activities. Feeder cell spots along with NR-dependent recipient cells (*npt1Δbna6Δpho5Δ*) were grown at 30˚C on YPD plate for 3 days.

***D**, rpd3Δ* and *hst1Δ* cells show increased intracellular storage of NR. The *hst1Δrpd3Δ* double mutant shows a further increase compared to the single mutants. Only the *rpd3Δ* mutant shows a significant increase in NR release. *E*, *rpd3Δ* and *hst1Δrpd3Δ* cells exhibit significantly reduced NAD^+ levels in standard SC medium. *F*, *rpd3Δ* cells display reduced NAD^+ levels in NA-free SC medium, while *hst1Δ* and *hst1Δrpd3Δ* display increased NAD^+ levels.

For *B, D, E,* and *F,* graphs are representative of the trend observed across three independent experiments. For *B* and *D,* error bars represent data from three technical replicates for each strain in an experiment. For *E* and *F,* error bars represent data from two biological replicates each with two technical replicates for each strain in an experiment. The *p* values are calculated using student's t test (*, $p<0.05$; *ns*, not significant).

FIGURE 2-3

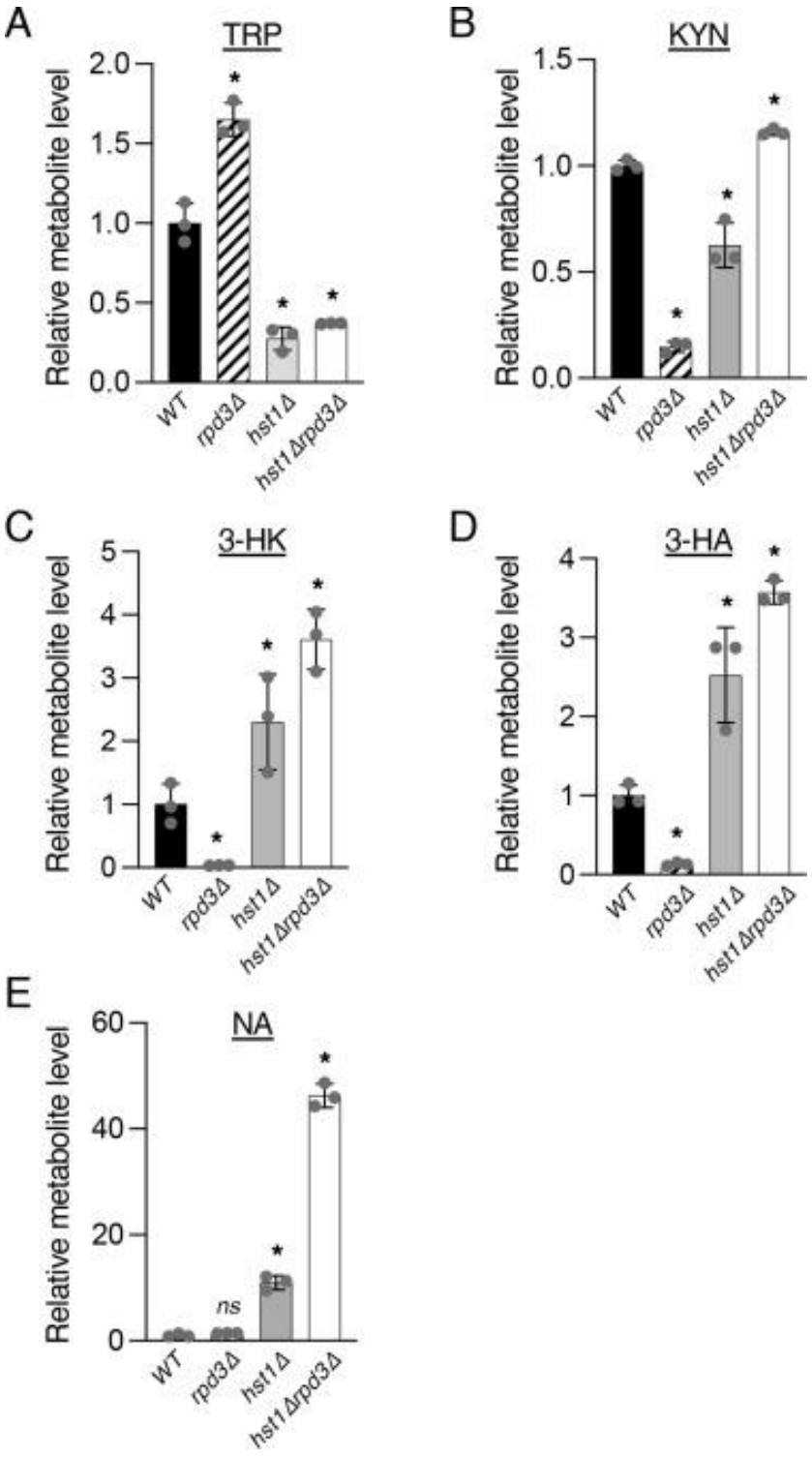
A
TRP
Relative metabolite level
2.0
1.5
1.0
0.5
0.0
*
*
*
WT
rpd3Δ
hst1Δ
hst1Δrpd3Δ
B
KYN
Relative metabolite level
1.5
1.0
0.5
0.0
*
*
*
WT
rpd3Δ
hst1Δ
hst1Δrpd3Δ
C
3-HK
Relative metabolite level
5
4
3
2
1
0
*
*
*
WT
rpd3Δ
hst1Δ
hst1Δrpd3Δ
D
3-HA
Relative metabolite level
4
3
2
1
0
*
*
*
WT
rpd3Δ
hst1Δ
hst1Δrpd3Δ
E
NA
Relative metabolite level
60
40
20
0
ns
*
*
WT
rpd3Δ
hst1Δ
hst1Δrpd3Δ

FIGURE 2-3. Rpd3 and Hst1 regulate homeostasis of *de novo* intermediates.
A, mass spectrometry analysis of TRP levels in *rpd3Δ*, *hst1Δ*, and *hst1Δrpd3Δ* cells. Deletion of *RPD3* leads to accumulation of TRP, while *hst1Δ*, and *hst1Δrpd3Δ* cells show reduced TRP levels.
B, *rpd3Δ* cells exhibit defective KYN production.
C, *rpd3Δ* cells show reduced 3-HK levels, while *hst1Δ* and *hst1Δrpd3Δ* cells show increased 3-HK levels.
D, *rpd3Δ* cells produce reduced levels of 3-HA, while *hst1Δ* and *hst1Δrpd3Δ* cells produce greater levels of 3-HA.
E, deletion of *HST1* and especially deletions of *RPD3* and *HST1* together increase NA levels.

All values for each metabolite are normalized to levels in WT cells. Error bars represent data from three technical replicates. The *p* values are calculated using student's t test (*, $p<0.05$; *ns*, not significant).

FIGURE 2-4

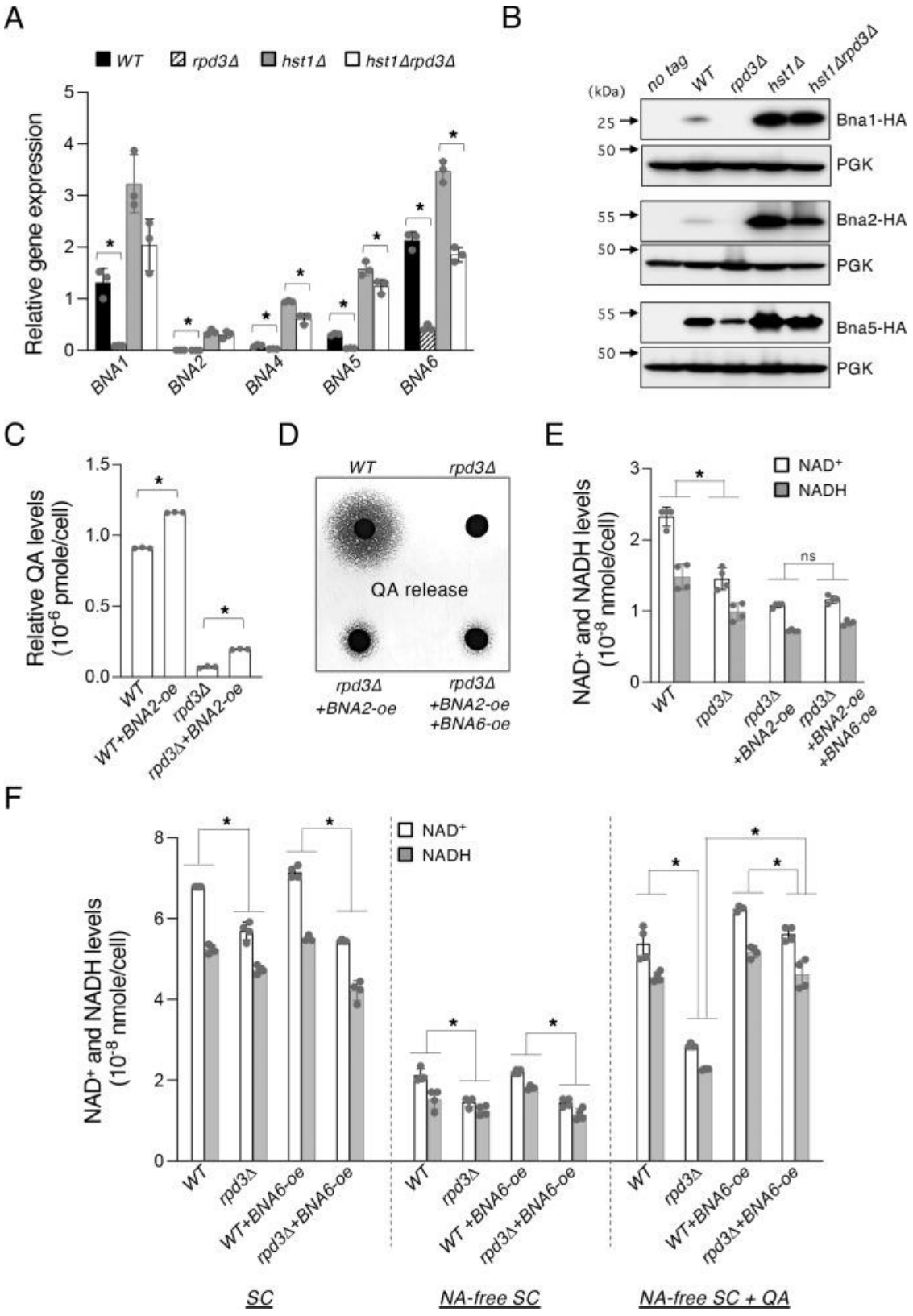
A
WT
rpd3Δ
hst1Δ
hst1Δrpd3Δ
Relative gene expression
BNA1
BNA2
BNA4
BNA5
BNA6
B
(kDa)
no tag
WT
rpd3Δ
hst1Δ
hst1Δrpd3Δ
Bna1-HA
PGK
Bna2-HA
PGK
Bna5-HA
PGK
C
Relative QA levels (10-6 pmole/cell)
WT
WT+BNA2-oe
rpd3Δ
rpd3Δ+BNA2-oe
D
WT
rpd3Δ
QA release
rpd3Δ +BNA2-oe
rpd3Δ +BNA2-oe +BNA6-oe
E
NAD+
NADH
NAD+ and NADH levels (10-8 nmole/cell)
ns
WT
rpd3Δ
rpd3Δ +BNA2-oe
rpd3Δ +BNA2-oe +BNA6-oe
F
NAD+
NADH
NAD+ and NADH levels (10-8 nmole/cell)
WT
rpd3Δ
WT+BNA6-oe
rpd3Δ+BNA6-oe
SC
NA-free SC
NA-free SC + QA

FIGURE 2-4. Rpd3 positively regulates *de novo* NAD^+ metabolism.
A, gene expression qPCR analysis of *BNA* mRNA in WT, *rpd3Δ*, *hst1Δ*, and *hst1Δrpd3Δ* cells. Values shown are relative expression levels normalized to *TAF10* as a control. Deletion of *RPD3* decreases expression of all *BNA* genes shown. *BNA* expression in *hst1Δrpd3Δ* cells is generally increased relative to WT cells and slightly less than levels in *hst1Δ* cells.
B, comparisons of Bna protein expression in HDAC mutants. HA-tagged Bna1, Bna2, and Bna5 proteins were generated in WT, *rpd3Δ, hst1Δ,* and *hst1Δrpd3Δ* cells. Protein expression was determined by Western blot analysis. Arrows make the positions of molecular weight markers.
C, overexpression of *BNA2* (*BNA2-oe*) slightly increases the levels of QA release.
D, *BNA2-oe* increases QA release in *rpd3Δ*, while overexpression of both *BNA2* and *BNA6* in *rpd3Δ* clears accumulated QA.
E, *BNA2-oe* alone or *BNA2-oe* and *BNA6-oe* together is insufficient to raise NAD^+ levels in *rpd3Δ* cells grown in SC. *F*, restoration of *de novo* pathway activity is necessary to rescue NAD^+ levels in *rpd3Δ* cells. NAD^+ levels in *rpd3Δ* cells are increased to WT levels when supplemented with QA (at 10 μM) and with *BNA6-oe*.

For *A*, *C*, *E*, and *F*, the graphs are representative of the trend observed across three independent experiments. For *A* and *C*, error bars represent data from three technical replicates for each strain in an experiment. For *E* and *F*, error bars represent data from two biological replicates each with two technical replicates for each strain in an experiment. The *p* values are calculated using student's t test (*, $p<0.05$; *ns*, not significant).

FIGURE 2-5

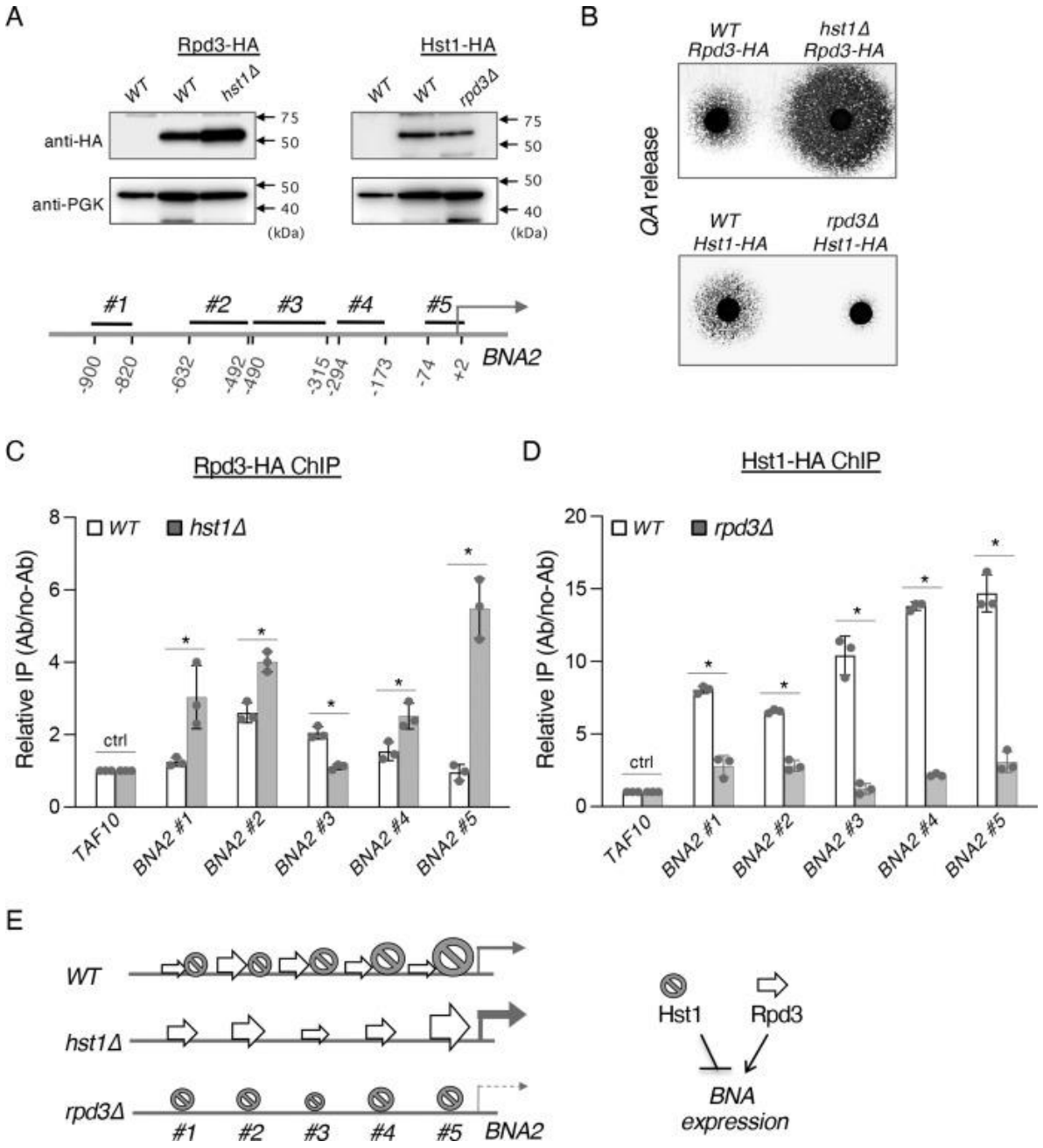
A
Rpd3-HA
Hst1-HA
WT
WT
hst1Δ
WT
WT
rpd3Δ
anti-HA
anti-PGK
75
50
50
40
(kDa)
#1
#2
#3
#4
#5
BNA2
-900
-820
-632
-492
-490
-315
-294
-173
-74
+2
B
WT Rpd3-HA
hst1Δ Rpd3-HA
WT Hst1-HA
rpd3Δ Hst1-HA
QA release
C
Rpd3-HA ChIP
WT
hst1Δ
Relative IP (Ab/no-Ab)
ctrl
TAF10
BNA2 #1
BNA2 #2
BNA2 #3
BNA2 #4
BNA2 #5
D
Hst1-HA ChIP
WT
rpd3Δ
Relative IP (Ab/no-Ab)
E
WT
hst1Δ
rpd3Δ
Hst1
Rpd3
BNA expression

FIGURE 2-5. Analysis of Rpd3 and Hst1 binding to the *BNA2* promoter.
A, design of the ChIP studies. HA-tagged Hst1 was generated in both WT and *rpd3Δ* cells. HA-tagged Rpd3 was generated in both WT and *hst1Δ* cells. Expression was confirmed by Western blot analysis (*top*). BNA2 promoter regions for ChIP studies are shown as *BNA2-#1, #2, #3, #4, and #5* (*bottom*).
B, Confirming the QA cross-feeding phenotypes of HA-tagged strains. Both Rpd3-HA WT and Hst1-HA WT cells show WT levels of QA release. Deletion of *HST1* in Rpd3-HA WT cells increases levels of QA release. Deletion of *RPD3* in Hst1-HA WT cells decreases levels of QA release.
C, ChIP analysis of Rpd3 binding to the *BNA2* promoter. The pattern of Rpd3 binding is altered in *hst1Δ* cells. Binding activity of Rpd3 is most significant near *BNA2-#2* in WT cells, which shifts to *BNA2-#5* in *hst1Δ* cells. Relative IP levels were normalized to *TAF10*.
D, Hst1 binding activity is the highest near the transcription start site (*BNA2-#5*) in an ascending pattern. Hst1 binding activity is decreased when Rpd3 is absent.

For *C* and *D*, the graphs are representative of the trend observed across three independent experiments. Error bars represent data from three technical replicates for each strain in an experiment. The *p* values are calculated using student's t test (*, $p<0.05$; *ns*, not significant). *E*, model of Rpd3 and Hst1 binding to the *BNA2* promoter.

FIGURE 2-6

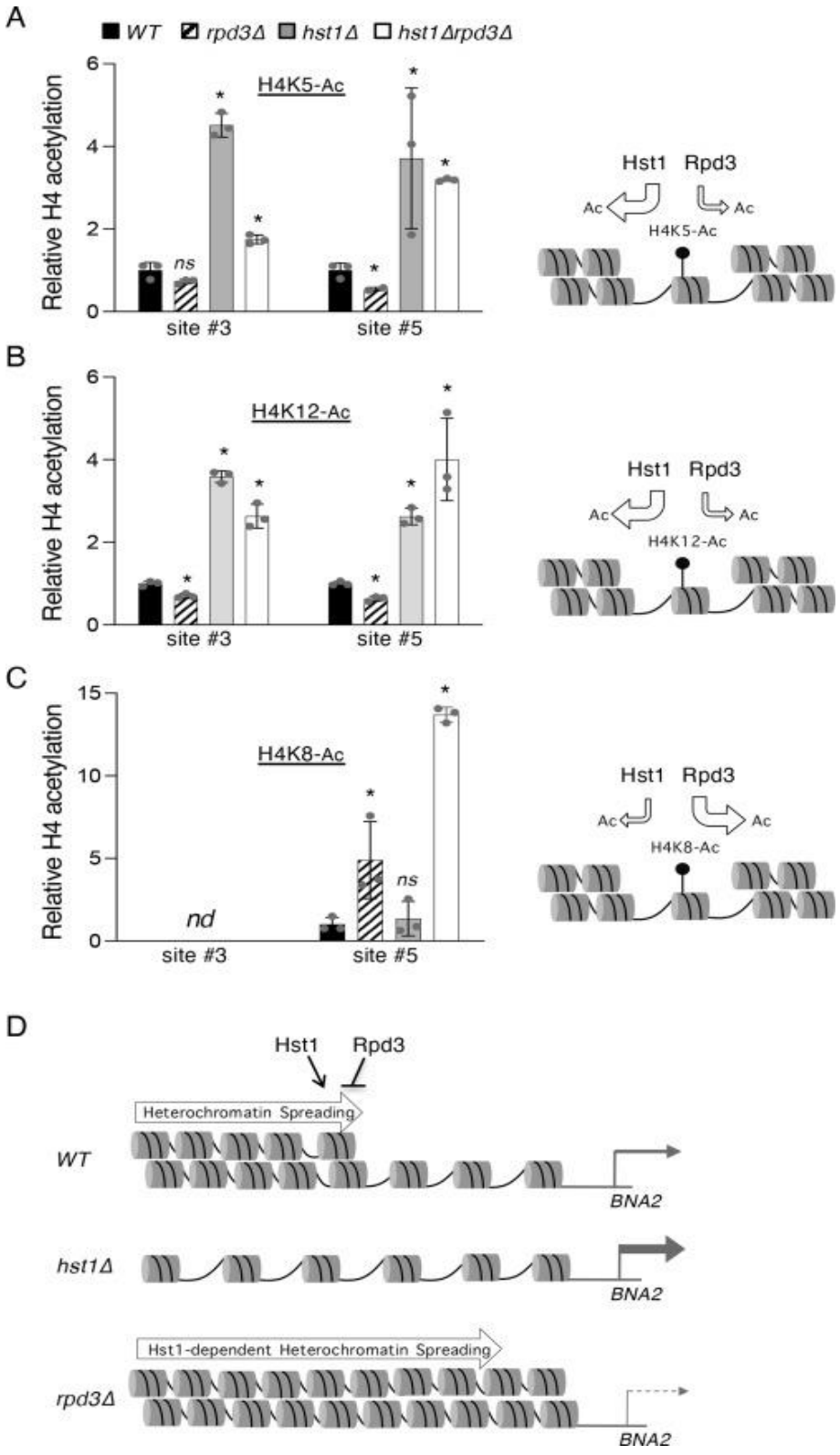
A
WT
rpd3Δ
hst1Δ
hst1Δrpd3Δ
H4K5-Ac
Relative H4 acetylation
ns
site #3
site #5
Hst1
Rpd3
Ac
Ac
H4K5-Ac
B
H4K12-Ac
Relative H4 acetylation
site #3
site #5
Hst1
Rpd3
Ac
Ac
H4K12-Ac
C
H4K8-Ac
Relative H4 acetylation
nd
ns
site #3
site #5
Hst1
Rpd3
Ac
Ac
H4K8-Ac
D
Hst1
Rpd3
Heterochromatin Spreading
WT
BNA2
hst1Δ
BNA2
Hst1-dependent Heterochromatin Spreading
rpd3Δ
BNA2

FIGURE 2-6. Rpd3 and Hst1 have opposing effects on histone H4 acetylation status at the *BNA2* promoter.
A, relative abundance of acetylated H4K5 (H4K5-Ac) at sites #3 and #5, depicted in Figure 5A, of the *BNA2* promoter (*left*). Deletion of RPD3 slightly decreases the amount of H4K5-Ac, while deletion of *HST1* as well as deletions of *RPD3* and *HST1* together increase the level of H4K5-Ac, suggesting that Hst1 is the main deacetylase for this residue (*right*).
B, relative abundance of H4K12-Ac at sites #3 and #5 of the *BNA2* promoter (*left*). *rpd3Δ* cells show reduced acetylation of H4K12, while *hst1Δ* and *hst1Δrpd3Δ* cells show increased acetylation of H4K12, suggesting that Hst1 is primarily responsible for the deacetylation of this residue (*right*).
C, relative abundance of H4K8-Ac at sites #3 and #5 of the *BNA2* promoter (*left*). *rpd3Δ* and *hst1rpd3Δ* cells show increased acetylation of H4K8, while deletion of *HST1* alone does not have a significant influence on H4K8-Ac levels, suggesting that Rpd3 is the main deacetylase for this residue.

Values are relative to levels of H4 protein-bound DNA in each strain and all values are normalized to those of WT cells. The graphs are representative of the trend observed across three independent experiments. Error bars represent data from three technical replicates for each strain in an experiment. The *p* values are calculated using student's t test (*, $p<0.05$; *ns*, not significant; *nd*, not detected).

D, model of *BNA2* expression and putative chromatin structure produced by the effects of Rpd3 and Hst1.

FIGURE 2-7

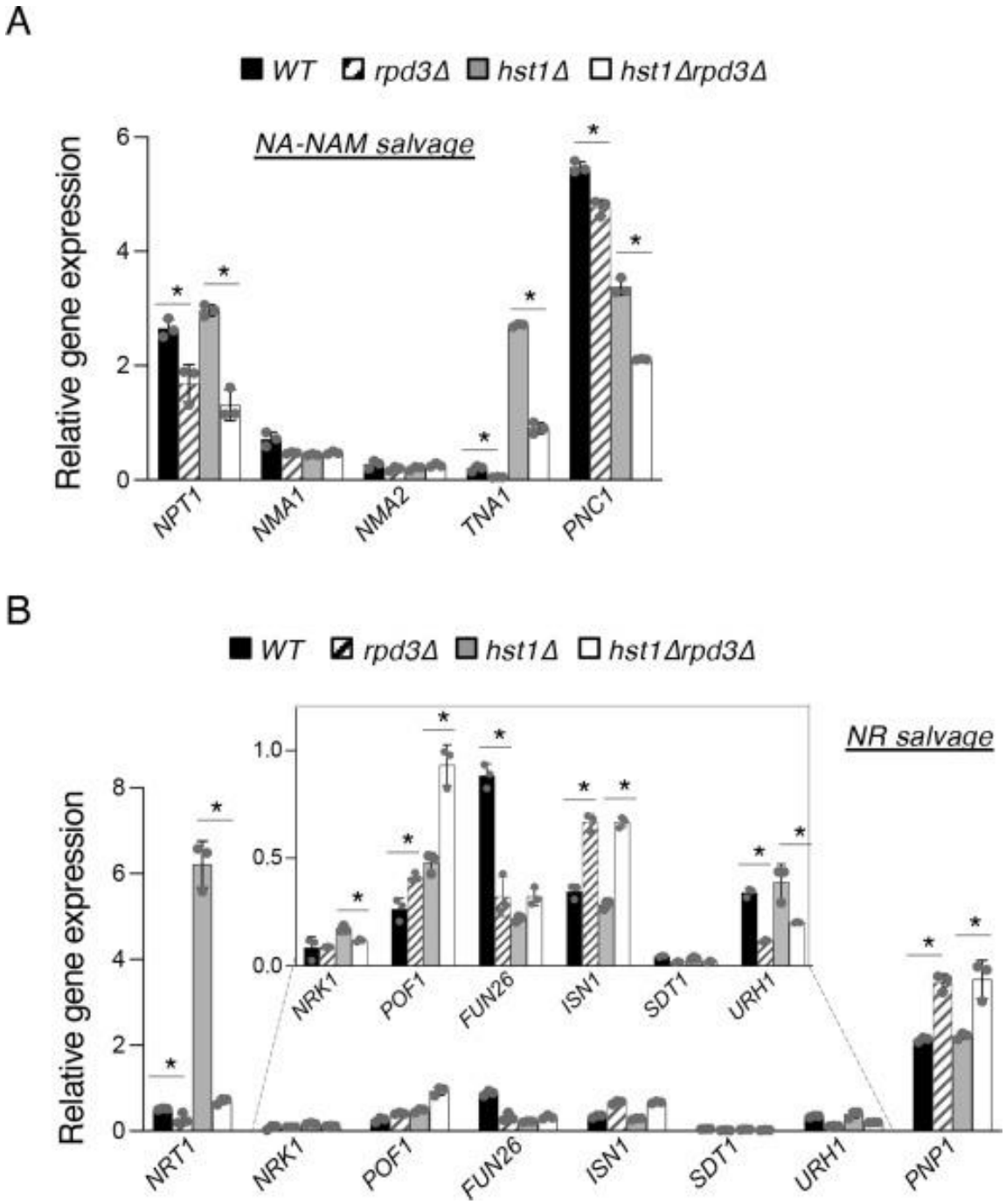
A
WT
rpd3Δ
hst1Δ
hst1Δrpd3Δ
NA-NAM salvage
Relative gene expression
NPT1
NMA1
NMA2
TNA1
PNC1
B
NR salvage
NRT1
NRK1
POF1
FUN26
ISN1
SDT1
URH1
PNP1

FIGURE 2-7. Rpd3 and Hst1 regulate different downstream target genes in NA-NAM and NR salvage pathways.
A, relative expression analysis of the genes of the NA-NAM (*left*) and NR (*right*) salvage pathways in WT, *rpd3Δ*, *hst1Δ*, and *hst1Δrpd3Δ* cells by qPCR.
B, relative expression analysis of the genes of the NR salvage pathway in WT, *rpd3Δ*, *hst1Δ*, and *hst1Δrpd3Δ* cells by qPCR.

All values shown are relative expression levels normalized to *TAF10* as a control. The graphs are representative of the trend observed across three independent experiments. Error bars represent data from three technical replicates for each strain in an experiment. The *p* values are calculated using student's t test (*, $p<0.05$; *ns*, not significant).

CHAPTER 3: The Histone Deacetylases Rpd3 and Hst1 and the Transcription Activator Pho2 Integrate *de novo* NAD^+ Metabolism with Phosphate Sensing in *Saccharomyces cerevisiae*

ABSTRACT

Nicotinamide adenine dinucleotide (NAD^+) is a critical enzymatic cofactor with a wide variety of roles in the cell. The regulation of NAD^+ metabolism and its integration with other aspects of the cellular metabolic network is incompletely elaborated and remains a rich topic for study. The histone deacetylases (HDACs) Hst1 and Rpd3 have previously been identified as engaging in antagonistic regulation of *de novo* NAD^+ metabolism. Hst1 serves as a negative regulator of the *de novo*-mediating *BNA* genes, while Rpd3 serves as a positive regulator. In this work, we show that Hst1 and the large Rpd3 complex (Rpd3L) link the regulation of *de novo* NAD^+ metabolism with certain aspects of the phosphate (Pi)-sensing *PHO* pathway. *De novo* NAD^+ metabolism and the *PHO* pathway have been independently linked to the transcription factor Pho2. We additionally demonstrate that competition for Pho2 usage between the *BNA*-activating Bas1-Pho2 complex and the *PHO*-activating Pho2-Pho4 complex balances *de novo* activity with *PHO* activity, and that the Bas1-Pho2 complex has genetic interactions with Hst1 and Rpd3 with respect to the regulation of the *BNA* genes. Finally, loss of the phosphate transporter Pho84 is shown to modify *de novo* NAD^+ metabolism in the absence of Hst1, in a fashion similar to phosphate depletion. This study helps to clarify the complex linkage between two different aspects of cellular metabolism.

INTRODUCTION

Nicotinamide adenine dinucleotide (NAD^+) is an essential enzymatic cofactor. NAD^+, its reduced form NADH, and the phosphorylated derivative $NADP^+$ serve a wide variety of critical roles in the cell. NAD/H is an oxidative electron acceptor in central metabolism, a source of electrons for mitochondrial respiration (58,264), and a cofactor for the sirtuin class of histone

deacetylases (14-16) and for the poly-ADP-ribose polymerase (PARP) class of DNA repair enzymes (19). Owing to its centrality and far-ranging influence in the cell, perturbations to NAD^+ homeostasis are associated with a considerable and diverse number of diseases, including various metabolic disorders (27), neurological disorders (265), cardiovascular disease (266), and numerous cancers (267-269). Supplementation of NAD^+ precursors has been shown to be efficacious in treating or alleviating symptoms of several diseases (270-272)

Owing to the complex regulatory networks governing the assimilation of these compounds into the cell's NAD^+ pool however, treatment of many disorders involving defective NAD^+ homeostasis is not always straightforward. In addition, NAD^+ precursors may interact with a large variety of signaling pathways in the cell, including diverse types of nutrient sensing as well as inflammation and various other responses to infection (7). As such, it is vital to understand the regulation of NAD^+ metabolism and its interaction with other cellular processes.

Biosynthesis of NAD^+ in budding yeast proceeds through the following pathways: NA-NAM salvage, NR salvage, and *de novo* biosynthesis from L-tryptophan (60). In the first pathway, NAM is deaminated to NA by Pnc1 (71), followed by phosphoribosylation to NaMN by Npt1 (16), adenylation to NaAD by Nma1/Nma2 (72,73), and finally amination to NAD^+ by Qns1 (74). NR salvage may merge with NA-NAM salvage via conversion to NAM by the nucleosidases Urh1 and Pnp1, or by phosphorylation to NMN by Nrk1 (45,76), followed by adenylation to NAD^+ by Pof1 and Nma1/Nma2 (68). *De novo* metabolism is mediated by the *BNA* genes and results in the formation of NaMN, at which point the pathway merges with NA/NAM salvage (Fig. 3-1*A*).

De novo metabolism, in addition to contributing toward the cell's NAD^+ pool, has a complex and reciprocal relationship with other signaling networks in the cell. The flux of

specific *de novo* metabolites, such as kynurenine and 3-hydroxykynurenine, is often affected, and itself in turn affects various signaling events induced by infection, inflammation, and nutrient sensing (7). Budding yeast represents a relatively simpler model in which to investigate the relationship of *de novo* activity with other aspects of NAD^+ biosynthesis and other cellular processes in general. The possibility of cross-talk between *de novo* metabolism and other branches of NAD^+ biosynthesis may be a promising avenue of investigation. The NAD^+-dependent HDAC Hst1, for instance, is itself a regulator of *de novo* NAD^+ biosynthesis (3,78,170), linking *de novo* activity with the status of the cell's NAD^+ pool. Furthermore, NR salvage activity has been seen to be sensitive to levels of the NAD^+ precursor NaMN (5). NR salvage is also mediated by the phosphate (Pi)-sensing PHO pathway targets Pho5 and Pho8, which dephosphorylate NMN to NR likely to replenish the cellular phosphate pool. As a result, NR salvage is strongly induced by phosphate limitation (5). Altogether, these connections invite the question of how different branches of NAD^+ metabolism may be integrated with each other and with other aspects of cellular metabolism.

In previous work, we have identified the histone deacetylase Rpd3 as a positive regulator of *de novo* NAD^+ metabolism, which acts specifically by antagonizing Hst1-dependent repression of the *BNA* genes (3). Rpd3 and Hst1 also appear to co-regulate many other additional NAD^+ metabolic factors, which suggest these two HDACs might co-ordinate *de novo* NAD^+ metabolism with other branches of the NAD^+ metabolic network or with other signaling pathways in the cell. Here we present evidence that the large Rpd3 complex (Rpd3L), Hst1, and the transcription factor Pho2 link the regulation of the *BNA* genes with targets of phosphate signaling and with NR salvage. Specifically, we show that Rpd3L and Hst1 together negatively regulate two cellular phosphatases responsible for the dephosphorylation of NR, *PHO5* and

PHO8, in addition to antagonistically regulating the *BNA* genes. Further, we establish a relationship between Hst1 and the transcription activation complex Bas1-Pho2 in the regulation of the *BNA* genes and identify competition for Pho2 between *PHO* and *BNA* promoters under conditions of phosphate depletion. Bas1-Pho2 is also known to be a sensor and regulator of *de novo* adenine and ATP biosynthesis (184,273), while Pho2-Pho4 is well characterized as a positive regulator of the *PHO* genes that is active under conditions of phosphate limitation (274,275). Lastly, we explore the relationship of the cellular phosphate transporter Pho84 with regulation of *de novo* metabolism. This work contributes to the ongoing elucidation of NAD^+ metabolism, its regulation, and its relationship with other metabolic pathways in the cell.

RESULTS

Rpd3 and Hst1 regulate targets of the *PHO* pathway – Rpd3 and Hst1 have been shown to regulate the *BNA* genes of *de novo* NAD^+ biosynthesis in an antagonistic fashion (3). In addition to this, Rpd3 (276-278) and Hst1 (78) have previously been identified as negative regulators of *PHO* pathway targets, while increased NR production has been shown to correlate with activation of the phosphate (Pi)-sensing *PHO* pathway (5). Moreover, two *PHO*-regulated phosphatases, Pho5 and Pho8, were shown to be able to convert NMN to NR (5,174). This collection of observations suggests that Rpd3 and Hst1 might coordinate *de novo* NAD^+ biosynthesis, Pi-sensing, and NR salvage (Fig. 3-1*B*).

To explore this nexus and to address whether and how Rpd3 and Hst1 interact at the *PHO5* and *PHO8* promoters, we determined the expression of *PHO5* and *PHO8* in cells lacking either or both HDACs. Interestingly, we found that levels of *PHO5* expression in *hst1Δrpd3Δ* cells are strikingly increased compared to WT, *rpd3*Δ, and *hst1*Δ cells, suggesting synergistic regulation of *PHO5* by Hst1 and Rpd3. Moreover, this large increase of *PHO5* expression in *hst1*Δ*rpd3*Δ cells

closely resembles the similarly elevated production of NR (a product of Pho5 activity) earlier observed in this strain (3). On the other hand, although *PHO8* expression was also increased in *rpd3*Δ and *hst1*Δ cells, it was not further increased in the double mutant (Fig. 1*C*). Notably, *rpd3*Δ cells show increased *PHO8* expression despite previous work demonstrating that Rpd3 does not affect the acetylation status of the *PHO8* promoter (279), suggesting an atypical form of regulation by Rpd3 at the *PHO8* promoter. These results are in agreement with previous studies, in which Rpd3 (277) and Hst1 (78) were independently shown to modulate *PHO5* expression. We next directly determined the phosphatase activities of Pho5 (Fig. 3-1*D*) and Pho8 (Fig. 3-1*E*), which also supported the expression results.

The Rpd3L complex is the main positive regulator of *de novo* NAD$^+$ metabolism - The Rpd3 complex exists in two forms, Rpd3L and Rpd3S (220,222,223). While Rpd3 has long been known as a negative regulator of *PHO5* expression (276-278), it was later established that only Rpd3L influences the expression of *PHO5* (280). Therefore, we wished to determine whether Rpd3L also regulates *de novo* NAD$^+$ metabolism. This would address whether Rpd3L HDAC activity does indeed link *de novo* metabolism with NR salvage and phosphate sensing. Since most QA is released into the extracellular environment (78), we determined the level of QA released by *rxt2*Δ and *rco1*Δ cells using a QA cross-feeding plate assay as described previously (3,78). Rxt2 is an essential subunit unique to Rpd3L, responsible for recruitment of Rpd3 to certain promoters via binding to trimethylated H3K4 (230,231).On the other hand, Rco1 is unique to Rpd3S and is required for its recruitment to open reading frames of targets genes via binding to methylated H3K36 (223,226,233). QA release in *rco1*Δ cells is slightly but visibly reduced relative to WT cells, while *rxt2*Δ cells show even greater reduction in released QA, similar to *rpd3Δ* cells. This is expected, as Rpd3 was previously seen to antagonize Hst1 activity in the promoter region of *BNA2*,

while Rpd3L, but not Rpd3S (223,226), is typically recruited to promoters (225,226). We confirmed the QA plate cross-feeding results by determining intra- and extracellular QA in the same strains, revealing that released QA levels are indeed significantly decreased in both *rco1*Δ and *rxt2*Δ cells (Figure 3-2*B*). *rxt2*Δ cells show less QA release compared to *rco1*Δ cells, but more than *rpd3Δ* cells. Interestingly however, the decrease in intracellular QA observed in *rco1*Δ cells is slightly stronger than that observed for *rxt2*Δ cells. Altogether, these results suggest that while Rpd3L is the primary form of Rpd3 active as a positive regulator of the *BNA* genes, Rpd3S also appears to have a significant role in the same capacity.

To explore this hypothesis, we then determined the influence of each complex on *BNA* expression and found that both Rpd3L and Rpd3S seem to be significant as activators of *BNA* expression (Fig. 3-2*C*). Similar to the case of *PHO5*, Rpd3L appears to be the main regulator of the *de novo* pathway. Notably, the relative influence of each seems to vary at each of the *BNA* genes, with *rxt2*Δ cells clearly showing greater reduction in expression of *BNA2*, *BNA4*, and *BNA5*. The stronger reduction in QA release observed in *rxt2*Δ cells is likely due to the fact that Rpd3L appears to be the main regulator of most *BNA* genes, and specifically of *BNA2*, which is the rate limiting step of the *de novo* pathway (78). Finally, we examined the influence of Rpd3L and Rpd3S on NAD^+ production to determine the degree to which each complex is responsible for the decreased NAD^+ levels observed in *rpd3*Δ cells. NAD^+ levels were measured in SC medium without NA, in order to reduce NA/NAM salvage activity and focus on the contribution of *de novo* activity to the cellular NAD^+ pool. We saw both *rxt2*Δ cells and *rco1*Δ cells to exhibit significant reduction in NAD^+ levels (Fig. 3-2*D*), confirming the importance of both as activators of the *de novo* pathway.

The Bas1-Pho2 complex interacts with Rpd3 and Hst1 - Having identified Rpd3 and Hst1 as regulators shared between the *PHO* genes, NR salvage, and *de novo* NAD^+ metabolism, we further investigated the interconnections between these pathways. First, we sought to determine the effect of Pi depletion on *BNA* expression. However, this question is difficult to address directly. Given that Pi depletion decreases cellular ATP levels (281), while ATP depletion itself leads to NAD^+ depletion (59), we would expect extended Pi-depletion to cause a corresponding drop in NAD^+ levels. This would have the ultimate indirect consequence of limiting NAD^+-dependent Hst1 activity and inducing *BNA* expression (Fig. 3-3*A*), as Hst1 is a critical negative regulator of *BNA* expression (78,170). Owing to these considerations, we attempted to identify a time window that would preserve the cellular NAD^+ pool while also sufficiently inducing *PHO* signaling. We found that, soon after transfer to Pi-depleted (low-Pi) medium, cellular NAD^+ levels significantly dropped (Fig. 3-3*B*). Interestingly, one of the first evident changes upon Pi depletion was a redox imbalance between NADH/NAD^+ (~5 min), with the ratio quickly rising and then leveling out over time. Since NAD^+ depletion appears to be an inevitable confounding factor of Pi limitation, we employed the *hst1*Δ mutant in our studies of phosphate depletion, which is not expected to be sensitive to changes in NAD^+ levels with respect to the regulation of *BNA* expression. In addition, we also sought to determine how the transcription factor Pho2, shared between two complexes formed with the *de novo*-activating Bas1 and the *PHO*-activating Pho4, might serve to integrate *de novo* NAD^+ metabolism and *PHO* signaling, alongside the aforementioned regulators (Fig. 3-3*C*). It has been shown that *ade16*Δ*ade17*Δ mutants, which are genetic mimics of adenine depletion, also have increased *BNA* expression through a mechanism in parallel to Hst1 (Fig. 3-3*C*) (59). In these cells, activation of *BNA* expression is mediated by a specific transcription complex Bas1-Pho2 stimulated by an adenine intermediate (5′-phosphoribosyl-5-amino-4-

imidazole carboxamide monophosphate, ZMP) that they accumulate (59). Although the primary function of Bas1-Pho2 complex is to activate genes for *de novo* adenine synthesis, they also activate *BNA* genes during adenine depletion or when cells accumulate ZMP metabolites (59). Therefore, we also deleted *ADE16* and *ADE17* in the *hst1*Δ background in order to induce *BNA* expression by this ZMP-Bas1-Pho2-dependent mechanism. As shown in Fig. 3-3*D*, expression of most *BNA* genes was already slightly but significantly reduced by Pi-depletion in *hst1*Δ cells, with the exception of *BNA6*. Expression of *PHO5* was included as a positive control of *PHO* activation. Interestingly, expression of *BNA2* and *BNA6* was further increased in the *hst1*Δ*ade16*Δ*ade17*Δ triple mutant (Fig. 3-3*D*). In addition, in this background we were able to observe that all *BNA* genes are sensitive to Pi-limitation, which reduces *BNA* gene expression. Lastly, the *hst1*Δ*ade16*Δ*ade17*Δ triple mutant also shows higher *BNA* expression relative to the *hst1*Δ mutant, suggesting that the mechanism of Bas1-Pho2-dependent *BNA* activation is at least partially independent of Hst1. These results also demonstrate an inverse correlation of *BNA* and *PHO* gene expression during Pi-limitation (Fig. 3-3*D*). Activation of *PHO* downstream genes is mediated by the Pho2-Pho4 transcription complex (Fig. 3-3*C*). Notably, the adenine precursor ZMP has also been shown to activate Pho2-Pho4 complex formation (184). Hence, our results suggest that Pho2 may be a limiting factor shared between the Bas1-Pho2 and Pho2-Pho4 complexes. Competition for limiting reserves of Pho2 may become particularly acute under conditions of ZMP accumulation (seen in the *ade16*Δ*ade17*Δ mutant (59)), which promotes the formation of both complexes (Fig. 3-3*C*). Indeed, competition between the two complexes has been suggested previously for the regulation of *PHO* genes and adenine biosynthesis *ADE* genes (184).

To test this model, we asked whether deleting *BAS1* would be sufficient to decrease *BNA* gene expression without Pi limitation. We found that *BAS1* deletion had no significant effect on *BNA*

expression in the WT background except for *BNA6* (Fig. 3-3*E*). We also examined *hst1*Δ cells, in which all *BNA* genes are de-repressed. As shown in Figure 3-3*E*, *BAS1* deletion reduced the expression of all *BNA* genes in *hst1*Δ cells. This suggests that the Bas1-Pho2 complex may only have a significant role as an activator of *BNA* expression under inducing conditions, whether due to ZMP accumulation or, as here, due to loss of Hst1 activity. However, it should be considered that deletion of *BAS1* causes a significant reduction in cellular ATP levels (282,283), which would be likely to reduce NAD^+ production downstream (59). Therefore, *BNA* expression in *bas1*Δ cells may be confounded by reduction or partial loss of Hst1 activity, masking the potential effect of Bas1 itself, which might only become evident in the *hst1*Δ background. Moreover, *hst1*Δ*bas1Δ* cells also showed a notable increase in *PHO5* and *PHO8* expression (Fig. 3-3*E*), lending support to the model that Bas1 and Pho4 are in competition for limiting reserves of Pho2 (Figure 3-3*C*). These studies also firmly indicate that Bas1/Pho2 is required for optimal *BNA* expression in *hst1*Δ cells even under adenine replete conditions.

Having observed a genetic interaction between the *hst1*Δ mutant and the *ade16*Δ*ade17*Δ (Fig. 3-3*D*) and *bas1*Δ mutants (Fig. 3-3*E*), we then examined whether Rpd3 also played a role in this context. Since Rpd3 antagonizes Hst1-mediated repression and promotes *BNA* expression, we examined whether Rpd3 was required for Bas1-Pho2 mediated activation of *BNA* expression in *ade16*Δ*ade17*Δ cells. As shown in Figure 3-3*F*, when we compared the *ade16*Δ*ade17*Δ and *rpd3*Δ*ade16*Δ*ade17*Δ mutants, *RPD3* deletion significantly reduced *BNA* expression in *ade16*Δ*ade17*Δ cells. Rpd3 may allow for improved recruitment of Bas1-Pho2 by preventing the spreading of repressive chromatin structure established by Hst1 (3). However, the *rpd3*Δ*ade16*Δ*ade17*Δ mutant still expressed most *BNA* genes to a level higher than that of *rpd3*Δ

cells, suggesting that the direct mechanism of Bas1-Pho2 recruitment might function independently of Rpd3.

ZMP induction alters cellular NR metabolism - Having observed significant decreases in *BNA* expression when *BAS1* is deleted in an *hst1*Δ background, we sought to investigate what effect the loss of Bas1 might have on QA production. Interestingly, *BAS1* deletion did not appear to decrease QA levels in either *WT* or *hst1*Δ cells (Figure 3-4*A*). It is likely that in *bas1*Δ cells, a small decrease in QA production may be masked by its decreased *BNA6* expression (Figure 3-3*E*), which is expected to cause QA accumulation (Figure 3-1*A*).

The QA production studies further support a role for Rpd3 as a positive regulator of *BNA* expression that is of primary significance, as suggested earlier (3). As shown in Fig. 3-4*B*, the *rpd3*Δ*ade16*Δ*ade17*Δ mutant did not release detectable QA, and displayed a similar phenotype observed in the *rpd3*Δ mutant (Fig. 3-2*A*). Surprisingly, although the *ade16*Δ*ade17*Δ mutant showed elevated *BNA* expression, these cells appeared to release less QA (Figure 3-4*B*). It is possible that a portion of produced QA is assimilated into NAD^+ due to especially high *BNA6* expression in these cells (Fig. 3-3*E*). In addition, unlike other *BNA* genes, *BNA1* expression was not increased in *ade16Δade17Δ* cells (Figure 3-3*F*), which may also contribute to observed lower QA levels (Fig. 3-4*B*). These results also suggest some *BNA* genes may be independently regulated by different mechanisms. Notably, although the *ade16*Δ*ade17*Δ mutant was shown to have increased levels of *BNA* expression and *de novo* pathway metabolites, it did not show increased NAD^+ levels (59). Therefore, we further examined whether other branches of NAD^+ metabolism are also affected in the *ade16*Δ*ade17*Δ mutant. Since *PHO* signaling is activated in this mutant, we examined whether it also produced more NR, as observed in *rpd3*Δ cells. We found that although the *ade16*Δ*ade17*Δ mutant did not appear to release more NR (Fig. 3-4*C*), its intracellular

NR was significantly increased (Fig. 3-4*D*). Direct Pi-depletion, which has previously been shown to induce NR production (5), caused comparatively greater NR production in WT cells as opposed to deletion of *ADE16* and *ADE17* (Fig. 3-4*D*). This is expected, as ZMP accumulation by itself (observed in the *ade16*Δ*ade17*Δ background) is predicted to be one of the many downstream consequences of Pi depletion. Moreover, the *ade16*Δ*ade17*Δ cells also showed increased intracellular NA-NAM levels (Figure 3-4*E*). This could be due to increased NR flow into the NA-NAM salvage pathway combined with a blockage in NA-NAM metabolism. To test this, we examined the expression of genes involved in NA (*NPT1*) and NAM (*PNC1*) metabolism. Moreover, higher intracellular NR and NA-NAM could also be due to increased import of these precursors, especially considering the quantities of these metabolites released extracellularly are not visibly increased. Therefore, expression of *TNA1* (NA and QA transporter), *NRT1* (NR transporter), and *FUN26* (vacuolar NR transporter) was also studied. As shown in Figure 3-4*F*, expression of *PNC1* was significantly reduced in *ade16*Δ*ade17*Δ cells while expression of the other genes was not significantly altered. Overall, our results showed that both increased NR production and a blockage in the conversion of NAM to NA (reduced *PNC1* expression) were observed in *ade16*Δ*ade17*Δ cells. Increased *PHO* signaling activity likely contributes to NR production (5), however, it remains unclear how *PNC1* expression is altered in *ade17*Δ*ade17*Δ cells.

Phosphate transport via Pho84 affects homeostasis of NAD^+ precursors - Rpd3 appears to be an important regulator in the recycling of cellular transporters, with several recycling factors being aberrantly expressed in *rpd3*Δ cells (249). It has also been shown that deletion of *RPD3* causes issues with the activity and localization of the cellular phosphate transporter Pho84, possibly due to this same recycling defect, ultimately leading to reduced uptake and storage of phosphate in

*rpd3*Δ cells (277). This leads to the further consequence of *PHO5* induction, independently of and additional to the baseline amount caused by *rpd3*Δ *per se*. For this reason, *rpd3*Δ cells also show increased induction of the *PHO* targets *PHO81*, *PHO84*, and *PHO86* under low Pi conditions, none of which are affected by the deletion of *RPD3* under standard, phosphate replete conditions (277). As these marked defects in Pho84 activity are downstream of *RPD3* deletion, loss of Pi transport may be an indirect contributor to the influence of Rpd3 upon *BNA* expression. In addition, having seen that Pi depletion may alter *de novo* NAD^+ metabolism (Figure 3-3*D*), the study of Pho84 may also provide an opportunity to confirm the connection between *BNA* and *PHO* regulation noted above. Therefore, we sought to investigate the possibility of a relationship between Pho84, Pi transport, and *de novo* metabolism.

As deletion of *PHO84* causes reduced intake and accumulation of Pi (284,285), we sought to investigate the effect of *PHO84* deletion on QA production in WT and *hst1*Δ cells. As opposed to the acute depletion of intracellular Pi and induction of *PHO* expression by transferring cells to low-Pi medium, *pho84*Δ cells may serve as a model of chronically reduced Pi levels. We found that deletion of *PHO84* slightly, but visibly, reduces QA release in WT and *hst1*Δ backgrounds (Fig. 3-5*A*). In the latter case, this may partly be due to competition between Bas1-Pho2 and Pho2-Pho4 caused by *PHO* activation, limiting the amount of Pho2 available for *BNA* induction. However, the decrease in QA release observed here exceeds that observed for full *BAS1* deletion (Fig. 3-4*A*), suggesting that other factors may be involved. We also examined the possibility that *PHO84* deletion and *PHO* pathway activation might cause increased NR production in *hst1*Δ cells, on an order comparable to the effect previously noted in WT cells (5). We saw that this indeed appeared to be the case, with *hst1*Δ*pho84*Δ cells showing increased release relative to *hst1*Δ cells, of a magnitude similar to the difference observed between WT and

*pho84*Δ cells (Fig. 3-5*B*). This suggests that the relationship between Pi sensing, *PHO* activation, and NR metabolism remains largely undisturbed in *hst1*Δ cells.

We expect that the above results are at least partially explained by the sequence of events described by Figure 3-3*A*: reduction of cellular Pi pools lowers ATP levels, which in turn depletes NAD^+. Pi depletion *per se* would cause *PHO* induction and increased NR production via Pho5 and Pho8. However, the predicted reduction of cellular NAD^+ levels would be anticipated to reduce Hst1 activity and thereby cause greater *de novo* activation and QA release in the NAD^+-sensitive WT background. This suggests that another factor might be involved that overrides the effect of reduced Hst1 activity. Alternatively, *pho84*Δ cells grow markedly more slowly than WT cells (data not shown); this alone is a likely explanation for the minor decrease of QA release caused by *PHO84* deletion in the WT and *hst1*Δ background.

To verify that the NAD^+ pool is indeed depleted by *PHO84* deletion, we measured NAD^+ levels in medium lacking NA (in which NAD^+ is derived mostly from *de novo* activity) (Fig. 3-5*C*) and standard SC medium (Fig. 3-5*D*). We found that NAD^+ levels are significantly reduced in both medium types, and particularly the latter. Most likely, this is primarily due to limitation of ATP available for the reactions catalyzed by Npt1 and Nma1/Nma2 (59). This suggests that *PHO84* deletion and Pi limitation indeed has a significant influence on Hst1 activity via reduction of NAD^+ levels. However, this effect is not strong enough to cause visible increases in QA release (Fig. 3-5*A*), nor does deletion of *HST1* have a significant influence on the relationship between *PHO* activation and NR metabolism (Fig. 3-5*B*), suggesting that the effect is largely independent of Hst1-dependent *PHO* repression (Fig. 3-1B) (78). Moreover, examination of NAD^+ levels in *pho84*Δ cells serves as an independent confirmation of the results shown in Fig. 3*B* and vindicates the use of *hst1*Δ cells to investigate the effect of low Pi on *BNA*

expression phenotypes: depletion of Pi leads to a decline in NAD^+ levels that is ultimately quite significant, causing conflicting adjustments to *BNA* regulation that involve, at minimum, alterations of Hst1 and Pho2 activity. Altogether, the effect that phosphate transport and storage exerts on *de novo* regulation is complex and multifaceted.

Lastly, the use of *PHO84* deletion affords us an opportunity to further solidify the competitive model elaborated above (Figure 3-3*C*) and may also serve as a model of chronic reduction of Pi levels, as opposed to acute depletion resulting from short periods of growth in low-Pi medium. If *PHO84* deletion and downstream *PHO* induction truly reduce *BNA* expression via competition for Pho2 between Bas1 and Pho4, then this effect should only be apparent in the *hst1*Δ background, as Bas1-Pho2 does not appear to be important for *BNA* expression under standard conditions (Fig. 3-3*E*). Consistent with this expectation, we saw almost no significant differences in *BNA* expression between WT and *pho84*Δ cells, while *BNA* expression was slightly but consistently reduced in *hst1*Δ*pho84*Δ cells compared to *hst1*Δ cells (Fig. 3-5*E*), closely resembling the differences observed by Pi depletion from the growth medium (Fig. 3-3*D*). However, it should again be noted that the reduction of ATP levels in *bas1*Δ cells (282,283) and of NAD^+ levels in *pho84*Δ cells (Fig. 3-5*D*) may complicate straightforward investigation of this model in non-*hst1*Δ backgrounds.

DISCUSSION

Rpd3 and Hst1 appear to play a role in co-regulating Pi-sensing *PHO* signaling and *de novo* NAD^+ metabolism (Fig. 3-6). Together with their antagonistic regulation of *de novo* metabolism (3), the two appear to employ a different mode of regulation at the *PHO5* and *PHO8* promoters, with both serving as negative regulators in this latter case (Figure 3-1*B*). The large Rpd3 complex, Rpd3L, appears to be specifically responsible for this link. As opposed to Rpd3S, it is the primary

regulator of both *PHO5* (280) and *BNA* expression (Fig. 3-2*C*), which is affected much more consistently and strongly by deletion of the Rpd3L subunit *RXT2* versus deletion of the Rpd3S subunit *RCO1*. However, Rpd3S does appear to assist Rpd3L in the positive regulation of *BNA* expression, though to a lesser degree. This invites the question of the nature of the coordination between the two complexes, their overlapping roles, and their mechanistic activities. It is typical for Rpd3L activity to be confined to the promoter region of target genes (225,226), while Rpd3S is generally active within the open-reading frame of its targets (223,226). It remains to understand how each of the two complexes contributes to the promotion of *BNA* and *PHO* expression.

Two transcription complexes, Pho2-Pho4 and Bas1-Pho2, are also active in this connection. The Pho2-Pho4 complex has long been known as an activator of *PHO* pathway targets (284,286,287), while the Bas1-Pho2 complex was recently identified as a positive regulator of *BNA* expression (59) (Fig. 3-6). In addition, the formation of both complexes is responsive to ZMP accumulation under conditions of ATP depletion and in the *ade16*Δ*ade17*Δ mutant (59,184). The sharing of Pho2 between these complexes provides an opportunity for coordination between *de novo* NAD^+ synthesis and *PHO* signaling pathways, considering that Pi depletion is also associated with reduction of cellular ATP levels (281) and NAD^+ levels (Fig. 3-3*B*). To study the specific effect of Pi-depletion on *BNA* expression independent of NAD^+ levels, we employed the *hst1*Δ mutant and showed that Pi-depletion in fact limits *BNA* expression in *hst1*Δ cells (Fig. 3-3*D*). These results indicate some degree of competition between Bas1 and Pho4 for binding to Pho2, which has also been suggested to occur between the *ADE* and *PHO* genes (184). The ultimate consequence of this would be two competing signals induced by low-Pi: low NAD^+ and ATP promotes *BNA* activation via loss of Hst1 activity and Bas1-Pho2 complex formation, respectively, while *PHO* activation limits *BNA* expression (Fig. 3-6). This

effect indeed becomes even more pronounced under conditions of ZMP accumulation in *hst1*Δ*ade16*Δ*ade17*Δ cells. Supporting this model, we showed that deleting *BAS1* indeed reduces *BNA* expression with a concomitant increase in *PHO* gene expression in *hst1*Δ cells (Fig. 3-3*E*). On the other hand, deletion of *BAS1* alone does not significantly alter *BNA* expression. It appears that the Bas1-Pho2 complex is not significant as a regulator of *BNA* expression under standard conditions, but that it is necessary for full *BNA* induction under inducing conditions, whether this be loss of Hst1 silencing activity or ZMP accumulation. As noted previously, however, the low ATP levels seen in *bas1*Δ cells (282,283) may cause declines in NAD^+ production and loss of Hst1 activity, confounding straightforward investigation of *BAS1* deletion in the WT background.

Indeed, a low level of ATP would generally be anticipated to cause NAD^+ depletion (59). As a sirtuin, Hst1 activity is limited by low NAD^+, resulting in de-repression of both the *BNA* genes and the *PHO* pathway (Fig. 3-6). Owing to these relationships, *PHO* gene expression is predicted to be activated in low Pi conditions not only by the main mechanism of Pho4 translocation to the nucleus, but also indirectly by reduction of ATP and NAD^+ levels under low Pi conditions (Fig. 3-3*A*). ATP limitation would cause increased production of ZMP, promoting Pho2-Pho4 complex formation, while NAD^+ depletion would limit negative regulation by Hst1. This series of events ultimately serves to strongly activate *PHO* targets, one result of which is the increased production of NR (Fig. 3-4*D*, Fig. 3-6). The *ade16Δade17Δ* cells also show reduced *PNC1* expression (Fig. 3-4*F*) and, consequently, NAM accumulation (Fig. 3-4*E*). It was shown previously that making NAD^+ from NA-NAM salvage requires more ATP than from the *de novo* pathway (59). Therefore, reduced *PNC1* expression may help decrease NA-NAM salvage activity to preserve ATP for other cellular functions. Increased NAM may also help de-repress

BNA genes to facilitate *de novo* NAD^+ synthesis. On the other hand, Rpd3 serves as an epigenetic regulator in this metabolic network independent of NAD^+ levels. This helps ensure that *PHO* activity and NR salvage remain controlled even when levels of NAD^+ are low. For example, in the case of *PHO5* expression and NR production, the removal of both Hst1 and Rpd3 leads to synergistically increased activity, which may be detrimental to cells. However, Rpd3 is required not only as a *PHO* repressor, but also seems to be required for full induction of *PHO5* (220,276), highlighting the intricate role of Rpd3 as a both a positive and negative epigenetic regulator depending on the context. As noted above, Rpd3 acts as a positive regulator of the *BNA* genes, as well as of the NR transporter *NRT1* and the NA/QA transporter *TNA1*, all of which are induced in *hst1Δ* or by limitation of NAD^+ (78). Interestingly, Nrt1 has also been shown to be a transporter of the ZMP precursor 5-Aminoimidazole-4-carboxamide-1-β-d-ribofuranoside (AICAR) (288). Collectively these results provide a model connecting *de novo* *BNA* expression, *PHO* signaling, and NR salvage.

As anticipated from the preceding relationship, the phosphate transporter Pho84 also appears to have a significant influence on regulation of *de novo* NAD^+ metabolism. It is likely that this primarily proceeds through the model outlined, as loss of *PHO84* is associated with reduced accumulation of Pi (285) and high levels of *PHO* induction (Fig. 3-5*E*) (289). As above, the relationship is likely twofold: loss of Hst1 activity due to decreased NAD^+ production and decreased availability of Pho2 via its increased recruitment into the *PHO*-activating Pho2-Pho4 complex. These two influences are predicted to have opposite effects on *BNA* expression, and the effect of reduced Hst1 activity would be predicted to predominate based on its significant control of BNA expression (3,78,170) relative to the more minor effect exerted by Bas1-Pho2 (59) (Fig. 3-3*E*; Fig. 3-4*A*). However, *pho84*Δ cells show almost no changes in *BNA* expression relative to

WT cells (Fig. 3-5*E*), suggesting that the two influences may be more balanced in degree. This could possibly be due to incomplete limitation of Hst1 activity at intermediate intracellular NAD^+ concentrations, or alternatively due to particular adaptations to chronically low Pi in *pho84*Δ cells (Fig. 3-5*D*).

In addition, the effect of Rpd3 on the transport of Pi via Pho84 cycling is a topic in need of further investigation. Having established the close relationship of both Pi-sensing and Rpd3 with the regulation of *de novo* metabolism, the two may interact in a variety of ways to influence the ultimate status of *BNA* gene expression. For instance, *rpd3*Δ cells are known to accumulate less Pi due to defective recycling of Pho84; this causes significant amounts of *PHO* induction independently of Rpd3 activity at *PHO* promoters (277), meaning that Pho4 might bind and sequester some amount of Pho2 away from Bas1, thereby indirectly reducing *BNA* expression. Although this effect is expected to be minor in comparison with the effect of Rpd3 as an epigenetic regulator of *BNA* expression *per se*, it provides a hint of the complexity involved in joining *de novo* NAD^+ metabolism, Pi-sensing, and NR salvage. Moreover, Pho84 recycling defects in *rpd3*Δ cells may partially explain the low NAD^+ phenotype of *rpd3*Δ cells in standard and -NA medium (3).

In summary, Rpd3, Hst1, and Pho2 appear to integrate the regulation of several disparate branches of NAD^+ metabolism, and their activities and targets also provide links to Pi sensing, purine metabolism, ATP production, and the overall status of the cell's NAD^+ pool. This set of regulators therefore helps to coordinate a variety of interrelated metabolic signals in budding yeast. Further work will be required to explore the mechanistic interactions among these regulators and to establish the means by which they compete and cooperate to influence the cellular pools of NAD^+ and its precursors. Altogether, this work contributes to the elaboration of

the relations by which NAD^+ metabolism is governed and helps to connect different branches of NAD^+ metabolism among each other and with other signaling networks in the cell.

EXPERIMENTAL PROCEDURES

Yeast strains, growth media, and plasmids – Yeast strain BY4742 *MATα his3Δ1 leu2Δ0 lys2Δ0 ura3Δ0* acquired from Open Biosystems (257) was used as the parental WT strain for this study. Standard growth media including synthetic minimal (SD), synthetic complete (SC), and yeast extract/peptone/dextrose (YPD) rich media were made as described (258). Special NA-free SD and NA-free SC were made by using niacin-free yeast nitrogen base acquired from Sunrise Science Products. Low phosphate (Low-Pi) medium was prepared by phosphate precipitation from SC as previously described (5). In brief, for each liter of Low-Pi SC medium, 2.46 g of $MgSO_4$ were first dissolved in SC. 8 ml of concentrated ammonia was then slowly added with gentle stirring to precipitate inorganic phosphate as $MgNH_4PO_4$. After filtration, the clear solution was adjusted to pH 6 with HCl and subjected to autoclave. Gene deletions were carried out by replacing the coding regions of WT genes with gene-specific PCR products generated using either the p*AG32-hphMX4* (2) or the reusable *loxP-kanMX-loxP* (pUG6) (1) cassettes as templates. Multiple gene deletions employed a galactose-inducible Cre recombinase to remove the *loxP-kanMX-loxP* cassette, followed by another round of gene deletion (1).

Quantitative PCR (qPCR) quantitation of gene expression – Approximately 40 A_{600} unit cells grown to early-logarithmic phase in SD (6 hr growth from A_{600} of 0.1) were collected by centrifugation. Total RNA was isolated using GeneJET RNA purification Kit (Thermo Scientific) and cDNA was synthesized using QuantiTect Reverse Transcription kit (Qiagen) according to the manufacturer's instructions. For each qPCR reaction, 50 ng of cDNA and 500 nM of each primer were used. qPCR reaction was run on Roche LightCycler 480 using

LightCycler 480 SYBR green I Master Mix (Roche) as previously described (68). Average size of the amplicon for each gene was ~ 150 bp. The target mRNA transcript levels were normalized to *TAF10* transcript levels.

Repressible acid phosphatase (rAPase) activity and alkaline phosphatase (rALPase) assays - The *rAPase* liquid assay was carried out as described (290) with modifications. In brief, about 2.5 A_{600} unit cells grown in SC for 6 hours were collected, washed, and resuspended in 150 μl sterile water. Next, 600 μl of substrate solution (5.6 mg/ml *p*-nitrophenylphosphate, pNPP, in 0.1 M sodium acetate, pH 4) was added to cell suspension, and the mixture was incubated at 30°C for 15 min. The reaction was stopped by adding 600 μl ice-cold 10% trichloroacetic acid. 600 μl of this final mixture was then added to 600 μl saturated Na_2CO_3 to allow color (neon yellow) development. Cells were pelleted to acquire the supernatant for A_{420} determination. The *rAPase* activities were determined by normalizing A_{420} readings of colorimetric phosphatase product *p*-nitrophenol (pNP) to total cell number (A_{600}). The cell extract-based *rALPase* activity assay was carried out as previously described (291) with modifications. About 2.5 A_{600} units of cells grown in SC for 6 hours were collected, washed in 0.85% NaCl with 1 mM PMSF as described (291). The resultant cell pellet was then resuspended in 600 μl lysis buffer (20 mM PIPES, 0.5 %, Triton X-100, 50 mM KCl, 100 mM potassium acetate, 10 mM $MgSO_4$, 10 μM $ZnSO_4$, 1 mM PMSF) followed by bead-beating. Cell lysates were then centrifuged at 13,200 rpm for 5 min at 4˚C to collect supernatant. 200 μl supernatant was added to 300 μl reaction buffer (333 mM Tris-HCl, pH 8.5, 0.53 % Triton X-100, 133 mM $MgSO_4$, 13.3 μM $ZnSO_4$, w/wo 1.66 mM pNPP) and then incubated at 37˚C for 20 min. Reactions were stopped by adding 500 μl stop buffer (1 M glycine/KOH, pH 11.0). Supernatants were then collected by centrifugation. The *rALPase*

activities were determined by normalizing A_{420} readings of colorimetric phosphatase product pNP to cell number.

QA and NR cross-feeding plate assays - These assays employed specific mutants, which depend on QA or NR for growth, as "recipient cells", and yeast strains of interest as "feeder cells". First, recipient cells were plated as a lawn on a solid agar plate (~10^4 cells/cm^2). Next, ~2x10^4 cells of each feeder cell strain (2 μl cell suspension made in sterile water at A_{600} of 1) was spotted onto the lawn of recipient cells. Plates were then incubated at 30˚C for 3 days. Since the growth media do not contain the NAD^+ intermediates needed for the growth of recipient cells, the extent of the recipient cell growth indicates the levels of specific NAD^+ intermediates released by feeder cells. QA cross-feeding was carried out on SC or SD using the QA dependent *npt1*Δ*nrk1*Δ*bna4*Δ mutant. NR cross-feeding was carried out on YPD or SC using the NR dependent *npt1*Δ*bna6*Δ*pho5*Δ mutant.

Measurement(s) of NAD^+, NADH, QA, NR and NA-NAM - Total intracellular levels of NAD^+ and NADH were determined using enzymatic cycling reactions as described (4). In brief, approximately 1 A_{600} unit (1 A_{600} unit = 1x10^7 cells/ml) cells grown to early-logarithmic phase in SC (~6 hr growth from A_{600} of 0.1) were collected in duplicate by centrifugation. Acid extraction was performed in one tube to obtain NAD^+, and alkali extraction was performed in the other to obtain NADH for 40 minutes at 60˚C. Amplification of NAD^+ or NADH in the form of malate was carried out using 3 µl or 4 µl of neutralized acid or alkali extracted lysate in 100 µl of cycling reaction for 1 hour at room temperature. The reaction was terminated by heating at 100˚C for 5 minutes. Next, malate produced from the cycling reaction was converted to oxaloacetate and then to aspartate and a-ketoglutarate by the addition of 1 ml malate indicator reagent for 20 minutes at room temperature. The reaction produced a corresponding amount of NADH as readout, which

was measured fluorometrically with excitation at 365 nm and emission monitored at 460 nm. Standard curves for determining NAD^+ and NADH concentrations were obtained as follows: NAD^+ and NADH were added into the acid and alkali buffer to a final concentration of 0, 2.5, and 7.5 μM, which were then treated with the same procedure along with other samples. The fluorometer was calibrated each time before use with 0, 5, 10, 20, 30, and 40 μM NADH to ensure that the detection was within a linear range. Levels of NAD^+ intermediates (QA, NR and NA-NAM) were determined by a liquid-based cross-feeding bioassay as previously described (5,77,174) with modifications. To prepare cell extracts for intracellular NAD^+ intermediates determination, approximately 200 A_{600} unit (for NR and NA-NAM) or 900 A_{600} unit (for QA) donor cells grown to late-logarithmic phase in SC (~16 hr growth from an A_{600} of 0.1) were collected by centrifugation and lysed by bead-beating (Biospec Products) in 400 μl (per 200 A_{600} unit cells) ice-cold 50 mM ammonium acetate solution. The supernatant was collected by centrifugation and the pellet was extracted two more times with 600 μl ice-cold 50 mM ammonium acetate solution, which generates 1600 μl cell lysate. After filter sterilization, 100-200 μl of clear extract (2.5 mL for QA) was used to supplement 8 ml cultures of recipient cells with starting A_{600} of 0.05 in SC. To determine extracellular NAD^+ intermediates levels, 20 ml supernatant of donor cell culture was collected, filter-sterilized, and then 4 ml was added to recipient cell culture in 2x SC to a final volume of 8 ml with total starting A_{600} of 0.05. A control culture of recipient cells in SC without supplementation was included in all experiments. For measuring relative QA levels, *npt1*Δ*nrk1*Δ*bna4*Δ and *npt1*Δ*nrk1*Δ*bna1*Δ mutants were used as recipient cells. The *npt1*Δ*bna6*Δ*pho5*Δ recipient cells were used to measure relative NR levels. To measure relative NA/NAM levels, the *bna6*Δ*nrk1*Δ*nrt1*Δ recipient cells were grown in NA-free SC. After incubation at 30˚C for 24 hours, growth of the recipient cells (A_{600}) was measured and normalized

to the cell number of each donor strain. A_{600} readings were then converted to concentrations of QA, NR, and NA/NAM using the standard curves established as previously described (77,174).

FIGURE 3-1

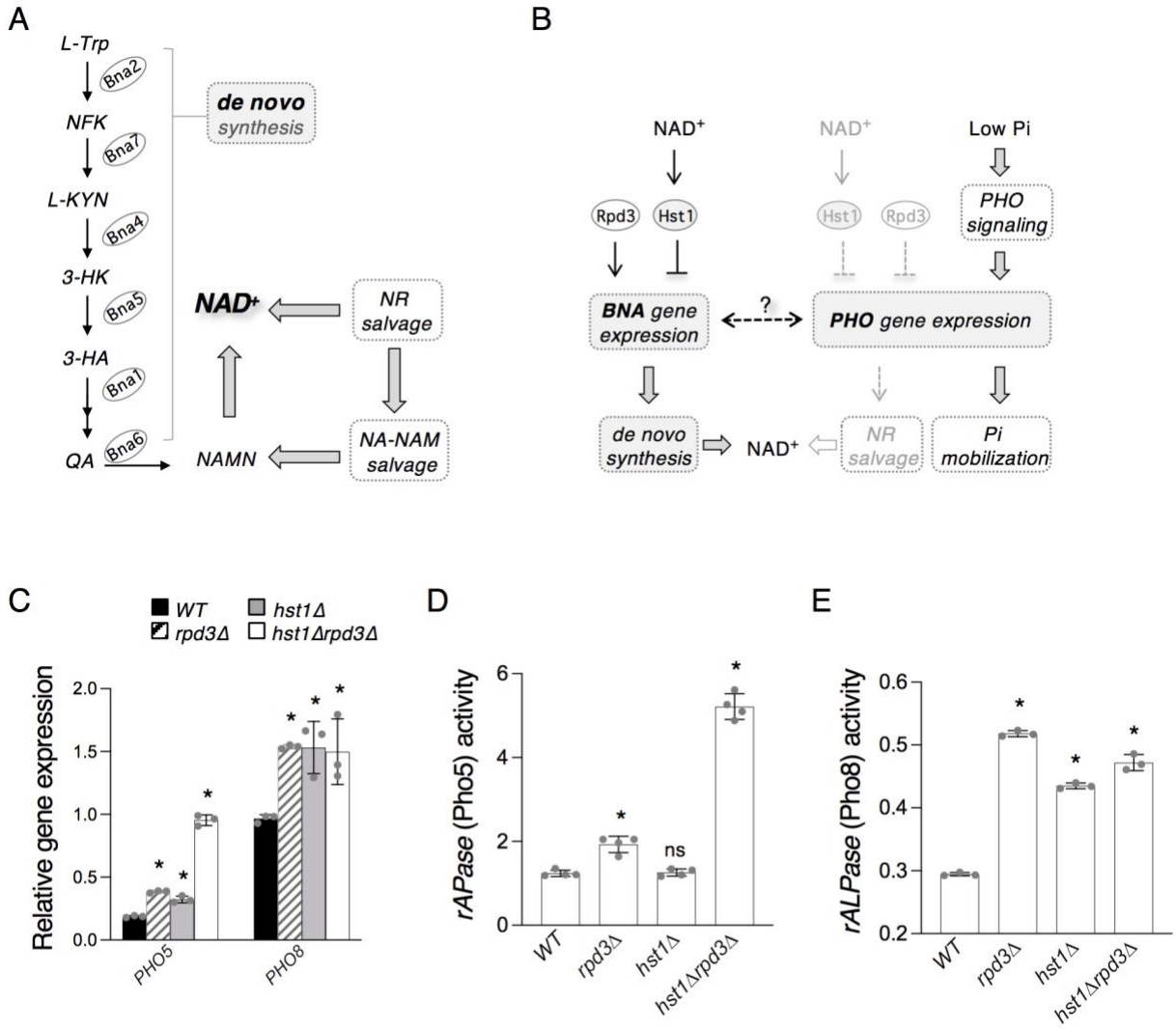
A
L-Trp
Bna2
NFK
Bna7
L-KYN
Bna4
3-HK
Bna5
3-HA
Bna1
QA
Bna6
de novo synthesis
NAD+
NR salvage
NAMN
NA-NAM salvage
B
NAD+
NAD+
Low Pi
Rpd3
Hst1
Hst1
Rpd3
PHO signaling
BNA gene expression
?
PHO gene expression
de novo synthesis
NAD+
NR salvage
Pi mobilization
C
WT
rpd3Δ
hst1Δ
hst1Δrpd3Δ
Relative gene expression
PHO5
PHO8
D
rAPase (Pho5) activity
ns
WT
rpd3Δ
hst1Δ
hst1Δrpd3Δ
E
rALPase (Pho8) activity
WT
rpd3Δ
hst1Δ
hst1Δrpd3Δ

FIGURE 3-1. Rpd3 and Hst1 negatively regulate the *PHO* pathway genes *PHO5* and *PHO8*.

A, abridged model of the NAD^+ biosynthetic pathways in *Saccharomyces cerevisiae*. *De novo* NAD^+ metabolism begins with TRP, which is converted into NaMN by the Bna enzymes (Bna2, -7, -4, -5, -1, -6) (left). NaMN is also produced by salvage of NA and NAM, which is further connected with salvage of NR (right). NA, nicotinic acid. NAM, nicotinamide. NR, nicotinamide riboside. QA, quinolinic acid. TRP, L-tryptophan. NFK, N-formylkynurenine. KYN, kynurenine. 3-HK, 3-hydroxykynurenine. 3-HA, 3-hydroxyanthranilic acid. ACMS, 2-amino-3-carboximuconate-6-semialdehyde. KA, kynurenic acid. NaMN, nicotinic acid mononucleotide. Abbreviations of protein names are shown in ovals. Bna2, tryptophan 2,3-dioxygenase. Bna7, kynurenine formamidase. Bna4, kynurenine 3-monooxygenase. Bna5, kynureninase. Bna1, 3-hydroxyanthranilate 3,4-dioxygenase. Bna6, quinolinic acid phosphoribosyl transferase.

B, relationship between *de novo* NAD^+ biosynthesis, NR salvage, and Pi sensing. Rpd3 and Hst1 antagonistically regulate the *BNA* genes of the de novo pathway and have previously been shown to negatively regulate certain *PHO* targets. *PHO* gene expression is sensitive to cellular Pi levels and is induced by Pi-depletion. Two *PHO* targets, the acid phosphatase Pho5 and the alkaline phosphatase Pho8, are known to convert NMN to NR.

C, gene expression qPCR analysis of *PHO5* and *PHO8* levels in WT, *rpd3*Δ, *hst1*Δ, and *hst1*Δ*rpd3*Δ cells. Values shown are relative expression levels normalized to *TAF10* as a control. *PHO5* expression is increased in *rpd3*Δ and *hst1*Δ cells, and is especially strongly raised in *hst1*Δ*rpd3*Δ cells. *PHO8* expression in *rpd3*Δ, *hst1*Δ, and *hst1*Δ*rpd3*Δ is raised to a similar extent relative to WT cells.

D, Pho5 acid phosphatase activity in WT, *rpd3*Δ, *hst1*Δ, and *hst1*Δ*rpd3*Δ cells. *hst1*Δ*rpd3*Δ cells show a large increase in Pho5 activity relative to WT, *rpd3*Δ, and *hst1*Δ cells.

E, Pho8 alkaline phosphatase activity in WT, *rpd3*Δ, *hst1*Δ, and *hst1*Δ*rpd3*Δ cells. *rpd3*Δ, *hst1*Δ, and *hst1*Δ*rpd3*Δ cells show comparable increases in Pho8 activity relative to WT cells.

For *C*, *D*, and *E*, the graphs are representative of the trend observed across three independent experiments. Error bars represent data from three technical replicates for each strain in an experiment. The *p* values are calculated using student's t test (*, $p<0.05$; *ns*, not significant).

FIGURE 3-2

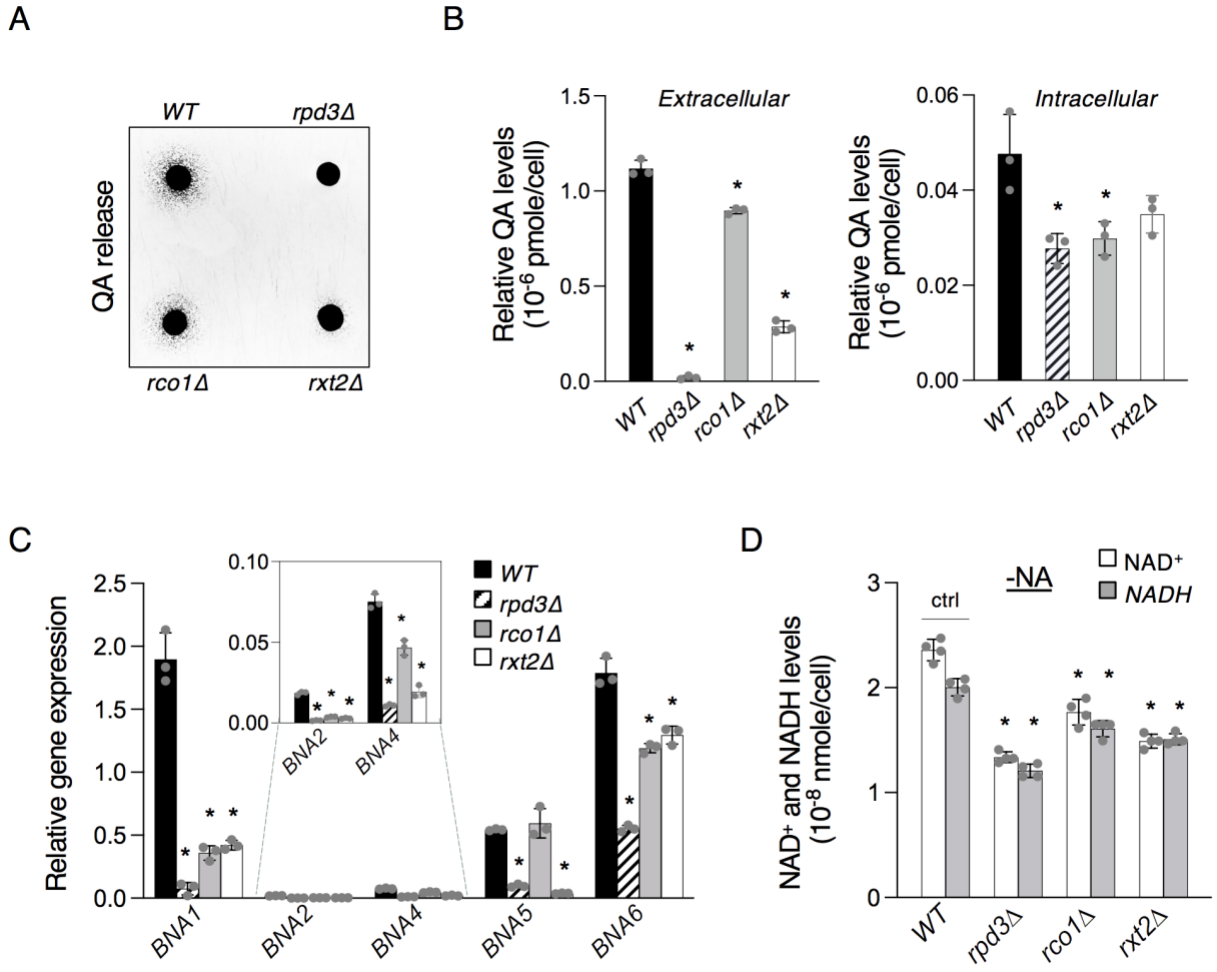
A
WT
rpd3Δ
QA release
rco1Δ
rxt2Δ
B
Extracellular
Relative QA levels (10-6 pmole/cell)
1.5
1.0
0.5
0.0
WT
rpd3Δ
rco1Δ
rxt2Δ
Intracellular
Relative QA levels (10-6 pmole/cell)
0.06
0.04
0.02
0.00
C
Relative gene expression
2.5
2.0
1.5
1.0
0.5
0.0
0.10
0.05
0.00
BNA2
BNA4
WT
rpd3Δ
rco1Δ
rxt2Δ
BNA1
BNA2
BNA4
BNA5
BNA6
D
NAD+ and NADH levels (10-8 nmole/cell)
ctrl
-NA
NAD+
NADH
3
2
1
0
WT
rpd3Δ
rco1Δ
rxt2Δ

FIGURE 3-2. Rpd3L is the main form of Rpd3 involved in positive regulation of *de novo* NAD^+ metabolism.
A, plate cross-feeding assay of QA release in WT, *rpd3*Δ, *rco1*Δ, and *rxt2*Δ cells. Rco1 is a subunit exclusive to the RpdS complex, while Rxt2 is found only in the Rpd3L complex. Spots of haploid single-deletion feeder cells were applied to a lawn of QA-dependent recipient cells (*bna1Δnrk1Δnpt1Δ*) and allow to grow for 2-3 days at 30˚C. The density of recipient cell growth around the feeder cell spots correlates with the amount of QA released by the feeder cells.
B, QA release is significantly decreased in *rco1*Δ and *rxt2*Δ cells. *rxt2*Δ cells show a comparatively greater level of decrease (left). Intracellular storage of QA in *rco1*Δ and *rxt2*Δ is reduced relative to WT cells, comparable to levels observed in *rpd3*Δ cells (right).
C, expression of the *de novo*-mediating *BNA* genes is reduced in *rco1*Δ and *rxt2*Δ cells. Values shown are relative expression levels normalized to *TAF10* as a control. *rxt2*Δ cells show greater and more extensive decreases compared to *rco1*Δ cells.
D, NAD^+ levels in WT, *rpd3*Δ, *rco1*Δ, and *rxt2*Δ cells, measured in SC medium lacking NA. *rco1*Δ and *rxt2*Δ cells show significant decreases in NAD^+ production, similar to *rpd3*Δ cells.

For *B*, *C*, and *D*, the graphs are representative of the trend observed across three independent experiments. Error bars represent data from three technical replicates for each strain in an experiment. The *p* values are calculated using student's t test (*, $p<0.05$; *ns*, not significant).

FIGURE 3-3

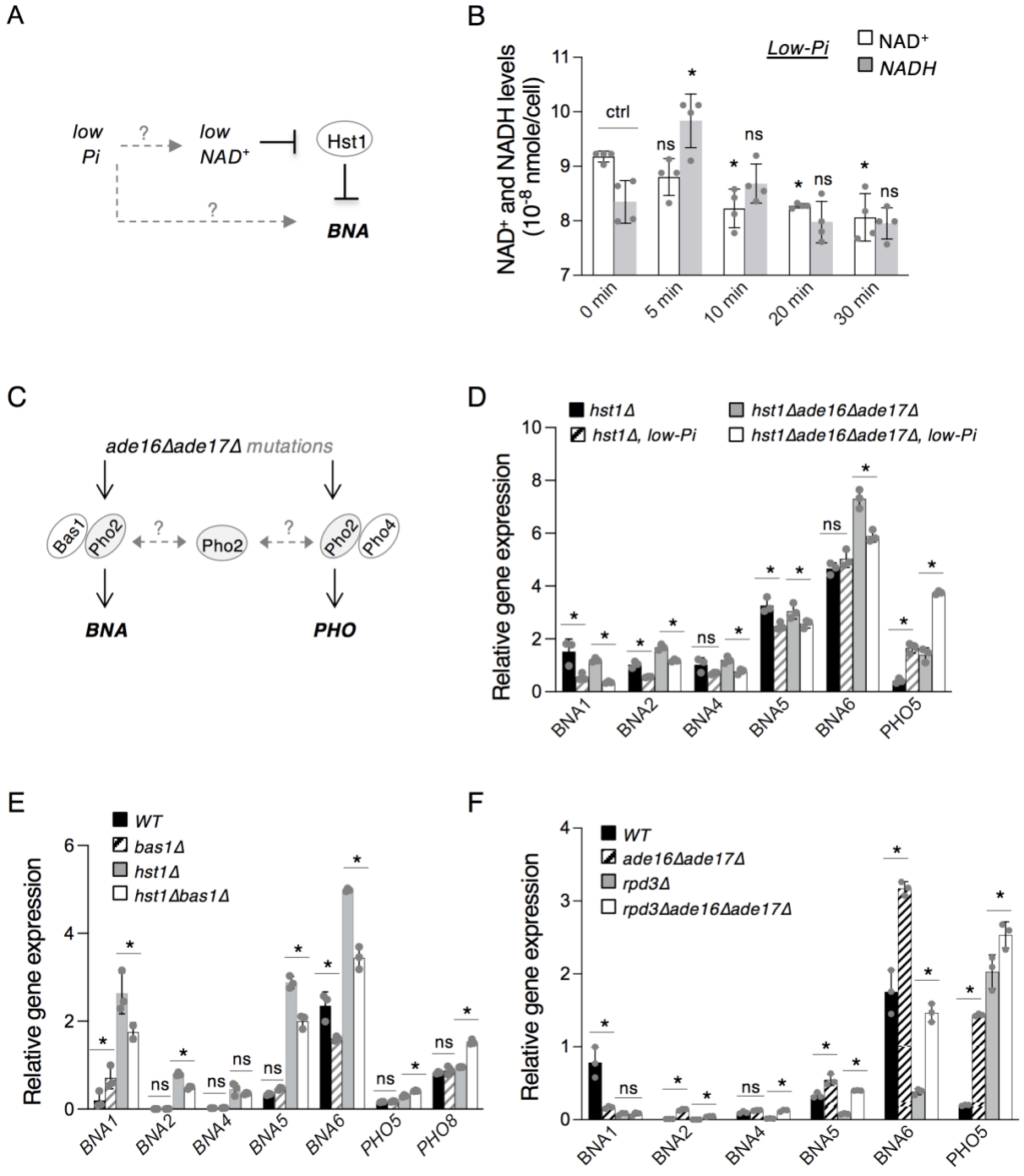
A
low Pi
?
low NAD+
Hst1
?
BNA
B
Low-Pi
NAD+
NADH
NAD+ and NADH levels (10-8 nmole/cell)
ctrl
ns
0 min
5 min
10 min
20 min
30 min
C
ade16Δade17Δ mutations
Bas1
Pho2
Pho2
Pho2
Pho4
BNA
PHO
D
hst1Δ
hst1Δ, low-Pi
hst1Δade16Δade17Δ
hst1Δade16Δade17Δ, low-Pi
Relative gene expression
BNA1
BNA2
BNA4
BNA5
BNA6
PHO5
E
WT
bas1Δ
hst1Δ
hst1Δbas1Δ
Relative gene expression
BNA1
BNA2
BNA4
BNA5
BNA6
PHO5
PHO8
F
WT
ade16Δade17Δ
rpd3Δ
rpd3Δade16Δade17Δ
Relative gene expression
BNA1
BNA2
BNA4
BNA5
BNA6
PHO5

FIGURE 3-3. Rpd3 and Hst1 interact with cellular phosphate sensing and the Bas1-Pho2 complex during regulation of *de novo* NAD^+ metabolism.
A, model of the proposed relationship between Pi depletion and reduction of cellular NAD^+ pools. Pi depletion causes decreases in ATP production and reduction of ATP levels leads to decreased NAD^+ production. By corollary, Pi depletion should lead to lower NAD^+ levels. Limitation of NAD^+ is predicted to reduce the activity of Hst1, which is an NAD^+-dependent HDAC. Loss of Hst1 activity would then lead to decreased silencing of the *BNA* promoters.
B, NAD^+ levels in low Pi medium over the course of 30 minutes. Cells transferred into SC medium without Pi rapidly begin to show altered NAD^+ homeostasis.
C, Pho2 is shared between the BNA-activating Bas1-Pho2 complex and the PHO-activating Pho2-Pho4 complex. Formation of both complexes is promoted by the adenine precursor ZMP, which is accumulated in *ade16*Δ*ade17*Δ cells.
D, Pi depletion reduces expression of the BNA genes in *hst1*Δ and *hst1*Δ*ade16*Δ*ade17*Δ backgrounds. Cells transferred to low Pi medium for 30 minutes show reduced expression of several *BNA* genes relative to cells maintained in standard SC medium. *PHO5* is included as a positive control for *PHO* activation. Values shown are relative expression levels normalized to *TAF10* as a control.
E, deletion of *BAS1* reduces expression of the *BNA* genes in an *hst1*Δ background. *bas1*Δ cells do not show significant differences in BNA expression relative to WT cells. *hst1*Δ*bas1*Δ cells exhibit slightly raised *PHO5* and *PHO8* expression relative to *hst1*Δ cells.
F, deletion of *ADE16/ADE17* in the *rpd3*Δ background significantly increases expression of most *BNA* genes relative to *rpd3*Δ cells, but does not fully restore *BNA* expression to levels in *ade16*Δ*ade17*Δ cells. *PHO5* is included as a positive control for *PHO* activation.

For *B, D, E,* and *F,* the graphs are representative of the trend observed across three independent experiments. Error bars represent data from three technical replicates for each strain in an experiment. The *p* values are calculated using student's t test (*, $p<0.05$; *ns*, not significant).

FIGURE 3-4

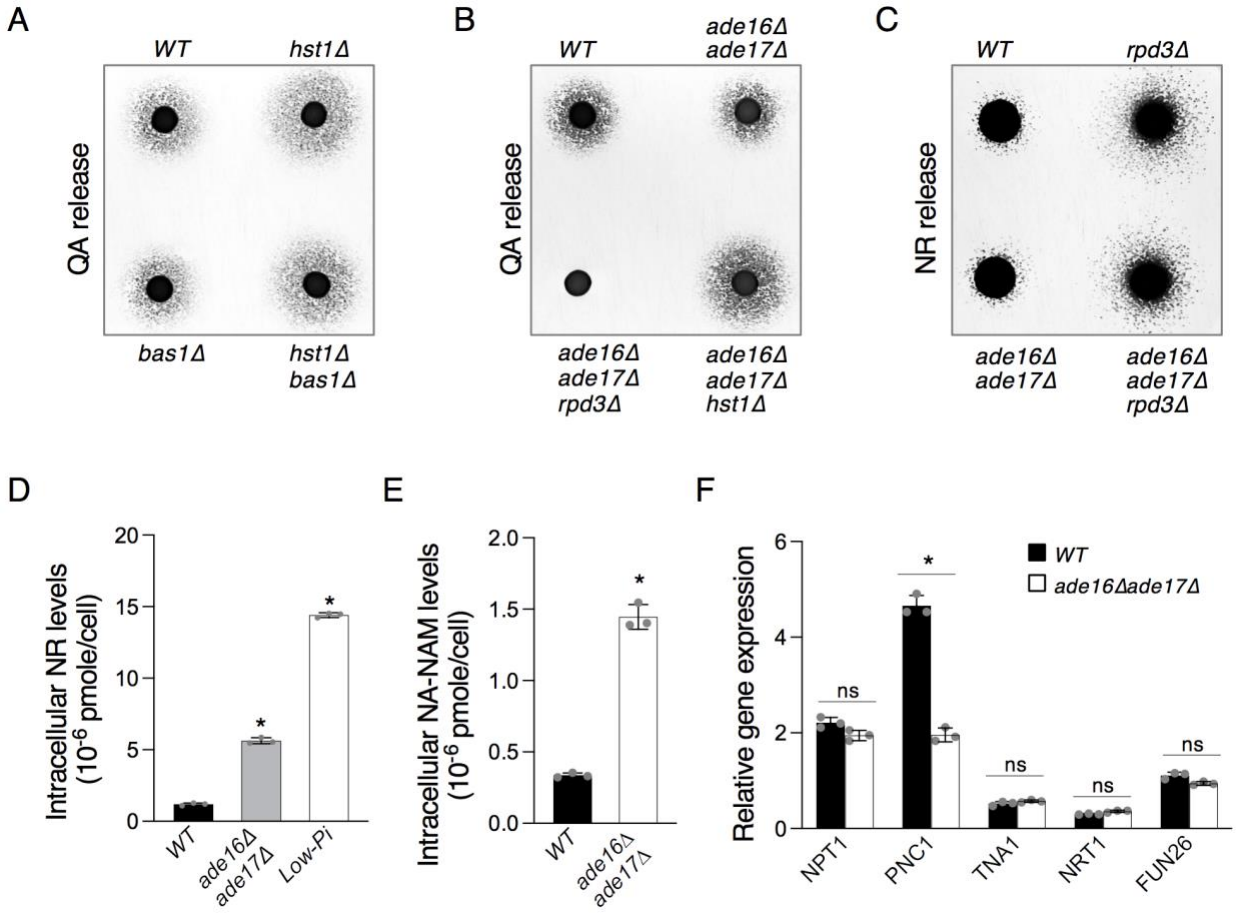
A
WT
hst1Δ
QA release
bas1Δ
hst1Δ bas1Δ
B
WT
ade16Δ ade17Δ
QA release
ade16Δ ade17Δ rpd3Δ
ade16Δ ade17Δ hst1Δ
C
WT
rpd3Δ
NR release
ade16Δ ade17Δ
ade16Δ ade17Δ rpd3Δ
D
Intracellular NR levels (10-6 pmole/cell)
20
15
10
5
0
*
*
WT
ade16Δ ade17Δ
Low-Pi
E
Intracellular NA-NAM levels (10-6 pmole/cell)
2.0
1.5
1.0
0.5
0.0
*
WT
ade16Δ ade17Δ
F
Relative gene expression
6
4
2
0
WT
ade16Δade17Δ
*
ns
ns
ns
ns
NPT1
PNC1
TNA1
NRT1
FUN26

FIGURE 3-4. The *ade16*Δ*ade17*Δ mutant cells show altered homeostasis of NAD^+ precursors.
A, deletion of *BAS1* does not markedly affect QA release in WT or *hst1*Δ backgrounds.
B, deletion of *ADE16/ADE17* does not visibly increase QA release in *rpd3*Δ cells. *rpd3*Δ*ade16*Δ*ade17*Δ cells release little to no QA.
C, deletion of *ADE16/ADE17* does not affect levels of NR release in WT or *hst1*Δ backgrounds. Feeder cell spots along with NR-dependent recipient cells (*npt1Δbna6Δpho5Δ*) were grown at 30˚C on YPD plate for 3 days.
D, *ade16*Δ*ade17*Δ cells produce more NR relative to WT cells.
E, *ade16*Δ*ade17*Δ cells produce more NA-NAM relative to WT cells.
F, *ade16*Δ*ade17*Δ cells do not show significant changes in expression of the NA/QA transporter Tna1 or the NR transporters Nrt1 and Fun26. Expression of *PNC*1, responsible for the conversion of NAM to NA, is reduced in *ade16*Δ*ade17*Δ cells. Values shown are relative expression levels normalized to *TAF10* as a control.

For *D, E,* and *F*, the graphs are representative of the trend observed across three independent experiments. Error bars represent data from three technical replicates for each strain in an experiment. The *p* values are calculated using student's t test (*, $p<0.05$; *ns*, not significant).

FIGURE 3-5

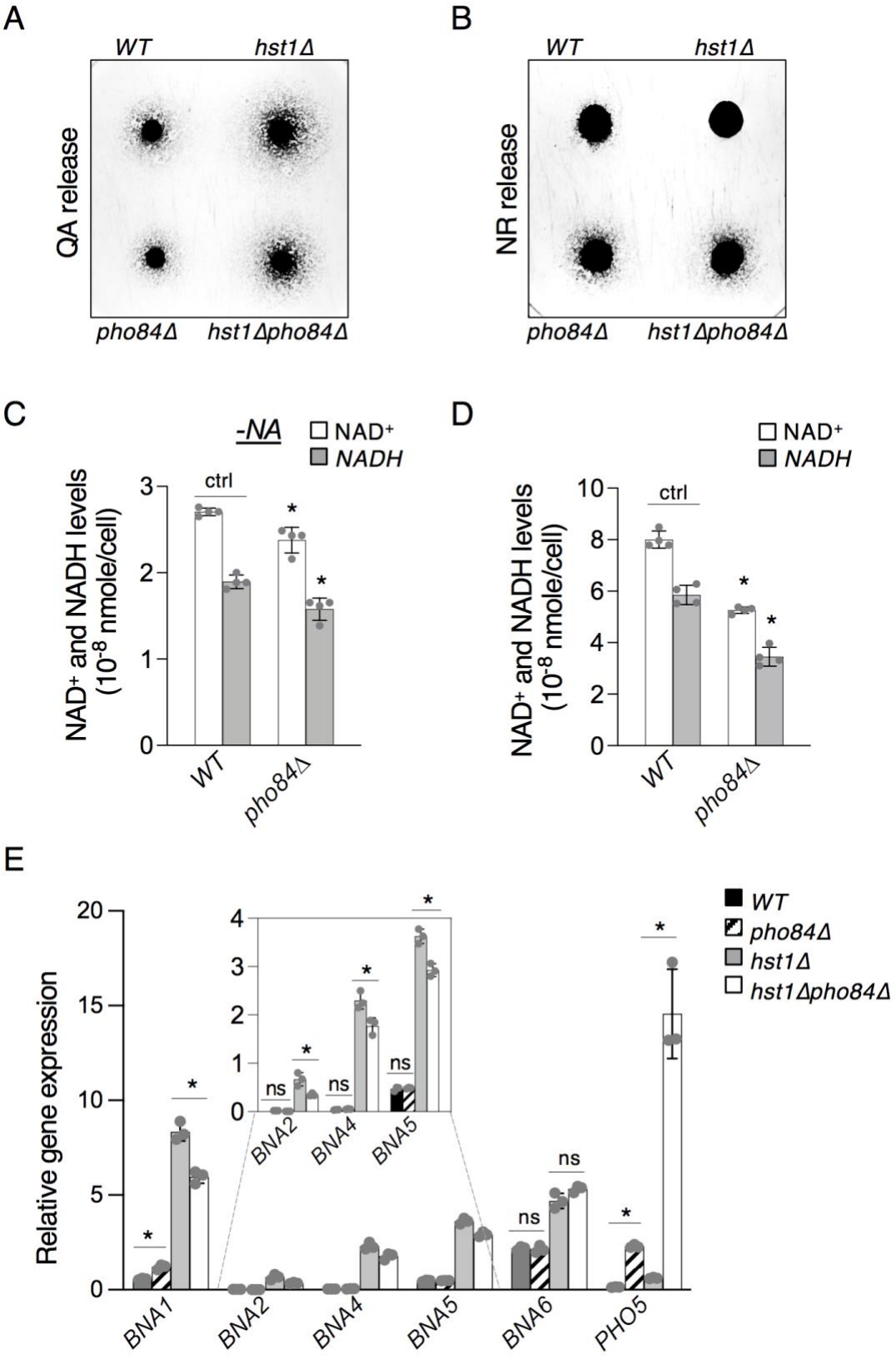
A
WT
hst1Δ
QA release
pho84Δ
hst1Δpho84Δ
B
WT
hst1Δ
NR release
pho84Δ
hst1Δpho84Δ
C
-NA
NAD+
NADH
NAD+ and NADH levels (10-8 nmole/cell)
ctrl
WT
pho84Δ
D
NAD+
NADH
NAD+ and NADH levels (10-8 nmole/cell)
ctrl
WT
pho84Δ
E
WT
pho84Δ
hst1Δ
hst1Δpho84Δ
Relative gene expression
BNA1
BNA2
BNA4
BNA5
BNA6
PHO5
ns

FIGURE 3-5. The phosphate transporter Pho84 influences cellular NAD^+ production.
A, *pho84*Δ cells do not show any difference in QA release relative to WT cells and *hst1*Δ*pho84*Δ do not show altered QA release relative to hst1 cells.
B, deletion of *PHO84* does not alter NR release in an *hst1*Δ background.
C, deletion of PHO84 reduces NAD/H levels when cells are grown in SC medium lacking NA.
D, *pho84*Δ cells show strongly reduced production of NAD/H relative to WT cells.
E, *pho84*Δ cells do not show markedly altered *BNA* expression compared to WT cells. *hst1*Δ*pho84*Δ cells exhibit small but significant reductions of *BNA* expression relative to *hst1*Δ cells. *PHO5* is included as a positive control for *PHO* activation. Values shown are relative expression levels normalized to *TAF10* as a control.

For *C, D,* and *E*, the graphs are representative of the trend observed across three independent experiments. Error bars represent data from three technical replicates for each strain in an experiment. The *p* values are calculated using student's t test (*, $p<0.05$; *ns*, not significant).

FIGURE 3-6

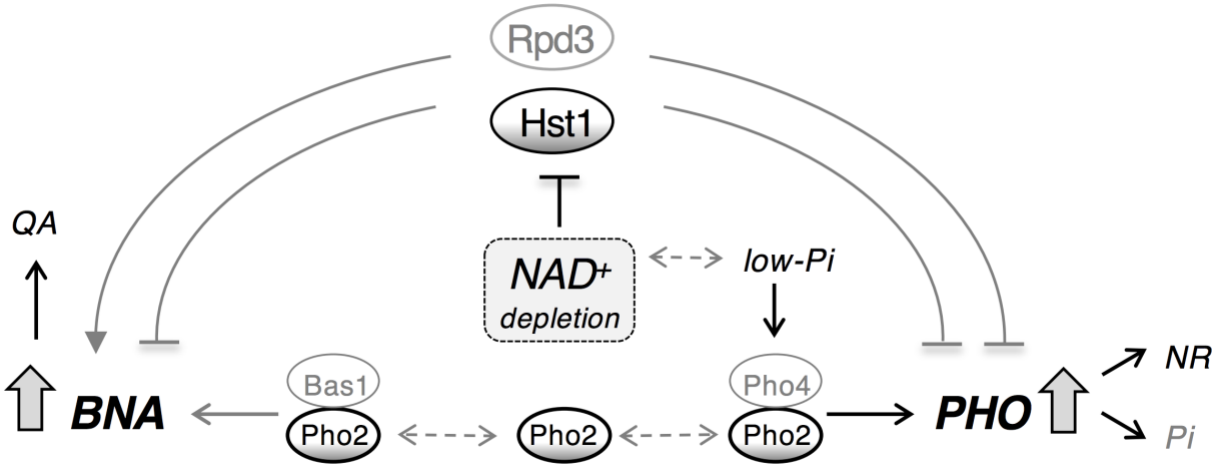
Rpd3
Hst1
QA
NAD+
depletion
low-Pi
BNA
Bas1
Pho2
Pho2
Pho4
Pho2
PHO
NR
Pi

FIGURE 3-6. Model of the interconnection of NAD^+ metabolism and *PHO* signaling by Hst1, Rpd3, and Pho2.

Rpd3 is a positive regulator of *de novo* NAD^+ metabolism, while Hst1 is a negative regulator of the same. On the other hand, both appear to be negative regulators of the *PHO* pathway. Hst1 activity is decreased by low NAD^+ levels, which may be caused by lowered ATP levels, which itself can be a consequence of phosphate depletion (low-Pi). This makes Hst1 sensitive to all three of these conditions, which consequently causes reduced silencing of *BNA* and *PHO* genes, leading to increased flux through *de novo* NAD^+ biosynthesis and NR salvage pathways. Low ATP also has the effect of increasing cellular ZMP levels, which promotes the formation of the Bas1-Pho2 and Pho2-Pho4 complexes, leading to increased *BNA* expression and *PHO* activity, respectively. Finally, low-Pi also promotes the translocation of Pho4 to the nucleus and increased Pho2-Pho4 complex formation. Under low-Pi conditions, the resultant lowered ATP and increased ZMP levels activate Bas1-Pho2 and Pho2-Pho4, while low-Pi itself leads to prioritization of *PHO* activation via Pho4-Pho2 over *BNA* activation via Bas1-Pho2. With its HDAC activity being independent of NAD^+ levels, Rpd3 remains an activator of *de novo* NAD^+ biosynthesis and NAD^+ precursor transport, as well as repressor of Pi sensing under all conditions described.

CHAPTER 4: Conclusion and future directions

Rpd3 and Hst1 are antagonistic regulators of *de novo* NAD$^+$ metabolism - Hst1 has long been known as a negative regulator of *de novo* NAD$^+$ metabolism (78,170). Our work demonstrates a novel role for the Class I HDAC Rpd3 as an antagonist of Hst1 activity, in which capacity it acts as a positive regulator of *de novo* NAD$^+$ metabolism. Specifically, Rpd3 appears to limit deacetylation of the 5th and 12th N-terminal lysines of histone H4 at the *BNA2* promoter by Hst1. Hst1 appears to be the primary and ultimate downstream regulator of *BNA* expression status. *BNA* expression (Fig. 2-4*A*) and production of *de novo* metabolites is greatly increased in the absence of Hst1 and highly reduced in the absence of Rpd3. When both *HST1* and *RPD3* are deleted, *de novo* metabolism and *BNA* expression are highly active to a degree almost matching that of *hst1*Δ cells (Fig. 2-1, Fig. 2-4*A*). Altogether, this leads toward a model in which Hst1 promotes heterochromatin formation at the promoters of the *BNA* genes and is limited in this function by Rpd3 (Fig. 2-6*D*). When the latter is absent, uncontrolled heterochromatin formation is likely to occur due to unchecked Hst1 activity, ultimately resulting in the silencing of *BNA* expression and the blockage of *de novo* metabolism.

Several questions remain to be addressed in the attempt to refine and validate this model. Namely, how might the particular mechanism(s) proceed by which Rpd3 opposes Hst1 activity? Currently, we have established an antagonism between the two HDACs in governing the acetylation status of histone H4. However, it remains unclear how Rpd3 might work to limit Hst1-dependent deacetylation of these residues. Several strategies are possible: first, Rpd3 might compete for several of the same targets as Hst1, potentially including H4K5-Ac and K4K12-Ac, thereby preventing their recognition by Hst1. Sirtuins have previously been shown to be recruited to chromatin by recognition of their acetylation targets (253); in this case, limited deacetylation by Rpd3 may prevent Hst1 from recognizing certain marks at the *BNA2* promoter

and thereby from initiating downstream deacetylation events. Another possibility is that Rpd3 might deacetylate certain key histone acetyl-lysine residues, potentially including H4K8-Ac, and thereby cause alterations in the chromatin structure that subsequently interfere with Hst1 HDAC activity. It is also possible that Rpd3 may be responsible for recruiting other downstream positive regulators to the *BNA* promoters, although no such factors were apparent in our QA cross-feeding screen of a genome-wide deletion collection (78). However, this would explain why *hst1*Δ*rpd3*Δ cells exhibit *BNA* expression levels slightly below those of *hst1*Δ cells (Fig. 2-4*A*). Lastly, Rpd3 may also target non-histone proteins as part of its regulatory activity. In a previous study of antagonism between Sir2 and Rpd3, the antagonistic function of Rpd3 did not appear to depend on any of its known histone targets (248).

In order to fully develop this model, it will also be necessary to examine the influence that Rpd3 and Hst1 have on the deacetylation of other histone residues. Rpd3 in particular affects a much wider range of histone residues than those included in the small subset investigated in Chapter 2 (220). Hst1 is at the very least known to deacetylate H3K4-Ac as well (217), which is interestingly not among the many known targets of Rpd3 (220). In addition to these studies, it will also be useful to determine the particular influence that each histone H4 acetyl-lysine investigated in these studies has on *BNA* expression and *de novo* activity. To these ends, strains carrying mutant Hhf1 proteins may be constructed, bearing either acetyl-mimic alanine substitutions (292) or non-acetyl-mimic glutamine substitutions (293) at H4K5, H4K8, and H4K12.

Lastly, it will also be useful to directly establish that Hst1 is responsible for producing a repressive chromatin structure at the *BNA2* promoter, while Rpd3 maintains de-repressed

chromatin status. This may be achieved by ATAC-seq analysis of the *BNA* promoters in *rpd3*Δ, *hst1*Δ, and *hst1*Δ*rpd3*Δ cells.

Recruitment of Rpd3 and Hst1 to the *BNA2* promoter - In addition to the need to establish a detailed mechanism of Rpd3 and Hst1 antagonism, it would also be useful to determine the means by which the two HDACs are initially recruited to the *BNA2* promoter. It is possible that Hst1 contacts the *BNA2* promoter via its chromatin binding subunit Sum1 (214). The recruitment of Rpd3 presents a more complex picture, as the HDAC may be targeted to chromatin by a wide variety of means, which include binding by Ume6 (222,227) or Ash1 (222,228), as well as recognition of di- (229) and trimethylated (230,231) H3K4. This last possibility is the most striking, following observations made regarding *BNA* induction in aged yeast cells. It was noted that deletion of *SPP1*, a subunit of the Set1/COMPASS methyltransferase, specifically reduces tri- but not mono- or dimethylation of this mark and that this has the effect of hindering *BNA* induction in aged cells (294). Because this specific modification is known to recruit Rpd3, and the effects of *RPD3* deletion resemble those of *SPP1* deletion, it is possible that Set1-dependent H3K4-3me formation may be responsible for Rpd3 recruitment to the *BNA2* promoter. On the other hand, no COMPASS subunit mutants were detected in our preliminary QA cross-feeding screen. This may however be due to the overlapping participation of COMPASS in mono-, di-, and trimethylation of H3K4, all of which modifications may have opposing influences on gene expression (294). Of note, H3K4 is also one of the known targets of Hst1 deacetylase activity (217). This residue is therefore a very intriguing subject of investigation in the context of *BNA* regulation.

Rpd3L, Hst1, and ZMP induction link *de novo* NAD^+ metabolism with phosphate sensing - Rpd3 (276-278) and Hst1 (78) are known to be negative regulators of *PHO5* expression. In this

work, we establish a broader role for Rpd3 and Hst1 as regulatory links between the *PHO* pathway and *de novo* pathway. Specifically, Hst1 and Rpd3 act as negative regulators of two phosphatases involved in NR salvage, *PHO5* and *PHO8*. Hst1 plays this same role in the regulation of the *BNA* genes, while Rpd3 has in this case the opposite effect. This indicates that the form of interaction between the two HDACs is fundamentally different between the *BNA* and *PHO* promoters. Moreover, the manners in which the two HDACs regulate *PHO5* and *PHO8* appear to be distinct, with a strong synergism being evident in the case of *PHO5* and likely redundant roles being employed in the case of *PHO8* (Fig. 3-1*C*).

In addition, Rpd3 and Hst1 appear to interact with the Bas1-Pho2 complex, another factor that coordinates phosphate sensing and *de novo* metabolism. Specifically, Rpd3 likely maintains an open chromatin structure necessary for full Bas1-Pho2 access to the *BNA* promoters (Fig. 3-3*F*). Bas1-Pho2 appears to promote *BNA* expression only under inducing conditions, whether this be due to loss of Hst1 activity or ZMP accumulation. Evidence supporting this conclusion includes the fact that *BAS1* deletion only significantly decreases *BNA* expression in an *hst1*Δ background (Fig. 3-3*E*), the observation that *ade16*Δ*ade17*Δ mutants no longer show *BNA* induction in the absence of Bas1 (59), as well as the fact that phosphate depletion only seems to reduce *BNA* expression (Fig. 3-3*D;* Fig. 3-5*F*) in an *hst1*Δ background. This latter fact is also likely due to the confounding influence of Hst1 activity being limited by reduced NAD^+ levels during phosphate starvation (Fig. 3-3B; Fig. 3-5D). However, it must also be considered that deletion of *BAS1*, as an activator of adenine biosynthesis, greatly reduces cellular ATP levels (282,283). This in all likelihood has the consequence of limiting NAD^+ production (59) and therefore interfering with Hst1 activity, indirectly causing at least partial *BNA* induction. Consequently, it is very much possible that the effect of Bas1-Pho2 as a potential positive

regulator of *BNA* expression under standard conditions is masked by this effect. Further work is needed to determine whether the Bas1-Pho2 complex might indeed significantly promote *BNA* expression when no ZMP is accumulated, but ATP and NAD^+ levels are controlled.

It appears ultimately that under phosphate depleted conditions, *de novo* metabolism and phosphate sensing compete for limited reserves of Pho2 as a shared member of Bas1-Pho2 and Pho2-Pho4, respectively, with the balance being shifted toward the *PHO* genes (Fig. 3-3*D*; Fig. 3-5*F*) during phosphate depletion, in which *PHO* activation is prioritized above *BNA* activation. This model is supported by the observation that deletion of *BAS1* causes a slight increase in *PHO5* activation (Fig. 3-3*F*), likely due to increased Pho2-Pho4 activity. Interestingly, deletion of *HST1* promotes the expression of multiple *PHO* genes: *PHO12* and *PHO84*, in addition to *PHO5* and *PHO8* (78). However, deletion of *HST1* also causes large increases in *BNA* expression (3,78,170); according to the competitive model outlined above, this should draw Bas1-Pho2 to the *BNA* promoters and limit the amount of Pho2 available for *PHO* activation. The fact that *PHO* expression is nevertheless significantly increased in *hst1*Δ cells suggests that Hst1 is likely quite important as a negative regulator of *PHO* expression and that, moreover, the true magnitude of its effect may be masked by the collateral influence of reduced Pho2 recruitment to the *PHO* promoters. This may also explain the less pronounced effect on *PHO5* expression and activity evident in *hst1*Δ vs. *rpd3*Δ *cells*.

It therefore remains to be investigated what roles Hst1 might have at the *PHO* promoters. While it is likely that the observed effect of *HST1* deletion upon *PHO* expression is caused directly by loss of Hst1-dependent negative regulation, it would be useful to examine the presence of Hst1 at the *PHO* promoters by ChIP analysis in order to confirm that Hst1 is a direct regulator of *PHO* expression. Moreover, ChIP analysis of Pho2 or Pho4 binding to the *PHO* and

BNA promoters in *hst1*Δ cells could be used to confirm our above hypothesis. As noted above, gene expression and enzyme activity analyses provide a good deal of evidence that Hst1 is a direct negative regulator of, at the very least, *PHO5* and *PHO8* (Fig. 3-1*C, D, E*). As to the influence of Rpd3 on *PHO* regulation, it would be illuminating to examine the binding of Rpd3 to these promoters, as well as the status of histone acetylation in *hst1*Δ and *rpd3*Δ cells, by ChIP, following the method used for the *BNA* genes.

It appears that the Bas1-Pho2 complex is only significant as an activator of *BNA* expression under inducing conditions. Under standard circumstances of adenine and NAD^+ repletion, Bas1-Pho2 has no significant influence on *de novo* activity (Fig. 3-3*E*; Fig. 3-4*A*). However, even when *de novo* metabolism is induced by ZMP accumulation, there is no apparent effect on QA production (Fig. 3-4*B)* or NAD^+ levels (59). Neither do the generally reduced levels of *BNA* expression observed in *bas1*Δ*hst1*Δ cells relative to *hst1*Δ cells cause any corresponding difference in the level of QA released by the two strains. Pinson, et al. also saw that *ade16*Δ*ade17*Δ cells show no significant increase of NAD^+ levels, though this group also noted increased levels of several *de novo* metabolites upstream of QA, in line with expectations (59). One possibility explaining these phenomena is the unique status of *BNA1* in this connection, which is directly responsible for the production of QA. We saw that *BNA1* appears to be negatively rather than positively regulated by Bas1-Pho2 under the conditions used (Fig. 3-3*E, 3*-3*F*). This may then lead to blockage of *de novo* metabolism at Bna1, thereby causing the apparent accumulation of early *de novo* metabolites and the accompanying lack of any corresponding increase in QA or NAD^+ levels downstream. We may test this hypothesis by overexpressing *BNA1* in *ade16*Δ*ade17*Δ cells, then examining QA and NAD^+ levels in this strain relative to WT cells overexpressing *BNA1*.

Influence of Rpd3, Hst1, and ZMP accumulation on the transport of NAD^+ precursors - Among all the potential shared targets of Rpd3 and Hst1 in the regulation of NAD^+ metabolism, only *TNA1* and *NRT1* appear to be regulated in an antagonistic manner comparable to the *BNA* genes (Fig. 2-7*A*, 2-7*B*). As in the latter case, Rpd3 appears to be a positive regulator of these genes, while Hst1 appears to be a negative regulator; moreover, *hst1*Δ*rpd3*Δ cells display an intermediate level of expression most similar to levels in WT cells. Significantly, both Tna1 and Nrt1 are involved in the transport of NAD^+ precursors. The former imports QA and, preferentially, NA (78), while the latter imports NR (81). The observed effect of each HDAC on these genes raises the question of their contribution to the regulation of NAD^+ metabolism via the modulation of transport activity. For instance, it is already apparent that *hst1*Δ cells simultaneously show increased NR production, but reduced NR release, due to drastically increased Nrt1 expression, ultimately resulting in the rapid re-uptake of released NR (78) (Fig. 2-2*C*, 2-2*D*, 2-7*B*).

A similar discrepancy between increased NR production and reduced NR release is evident in *ade16*Δ*ade17*Δ cells as well (Fig. 3-4*C*, 3-4*D*). The cause of this phenomenon is still unknown. Predicting that ZMP accumulation and promotion of either Pho2-Pho4 or Bas1-Pho2 complex formation might, like Rpd3 and Hst1, regulate the transporters of NAD^+ precursors, we examined the expression *TNA1*, *NRT1*, and *FUN26* in *ade16*Δ*ade17*Δ cells. Surprisingly, no effect on any of these genes was observed (Fig. 3-4*F*). Consequently, the particular reason for the decline in NR release observed for *ade16*Δ*ade17*Δ cells remains enigmatic. Interestingly, Nrt1 is also a transporter of the ZMP derivative, AICAR (288). It may be that transport of this compound, possibly accumulated in *ade16*Δ*ade17*Δ cells, somehow influences the movement of NR in and out of the cell. As to the cause of increased NR accumulation in *ade16*Δ*ade17*Δ cells,

we anticipate that this is likely at least in part due to increased *PHO* activity, inclusive of the NR-producing phosphatases Pho5 and Pho8, in *ade16*Δ*ade17*Δ cells (184). This remains to be demonstrated directly, as does the cause of the stark increase in NR production observed in *hst1*Δ*rpd3*Δ cells (Fig. 2-2*D*). We also observed significant reduction of *PNC1* expression in *ade16*Δ*ade17*Δ cells (Fig. 3-4*F*). It remains to determine whether ZMP promotion of Bas1-Pho2 or Pho2-Pho4 complex formation is specifically responsible for this phenomenon.

Rpd3 has previously been implicated in promoting the recycling of cell-surface transporters (277) (249). Indeed, Rpd3 directly regulates the activity of several cell-surface recycling factors (249). If these defects in transporter recycling in the absence of Rpd3 are of a general nature and common to all or most transporters, this indicates a further role for Rpd3 as a regulator of NAD^+ precursor transport, independent of its activity as an activator of *TNA1* and *NRT1* expression. The potential role of Rpd3 as an indirect regulator of NAD^+ metabolism via the promotion of transporter recycling is quite far-ranging in its implications. For instance, the observed effect of Rpd3 on Pho84 recycling (277) may be further connected with phosphate importation, downstream of which *PHO* activity, NR salvage, *de novo* metabolism, and ultimately NAD^+ levels are altered. In addition, the observed effect of Rpd3 on the recycling of the Tat2 TRP transporter may modify the level of TRP available as an input for *de novo* metabolism. It is possible as well that this recycling defect seen in the absence of Rpd3 further affects Tna1 and Nrt1 activity. This scenario presents a rich topic for future study.

Conclusion - NAD^+ is a key cellular cofactor necessary for the operation of many and diverse processes, including catabolism, DNA repair, and gene regulation. Maintenance of the NAD^+ pool and balancing the homeostasis of NAD^+ precursors is therefore a critical part of securing cellular health. Moreover, these NAD^+ precursors are often highly significant in their own right,

having an extensive range of connections with immune signaling, nutrient sensing, and infection. In this work, we have demonstrated a crucial role for Rpd3 as a positive regulator of *de novo* NAD^+ metabolism, which acts in this capacity by means of limiting Hst1-dependent repression of the *BNA* genes. In addition, we have identified a multifarious connection between *de novo* metabolism, NR salvage, and phosphate sensing. Specifically, we have shown that the Bas1-Pho2 complex may activate *BNA* expression only under conditions of ZMP accumulation or limited Hst1 activity, and that this role of Bas1-Pho2 is further modulated by competition with the Pho2-Pho4 complex and the phosphate sensing pathway for the use of Pho2. These studies contribute to the greater understanding of NAD^+ metabolism and the complexity of its integration with other processes in the cell. In particular, Rpd3 is characterized as a major regulator of *de novo* metabolism and a point of connection between this pathway and the vast expanse of the genome under its epigenetic control. This relationship offers a wealth of matters for future inquiry.

REFERENCES

1. Guldener, U., Heck, S., Fielder, T., Beinhauer, J., and Hegemann, J. H. (1996) A new efficient gene disruption cassette for repeated use in budding yeast. *Nucleic Acids Res* **24**, 2519-2524
2. Goldstein, A. L., and McCusker, J. H. (1999) Three new dominant drug resistance cassettes for gene disruption in Saccharomyces cerevisiae. *Yeast* **15**, 1541-1553
3. Groth, B., Huang, C. C., and Lin, S. J. (2022) The histone deacetylases Rpd3 and Hst1 antagonistically regulate de novo NAD(+) metabolism in the budding yeast Saccharomyces cerevisiae. *J Biol Chem* **298**, 102410
4. Easlon, E., Tsang, F., Skinner, C., Wang, C., and Lin, S. J. (2008) The malate-aspartate NADH shuttle components are novel metabolic longevity regulators required for calorie restriction-mediated life span extension in yeast. *Genes Dev* **22**, 931-944
5. Lu, S. P., and Lin, S. J. (2011) Phosphate-responsive signaling pathway is a novel component of NAD+ metabolism in Saccharomyces cerevisiae. *J Biol Chem* **286**, 14271-14281
6. Longtine, M. S., McKenzie, A., 3rd, Demarini, D. J., Shah, N. G., Wach, A., Brachat, A., Philippsen, P., and Pringle, J. R. (1998) Additional modules for versatile and economical PCR-based gene deletion and modification in Saccharomyces cerevisiae. *Yeast* **14**, 953-961
7. Groth, B., Venkatakrishnan, P., and Lin, S. J. (2021) NAD(+) Metabolism, Metabolic Stress, and Infection. *Front Mol Biosci* **8**, 686412
8. Harden, A., and Young, W. J. (1906) The alcoholic ferment of yeast-juice. *Proceedings of the Royal Society of London. Series B, Containing Papers of a Biological Character* **77**, 405-420
9. Harden, A., and Young, W. J. (1906) The alcoholic ferment of yeast-juice. Part II.—The coferment of yeast-juice. . *Proceedings of the Royal Society of London. Series B, Containing Papers of a Biological Character* **78**, 369-375
10. Euler, H., and Myrbäck, K. (1923) Gärungs-Co-Enzym (Co-Zymase) der Hefe. I. **131**, 179-203
11. Euler-Chelpin, H. v. (1930) Fermentation of Sugars and Fermentative Enzymes. *Nobel Lecture* **NobelPrize.org**
12. Schlenk, F., and v. Euler, H. (1936) Cozymase. *Naturwissenschaften* **24**, 794-795
13. Warburg, O., and Christian, W. (1936) Pyridin, der wasserstoffübertragende Bestandteil von Gärungsfermenten. *Helvetica* **19**, E79-E88
14. Landry, J., Sutton, A., Tafrov, S. T., Heller, R. C., Stebbins, J., Pillus, L., and Sternglanz, R. (2000) The silencing protein SIR2 and its homologs are NAD-dependent protein deacetylases. *Proc Natl Acad Sci U S A* **97**, 5807-5811
15. Imai, S., Armstrong, C. M., Kaeberlein, M., and Guarente, L. (2000) Transcriptional silencing and longevity protein Sir2 is an NAD-dependent histone deacetylase. *Nature* **403**, 795-800

16. Smith, J. S., Brachmann, C. B., Celic, I., Kenna, M. A., Muhammad, S., Starai, V. J., Avalos, J. L., Escalante-Semerena, J. C., Grubmeyer, C., Wolberger, C., and Boeke, J. D. (2000) A phylogenetically conserved NAD+-dependent protein deacetylase activity in the Sir2 protein family. *Proc Natl Acad Sci U S A* **97**, 6658-6663

17. Chambon, P., Weill, J. D., and Mandel, P. (1963) Nicotinamide mononucleotide activation of new DNA-dependent polyadenylic acid synthesizing nuclear enzyme. *Biochemical and biophysical research communications* **11**, 39-43

18. Chambon, P., Weill, J. D., Doly, J., Strosser, M. T., and Mandel, P. (1966) On the formation of a novel adenylic compound by enzymatic extracts of liver nuclei. *Biochemical and Biophysical Research Communications* **25**, 638-643

19. Kraus, W. L. (2015) PARPs and ADP-Ribosylation: 50 Years … and Counting. *Mol Cell* **58**, 902-910

20. Camacho-Pereira, J., Tarragó, M. G., Chini, C. C., Nin, V., Escande, C., Warner, G. M., Puranik, A. S., Schoon, R. A., Reid, J. M., and Galina, A. (2016) CD38 dictates age-related NAD decline and mitochondrial dysfunction through an SIRT3-dependent mechanism. *Cell metabolism* **23**, 1127-1139

21. Tarragó, M. G., Chini, C. C. S., Kanamori, K. S., Warner, G. M., Caride, A., de Oliveira, G. C., Rud, M., Samani, A., Hein, K. Z., Huang, R., Jurk, D., Cho, D. S., Boslett, J. J., Miller, J. D., Zweier, J. L., Passos, J. F., Doles, J. D., Becherer, D. J., and Chini, E. N. (2018) A Potent and Specific CD38 Inhibitor Ameliorates Age-Related Metabolic Dysfunction by Reversing Tissue NAD(+) Decline. *Cell Metab* **27**, 1081-1095.e1010

22. Kato, M., and Lin, S. J. (2014) Regulation of NAD+ metabolism, signaling and compartmentalization in the yeast Saccharomyces cerevisiae. *DNA Repair (Amst)* **23**, 49-58

23. Nikiforov, A., Kulikova, V., and Ziegler, M. (2015) The human NAD metabolome: Functions, metabolism and compartmentalization. *Critical reviews in biochemistry and molecular biology* **50**, 284-297

24. Chini, C. C., Tarrago, M. G., and Chini, E. N. (2016) NAD and the aging process: Role in life, death and everything in between. *Molecular and cellular endocrinology*

25. Imai, S. I., and Guarente, L. (2014) NAD and sirtuins in aging and disease. *Trends Cell Biol*

26. Yoshino, J., Baur, J. A., and Imai, S. I. (2018) NAD(+) Intermediates: The Biology and Therapeutic Potential of NMN and NR. *Cell Metab* **27**, 513-528

27. Okabe, K., Yaku, K., Tobe, K., and Nakagawa, T. (2019) Implications of altered NAD metabolism in metabolic disorders. *Journal of Biomedical Science* **26**, 34

28. Castro-Portuguez, R., and Sutphin, G. L. (2020) Kynurenine pathway, NAD(+) synthesis, and mitochondrial function: Targeting tryptophan metabolism to promote longevity and healthspan. *Exp Gerontol* **132**, 110841

29. Garten, A., Schuster, S., Penke, M., Gorski, T., de Giorgis, T., and Kiess, W. (2015) Physiological and pathophysiological roles of NAMPT and NAD metabolism. *Nature reviews. Endocrinology* **11**, 535-546

30. Verdin, E. (2015) NAD(+) in aging, metabolism, and neurodegeneration. *Science* **350**, 1208-1213

31. Cantó, C., Menzies, K. J., and Auwerx, J. (2015) NAD(+) Metabolism and the Control of Energy Homeostasis: A Balancing Act between Mitochondria and the Nucleus. *Cell Metab* **22**, 31-53

32. Yang, Y., and Sauve, A. A. (2016) NAD(+) metabolism: Bioenergetics, signaling and manipulation for therapy. *Biochim Biophys Acta* **1864**, 1787-1800

33. Cheng, A., Yang, Y., Zhou, Y., Maharana, C., Lu, D., Peng, W., Liu, Y., Wan, R., Marosi, K., and Misiak, M. (2016) Mitochondrial SIRT3 mediates adaptive responses of neurons to exercise and metabolic and excitatory challenges. *Cell metabolism* **23**, 128-142

34. Liu, H. W., Smith, C. B., Schmidt, M. S., Cambronne, X. A., Cohen, M. S., Migaud, M. E., Brenner, C., and Goodman, R. H. (2018) Pharmacological bypass of NAD(+) salvage pathway protects neurons from chemotherapy-induced degeneration. *Proc Natl Acad Sci U S A* **115**, 10654-10659

35. Poyan Mehr, A., Tran, M. T., Ralto, K. M., Leaf, D. E., Washco, V., Messmer, J., Lerner, A., Kher, A., Kim, S. H., Khoury, C. C., Herzig, S. J., Trovato, M. E., Simon-Tillaux, N., Lynch, M. R., Thadhani, R. I., Clish, C. B., Khabbaz, K. R., Rhee, E. P., Waikar, S. S., Berg, A. H., and Parikh, S. M. (2018) De novo NAD(+) biosynthetic impairment in acute kidney injury in humans. *Nat Med* **24**, 1351-1359

36. Schwarcz, R., Bruno, J. P., Muchowski, P. J., and Wu, H. Q. (2012) Kynurenines in the mammalian brain: when physiology meets pathology. *Nat Rev Neurosci* **13**, 465-477

37. Williams, P. A., Harder, J. M., Foxworth, N. E., Cochran, K. E., Philip, V. M., Porciatti, V., Smithies, O., and John, S. W. (2017) Vitamin B(3) modulates mitochondrial vulnerability and prevents glaucoma in aged mice. *Science* **355**, 756-760

38. Yaku, K., Okabe, K., Hikosaka, K., and Nakagawa, T. (2018) NAD Metabolism in Cancer Therapeutics. *Front Oncol* **8**, 622

39. Katsyuba, E., Romani, M., Hofer, D., and Auwerx, J. (2020) NAD(+) homeostasis in health and disease. *Nature metabolism* **2**, 9-31

40. Covarrubias, A. J., Perrone, R., Grozio, A., and Verdin, E. (2021) NAD(+) metabolism and its roles in cellular processes during ageing. *Nat Rev Mol Cell Biol* **22**, 119-141

41. Chini, C. C. S., Peclat, T. R., Warner, G. M., Kashyap, S., Espindola-Netto, J. M., de Oliveira, G. C., Gomez, L. S., Hogan, K. A., Tarragó, M. G., Puranik, A. S., Agorrody, G., Thompson, K. L., Dang, K., Clarke, S., Childs, B. G., Kanamori, K. S., Witte, M. A., Vidal, P., Kirkland, A. L., De Cecco, M., Chellappa, K., McReynolds, M. R., Jankowski, C., Tchkonia, T., Kirkland, J. L., Sedivy, J. M., van Deursen, J. M., Baker, D. J., van Schooten, W., Rabinowitz, J. D., Baur, J. A., and Chini, E. N. (2020) CD38 ecto-enzyme in immune cells is induced during aging and regulates NAD(+) and NMN levels. *Nature metabolism* **2**, 1284-1304

42. Covarrubias, A. J., Kale, A., Perrone, R., Lopez-Dominguez, J. A., Pisco, A. O., Kasler, H. G., Schmidt, M. S., Heckenbach, I., Kwok, R., Wiley, C. D., Wong, H. S., Gibbs, E.,

Iyer, S. S., Basisty, N., Wu, Q., Kim, I. J., Silva, E., Vitangcol, K., Shin, K. O., Lee, Y. M., Riley, R., Ben-Sahra, I., Ott, M., Schilling, B., Scheibye-Knudsen, M., Ishihara, K., Quake, S. R., Newman, J., Brenner, C., Campisi, J., and Verdin, E. (2020) Senescent cells promote tissue NAD(+) decline during ageing via the activation of CD38(+) macrophages. *Nature metabolism* **2**, 1265-1283

43. Brown, K. D., Maqsood, S., Huang, J. Y., Pan, Y., Harkcom, W., Li, W., Sauve, A., Verdin, E., and Jaffrey, S. R. (2014) Activation of SIRT3 by the NAD(+) precursor nicotinamide riboside protects from noise-induced hearing loss. *Cell Metab* **20**, 1059-1068

44. Lin, J. B., Kubota, S., Ban, N., Yoshida, M., Santeford, A., Sene, A., Nakamura, R., Zapata, N., Kubota, M., Tsubota, K., Yoshino, J., Imai, S., and Apte, R. S. (2016) NAMPT-Mediated NAD(+) Biosynthesis Is Essential for Vision In Mice. *Cell Rep* **17**, 69-85

45. Belenky, P., Racette, F. G., Bogan, K. L., McClure, J. M., Smith, J. S., and Brenner, C. (2007) Nicotinamide riboside promotes Sir2 silencing and extends lifespan via Nrk and Urh1/Pnp1/Meu1 pathways to NAD+. *Cell* **129**, 473-484

46. Katsyuba, E., Mottis, A., Zietak, M., De Franco, F., van der Velpen, V., Gariani, K., Ryu, D., Cialabrini, L., Matilainen, O., Liscio, P., Giacche, N., Stokar-Regenscheit, N., Legouis, D., de Seigneux, S., Ivanisevic, J., Raffaelli, N., Schoonjans, K., Pellicciari, R., and Auwerx, J. (2018) De novo NAD(+) synthesis enhances mitochondrial function and improves health. *Nature* **563**, 354-359

47. Yang, Y., Mohammed, F. S., Zhang, N., and Sauve, A. A. (2019) Dihydronicotinamide riboside is a potent NAD(+) concentration enhancer in vitro and in vivo. *J Biol Chem* **294**, 9295-9307

48. Sambeat, A., Ratajczak, J., Joffraud, M., Sanchez-Garcia, J. L., Giner, M. P., Valsesia, A., Giroud-Gerbetant, J., Valera-Alberni, M., Cercillieux, A., Boutant, M., Kulkarni, S. S., Moco, S., and Canto, C. (2019) Endogenous nicotinamide riboside metabolism protects against diet-induced liver damage. *Nat Commun* **10**, 4291

49. Vannini, N., Campos, V., Girotra, M., Trachsel, V., Rojas-Sutterlin, S., Tratwal, J., Ragusa, S., Stefanidis, E., Ryu, D., Rainer, P. Y., Nikitin, G., Giger, S., Li, T. Y., Semilietof, A., Oggier, A., Yersin, Y., Tauzin, L., Pirinen, E., Cheng, W. C., Ratajczak, J., Canto, C., Ehrbar, M., Sizzano, F., Petrova, T. V., Vanhecke, D., Zhang, L., Romero, P., Nahimana, A., Cherix, S., Duchosal, M. A., Ho, P. C., Deplancke, B., Coukos, G., Auwerx, J., Lutolf, M. P., and Naveiras, O. (2019) The NAD-Booster Nicotinamide Riboside Potently Stimulates Hematopoiesis through Increased Mitochondrial Clearance. *Cell Stem Cell* **24**, 405-418 e407

50. Meng, Y., Ren, Z., Xu, F., Zhou, X., Song, C., Wang, V. Y., Liu, W., Lu, L., Thomson, J. A., and Chen, G. (2018) Nicotinamide Promotes Cell Survival and Differentiation as Kinase Inhibitor in Human Pluripotent Stem Cells. *Stem Cell Reports* **11**, 1347-1356

51. Mitchell, S. J., Bernier, M., Aon, M. A., Cortassa, S., Kim, E. Y., Fang, E. F., Palacios, H. H., Ali, A., Navas-Enamorado, I., Di Francesco, A., Kaiser, T. A., Waltz, T. B., Zhang, N., Ellis, J. L., Elliott, P. J., Frederick, D. W., Bohr, V. A., Schmidt, M. S., Brenner, C., Sinclair, D. A., Sauve, A. A., Baur, J. A., and de Cabo, R. (2018)

Nicotinamide Improves Aspects of Healthspan, but Not Lifespan, in Mice. *Cell Metab* **27**, 667-676 e664

52. Rajman, L., Chwalek, K., and Sinclair, D. A. (2018) Therapeutic Potential of NAD-Boosting Molecules: The In Vivo Evidence. *Cell Metab* **27**, 529-547

53. Edwards, C., Canfield, J., Copes, N., Brito, A., Rehan, M., Lipps, D., Brunquell, J., Westerheide, S. D., and Bradshaw, P. C. (2015) Mechanisms of amino acid-mediated lifespan extension in Caenorhabditis elegans. *BMC Genet* **16**, 8

54. Pirinen, E., Auranen, M., Khan, N. A., Brilhante, V., Urho, N., Pessia, A., Hakkarainen, A., Kuula, J., Heinonen, U., Schmidt, M. S., Haimilahti, K., Piirilä, P., Lundbom, N., Taskinen, M. R., Brenner, C., Velagapudi, V., Pietiläinen, K. H., and Suomalainen, A. (2020) Niacin Cures Systemic NAD(+) Deficiency and Improves Muscle Performance in Adult-Onset Mitochondrial Myopathy. *Cell Metab* **31**, 1078-1090.e1075

55. Zhang, H., Ryu, D., Wu, Y., Gariani, K., Wang, X., Luan, P., D'Amico, D., Ropelle, E. R., Lutolf, M. P., Aebersold, R., Schoonjans, K., Menzies, K. J., and Auwerx, J. (2016) NAD^+ repletion improves mitochondrial and stem cell function and enhances life span in mice. *Science* **352**, 1436-1443

56. Ryu, D., Zhang, H., Ropelle, E. R., Sorrentino, V., Mázala, D. A., Mouchiroud, L., Marshall, P. L., Campbell, M. D., Ali, A. S., Knowels, G. M., Bellemin, S., Iyer, S. R., Wang, X., Gariani, K., Sauve, A. A., Cantó, C., Conley, K. E., Walter, L., Lovering, R. M., Chin, E. R., Jasmin, B. J., Marcinek, D. J., Menzies, K. J., and Auwerx, J. (2016) NAD+ repletion improves muscle function in muscular dystrophy and counters global PARylation. *Science translational medicine* **8**, 361ra139

57. Hui, F., Tang, J., Williams, P. A., McGuinness, M. B., Hadoux, X., Casson, R. J., Coote, M., Trounce, I. A., Martin, K. R., van Wijngaarden, P., and Crowston, J. G. (2020) Improvement in inner retinal function in glaucoma with nicotinamide (vitamin B3) supplementation: A crossover randomized clinical trial. *Clinical & experimental ophthalmology* **48**, 903-914

58. Croft, T., Venkatakrishnan, P., and Lin, S. J. (2020) NAD(+) Metabolism and Regulation: Lessons From Yeast. *Biomolecules* **10**

59. Pinson, B., Ceschin, J., Saint-Marc, C., and Daignan-Fornier, B. (2019) Dual control of NAD+ synthesis by purine metabolites in yeast. *eLife* **8**, e43808

60. Tsang, F., and Lin, S.-J. (2015) Less is more: Nutrient limitation induces cross-talk of nutrient sensing pathways with NAD+ homeostasis and contributes to longevity. *Frontiers in biology* **10**, 333-357

61. Cervenka, I., Agudelo, L. Z., and Ruas, J. L. (2017) Kynurenines: Tryptophan's metabolites in exercise, inflammation, and mental health. *Science* **357**, eaaf9794

62. Höglund, E., Øverli, Ø., and Winberg, S. (2019) Tryptophan Metabolic Pathways and Brain Serotonergic Activity: A Comparative Review. *Frontiers in endocrinology* **10**, 158

63. Braidy, N., and Grant, R. (2017) Kynurenine pathway metabolism and neuroinflammatory disease. *Neural regeneration research* **12**, 39-42

64. Sporty, J., Lin, S. J., Kato, M., Ognibene, T., Stewart, B., Turteltaub, K., and Bench, G. (2009) Quantitation of NAD+ biosynthesis from the salvage pathway in Saccharomyces cerevisiae. *Yeast* **26**, 363-369

65. Elvehjem, C. A., Madden, R. J., Strong, F. M., and Woolley, D. W. (1938) THE ISOLATION AND IDENTIFICATION OF THE ANTI-BLACK TONGUE FACTOR. *Journal of Biological Chemistry* **123**, 137-149

66. Axelrod, A. E., Madden, R. J., and Elvehjem, C. A. (1939) THE EFFECT OF A NICOTINIC ACID DEFICIENCY UPON THE COENZYME I CONTENT OF ANIMAL TISSUES. *Journal of Biological Chemistry* **131**, 85-93

67. Kornberg, A. (1948) THE PARTICIPATION OF INORGANIC PYROPHOSPHATE IN THE REVERSIBLE ENZYMATIC SYNTHESIS OF DIPHOSPHOPYRIDINE NUCLEOTIDE. *Journal of Biological Chemistry* **176**, 1475-1476

68. Kato, M., and Lin, S. J. (2014) YCL047C/POF1 Is a Novel Nicotinamide Mononucleotide Adenylyltransferase (NMNAT) in Saccharomyces cerevisiae. *J Biol Chem* **289**, 15577-15587

69. Preiss, J., and Handler, P. (1958) Biosynthesis of diphosphopyridine nucleotide. I. Identification of intermediates. *J Biol Chem* **233**, 488-492

70. Preiss, J., and Handler, P. (1958) Biosynthesis of diphosphopyridine nucleotide. II. Enzymatic aspects. *J Biol Chem* **233**, 493-500

71. Ghislain, M., Talla, E., and Francois, J. M. (2002) Identification and functional analysis of the Saccharomyces cerevisiae nicotinamidase gene, PNC1. *Yeast* **19**, 215-224

72. Emanuelli, M., Carnevali, F., Lorenzi, M., Raffaelli, N., Amici, A., Ruggieri, S., and Magni, G. (1999) Identification and characterization of YLR328W, the Saccharomyces cerevisiae structural gene encoding NMN adenylyltransferase. Expression and characterization of the recombinant enzyme. *FEBS Lett* **455**, 13-17

73. Anderson, R. M., Bitterman, K. J., Wood, J. G., Medvedik, O., Cohen, H., Lin, S. S., Manchester, J. K., Gordon, J. I., and Sinclair, D. A. (2002) Manipulation of a nuclear NAD+ salvage pathway delays aging without altering steady-state NAD+ levels. *J Biol Chem* **277**, 18881-18890

74. Bieganowski, P., Pace, H. C., and Brenner, C. (2003) Eukaryotic NAD+ synthetase Qns1 contains an essential, obligate intramolecular thiol glutamine amidotransferase domain related to nitrilase. *J Biol Chem* **278**, 33049-33055

75. Shats, I., Williams, J. G., Liu, J., Makarov, M. V., Wu, X., Lih, F. B., Deterding, L. J., Lim, C., Xu, X., Randall, T. A., Lee, E., Li, W., Fan, W., Li, J. L., Sokolsky, M., Kabanov, A. V., Li, L., Migaud, M. E., Locasale, J. W., and Li, X. (2020) Bacteria Boost Mammalian Host NAD Metabolism by Engaging the Deamidated Biosynthesis Pathway. *Cell Metab* **31**, 564-579 e567

76. Bieganowski, P., and Brenner, C. (2004) Discoveries of nicotinamide riboside as a nutrient and conserved NRK genes establish a Preiss-Handler independent route to NAD+ in fungi and humans. *Cell* **117**, 495-502

77. Croft, T., Raj, C. J. T., Salemi, M., Phinney, B. S., and Lin, S.-J. (2018) A functional link between NAD+ homeostasis and N-terminal protein acetylation in Saccharomyces cerevisiae. *J Biol Chem* **293**, 2927-2938

78. James Theoga Raj, C., Croft, T., Venkatakrishnan, P., Groth, B., Dhugga, G., Cater, T., and Lin, S. J. (2019) The copper-sensing transcription factor Mac1, the histone deacetylase Hst1, and nicotinic acid regulate de novo NAD(+) biosynthesis in budding yeast. *J Biol Chem* **294**, 5562-5575

79. Llorente, B., and Dujon, B. (2000) Transcriptional regulation of the Saccharomyces cerevisiae DAL5 gene family and identification of the high affinity nicotinic acid permease TNA1 (YGR260w). *FEBS Lett* **475**, 237-241

80. Ohashi, K., Kawai, S., and Murata, K. (2013) Secretion of quinolinic acid, an intermediate in the kynurenine pathway, for utilization in NAD+ biosynthesis in the yeast Saccharomyces cerevisiae. *Eukaryot Cell* **12**, 648-653

81. Belenky, P. A., Moga, T. G., and Brenner, C. (2008) Saccharomyces cerevisiae YOR071C encodes the high affinity nicotinamide riboside transporter Nrt1. *J Biol Chem* **283**, 8075-8079

82. Panozzo, C., Nawara, M., Suski, C., Kucharczyka, R., Skoneczny, M., Becam, A. M., Rytka, J., and Herbert, C. J. (2002) Aerobic and anaerobic NAD+ metabolism in Saccharomyces cerevisiae. *FEBS Lett* **517**, 97-102

83. Ternes, C. M., and Schönknecht, G. (2014) Gene transfers shaped the evolution of de novo NAD+ biosynthesis in eukaryotes. *Genome Biol Evol* **6**, 2335-2349

84. Wogulis, M., Chew, E. R., Donohoue, P. D., and Wilson, D. K. (2008) Identification of formyl kynurenine formamidase and kynurenine aminotransferase from Saccharomyces cerevisiae using crystallographic, bioinformatic and biochemical evidence. *Biochemistry* **47**, 1608-1621

85. Kucharczyk, R., Zagulski, M., Rytka, J., and Herbert, C. J. (1998) The yeast gene YJR025c encodes a 3-hydroxyanthranilic acid dioxygenase and is involved in nicotinic acid biosynthesis. *FEBS Lett* **424**, 127-130

86. Lin, S. J., Defossez, P. A., and Guarente, L. (2000) Requirement of NAD and SIR2 for life-span extension by calorie restriction in Saccharomyces cerevisiae. *Science* **289**, 2126-2128

87. Ohashi, K., Chaleckis, R., Takaine, M., Wheelock, C. E., and Yoshida, S. (2017) Kynurenine aminotransferase activity of Aro8/Aro9 engage tryptophan degradation by producing kynurenic acid in Saccharomyces cerevisiae. *Sci Rep* **7**, 12180

88. Fallarino, F., Grohmann, U., and Puccetti, P. (2012) Indoleamine 2,3-dioxygenase: from catalyst to signaling function. *European journal of immunology* **42**, 1932-1937

89. Amaral, M., Levy, C., Heyes, D. J., Lafite, P., Outeiro, T. F., Giorgini, F., Leys, D., and Scrutton, N. S. (2013) Structural basis of kynurenine 3-monooxygenase inhibition. *Nature* **496**, 382-385

90. Schwarcz, R., and Stone, T. W. (2017) The kynurenine pathway and the brain: Challenges, controversies and promises. *Neuropharmacology* **112**, 237-247

91. Wang, Q., Liu, D., Song, P., and Zou, M. H. (2015) Tryptophan-kynurenine pathway is dysregulated in inflammation, and immune activation. *Frontiers in bioscience (Landmark edition)* **20**, 1116-1143

92. Yuasa, H. J., and Ball, H. J. (2015) Efficient tryptophan-catabolizing activity is consistently conserved through evolution of TDO enzymes, but not IDO enzymes. *Journal of experimental zoology. Part B, Molecular and developmental evolution* **324**, 128-140

93. Belladonna, M. L., Volpi, C., Bianchi, R., Vacca, C., Orabona, C., Pallotta, M. T., Boon, L., Gizzi, S., Fioretti, M. C., Grohmann, U., and Puccetti, P. (2008) Cutting edge: Autocrine TGF-beta sustains default tolerogenesis by IDO-competent dendritic cells. *Journal of immunology (Baltimore, Md. : 1950)* **181**, 5194-5198

94. Pemberton, L. A., Kerr, S. J., Smythe, G., and Brew, B. J. (1997) Quinolinic acid production by macrophages stimulated with IFN-gamma, TNF-alpha, and IFN-alpha. *Journal of interferon & cytokine research : the official journal of the International Society for Interferon and Cytokine Research* **17**, 589-595

95. Munn, D. H. (2011) Indoleamine 2,3-dioxygenase, Tregs and cancer. *Curr Med Chem* **18**, 2240-2246

96. Smith, J. R., Evans, K. J., Wright, A., Willows, R. D., Jamie, J. F., and Griffith, R. (2012) Novel indoleamine 2,3-dioxygenase-1 inhibitors from a multistep in silico screen. *Bioorganic & medicinal chemistry* **20**, 1354-1363

97. Takikawa, O., Yoshida, R., Kido, R., and Hayaishi, O. (1986) Tryptophan degradation in mice initiated by indoleamine 2,3-dioxygenase. *J Biol Chem* **261**, 3648-3653

98. Heyes, M. P., Chen, C. Y., Major, E. O., and Saito, K. (1997) Different kynurenine pathway enzymes limit quinolinic acid formation by various human cell types. *Biochem J* **326 (Pt 2)**, 351-356

99. Song, P., Ramprasath, T., Wang, H., and Zou, M. H. (2017) Abnormal kynurenine pathway of tryptophan catabolism in cardiovascular diseases. *Cell Mol Life Sci* **74**, 2899-2916

100. Guillemin, G. J. (2012) Quinolinic acid: neurotoxicity. *FEBS J* **279**, 1355

101. Hassanain, H. H., Chon, S. Y., and Gupta, S. L. (1993) Differential regulation of human indoleamine 2,3-dioxygenase gene expression by interferons-gamma and -alpha. Analysis of the regulatory region of the gene and identification of an interferon-gamma-inducible DNA-binding factor. *J Biol Chem* **268**, 5077-5084

102. Guillemin, G. J., Kerr, S. J., Smythe, G. A., Smith, D. G., Kapoor, V., Armati, P. J., Croitoru, J., and Brew, B. J. (2001) Kynurenine pathway metabolism in human astrocytes: a paradox for neuronal protection. *Journal of neurochemistry* **78**, 842-853

103. Musso, T., Gusella, G. L., Brooks, A., Longo, D. L., and Varesio, L. (1994) Interleukin-4 inhibits indoleamine 2,3-dioxygenase expression in human monocytes. *Blood* **83**, 1408-1411

104. Chaves, A. C., Cerávolo, I. P., Gomes, J. A., Zani, C. L., Romanha, A. J., and Gazzinelli, R. T. (2001) IL-4 and IL-13 regulate the induction of indoleamine 2,3-dioxygenase

activity and the control of Toxoplasma gondii replication in human fibroblasts activated with IFN-gamma. *European journal of immunology* **31**, 333-344

105. Yan, M. L., Wang, Y. D., Tian, Y. F., Lai, Z. D., and Yan, L. N. (2010) Inhibition of allogeneic T-cell response by Kupffer cells expressing indoleamine 2,3-dioxygenase. *World journal of gastroenterology* **16**, 636-640

106. Moffett, J. R., Arun, P., Puthillathu, N., Vengilote, R., Ives, J. A., Badawy, A. A., and Namboodiri, A. M. (2020) Quinolinate as a Marker for Kynurenine Metabolite Formation and the Unresolved Question of NAD(+) Synthesis During Inflammation and Infection. *Frontiers in immunology* **11**, 31

107. Smith, L. M., Wells, J. D., Vachharajani, V. T., Yoza, B. K., McCall, C. E., and Hoth, J. J. (2015) SIRT1 mediates a primed response to immune challenge after traumatic lung injury. *The journal of trauma and acute care surgery* **78**, 1034-1038

108. Liu, T. F., Yoza, B. K., El Gazzar, M., Vachharajani, V. T., and McCall, C. E. (2011) NAD+-dependent SIRT1 deacetylase participates in epigenetic reprogramming during endotoxin tolerance. *J Biol Chem* **286**, 9856-9864

109. Chang, K. H., Cheng, M. L., Tang, H. Y., Huang, C. Y., Wu, Y. R., and Chen, C. M. (2018) Alternations of Metabolic Profile and Kynurenine Metabolism in the Plasma of Parkinson's Disease. *Molecular neurobiology* **55**, 6319-6328

110. Jia, S. H., Li, Y., Parodo, J., Kapus, A., Fan, L., Rotstein, O. D., and Marshall, J. C. (2004) Pre-B cell colony-enhancing factor inhibits neutrophil apoptosis in experimental inflammation and clinical sepsis. *J Clin Invest* **113**, 1318-1327

111. Zhang, J., Tao, J., Ling, Y., Li, F., Zhu, X., Xu, L., Wang, M., Zhang, S., McCall, C. E., and Liu, T. F. (2019) Switch of NAD Salvage to de novo Biosynthesis Sustains SIRT1-RelB-Dependent Inflammatory Tolerance. *Frontiers in immunology* **10**, 2358

112. Pfefferkorn, E. R. (1984) Interferon gamma blocks the growth of Toxoplasma gondii in human fibroblasts by inducing the host cells to degrade tryptophan. *Proc Natl Acad Sci U S A* **81**, 908-912

113. Schröcksnadel, K., Wirleitner, B., Winkler, C., and Fuchs, D. (2006) Monitoring tryptophan metabolism in chronic immune activation. *Clinica chimica acta; international journal of clinical chemistry* **364**, 82-90

114. Suzuki, Y., Suda, T., Asada, K., Miwa, S., Suzuki, M., Fujie, M., Furuhashi, K., Nakamura, Y., Inui, N., Shirai, T., Hayakawa, H., Nakamura, H., and Chida, K. (2012) Serum indoleamine 2,3-dioxygenase activity predicts prognosis of pulmonary tuberculosis. *Clinical and vaccine immunology : CVI* **19**, 436-442

115. Wang, D., Saga, Y., Mizukami, H., Sato, N., Nonaka, H., Fujiwara, H., Takei, Y., Machida, S., Takikawa, O., Ozawa, K., and Suzuki, M. (2012) Indoleamine-2,3-dioxygenase, an immunosuppressive enzyme that inhibits natural killer cell function, as a useful target for ovarian cancer therapy. *International journal of oncology* **40**, 929-934

116. Divanovic, S., Sawtell, N. M., Trompette, A., Warning, J. I., Dias, A., Cooper, A. M., Yap, G. S., Arditi, M., Shimada, K., Duhadaway, J. B., Prendergast, G. C., Basaraba, R. J., Mellor, A. L., Munn, D. H., Aliberti, J., and Karp, C. L. (2012) Opposing biological

functions of tryptophan catabolizing enzymes during intracellular infection. *The Journal of infectious diseases* **205**, 152-161

117. Munn, D. H., Zhou, M., Attwood, J. T., Bondarev, I., Conway, S. J., Marshall, B., Brown, C., and Mellor, A. L. (1998) Prevention of allogeneic fetal rejection by tryptophan catabolism. *Science* **281**, 1191-1193

118. Grohmann, U., Bianchi, R., Belladonna, M. L., Silla, S., Fallarino, F., Fioretti, M. C., and Puccetti, P. (2000) IFN-gamma inhibits presentation of a tumor/self peptide by CD8 alpha- dendritic cells via potentiation of the CD8 alpha+ subset. *Journal of immunology (Baltimore, Md. : 1950)* **165**, 1357-1363

119. Belladonna, M. L., Grohmann, U., Guidetti, P., Volpi, C., Bianchi, R., Fioretti, M. C., Schwarcz, R., Fallarino, F., and Puccetti, P. (2006) Kynurenine pathway enzymes in dendritic cells initiate tolerogenesis in the absence of functional IDO. *Journal of immunology (Baltimore, Md. : 1950)* **177**, 130-137

120. O'Farrell, K., and Harkin, A. (2017) Stress-related regulation of the kynurenine pathway: Relevance to neuropsychiatric and degenerative disorders. *Neuropharmacology* **112**, 307-323

121. Hill, M., Tanguy-Royer, S., Royer, P., Chauveau, C., Asghar, K., Tesson, L., Lavainne, F., Rémy, S., Brion, R., Hubert, F. X., Heslan, M., Rimbert, M., Berthelot, L., Moffett, J. R., Josien, R., Grégoire, M., and Anegon, I. (2007) IDO expands human CD4+CD25high regulatory T cells by promoting maturation of LPS-treated dendritic cells. *European journal of immunology* **37**, 3054-3062

122. Mezrich, J. D., Fechner, J. H., Zhang, X., Johnson, B. P., Burlingham, W. J., and Bradfield, C. A. (2010) An interaction between kynurenine and the aryl hydrocarbon receptor can generate regulatory T cells. *Journal of immunology (Baltimore, Md. : 1950)* **185**, 3190-3198

123. Kwidzinski, E., and Bechmann, I. (2007) IDO expression in the brain: a double-edged sword. *Journal of molecular medicine (Berlin, Germany)* **85**, 1351-1359

124. Krause, D., Suh, H. S., Tarassishin, L., Cui, Q. L., Durafourt, B. A., Choi, N., Bauman, A., Cosenza-Nashat, M., Antel, J. P., Zhao, M. L., and Lee, S. C. (2011) The tryptophan metabolite 3-hydroxyanthranilic acid plays anti-inflammatory and neuroprotective roles during inflammation: role of hemeoxygenase-1. *The American journal of pathology* **179**, 1360-1372

125. Berger, M., Gray, J. A., and Roth, B. L. (2009) The expanded biology of serotonin. *Annual review of medicine* **60**, 355-366

126. Reiter, R. J., Tan, D. X., Rosales-Corral, S., Galano, A., Zhou, X. J., and Xu, B. (2018) Mitochondria: Central Organelles for Melatonin's Antioxidant and Anti-Aging Actions. *Molecules (Basel, Switzerland)* **23**

127. Emens, J. S., and Burgess, H. J. (2015) Effect of Light and Melatonin and Other Melatonin Receptor Agonists on Human Circadian Physiology. *Sleep medicine clinics* **10**, 435-453

128. Beas, A. O., Gordon, P. B., Prentiss, C. L., Olsen, C. P., Kukurugya, M. A., Bennett, B. D., Parkhurst, S. M., and Gottschling, D. E. (2020) Independent regulation of age associated fat accumulation and longevity. *Nat Commun* **11**, 2790

129. Breda, C., Sathyasaikumar, K. V., Sograte Idrissi, S., Notarangelo, F. M., Estranero, J. G., Moore, G. G., Green, E. W., Kyriacou, C. P., Schwarcz, R., and Giorgini, F. (2016) Tryptophan-2,3-dioxygenase (TDO) inhibition ameliorates neurodegeneration by modulation of kynurenine pathway metabolites. *Proc Natl Acad Sci U S A* **113**, 5435-5440

130. Goda, K., Kishimoto, R., Shimizu, S., Hamane, Y., and Ueda, M. (1996) Quinolinic acid and active oxygens. Possible contribution of active Oxygens during cell death in the brain. *Advances in experimental medicine and biology* **398**, 247-254

131. Stípek, S., Stastný, F., Pláteník, J., Crkovská, J., and Zima, T. (1997) The effect of quinolinate on rat brain lipid peroxidation is dependent on iron. *Neurochemistry international* **30**, 233-237

132. Heyes, M. P., Ellis, R. J., Ryan, L., Childers, M. E., Grant, I., Wolfson, T., Archibald, S., and Jernigan, T. L. (2001) Elevated cerebrospinal fluid quinolinic acid levels are associated with region-specific cerebral volume loss in HIV infection. *Brain : a journal of neurology* **124**, 1033-1042

133. Guillemin, G. J., Williams, K. R., Smith, D. G., Smythe, G. A., Croitoru-Lamoury, J., and Brew, B. J. (2003) Quinolinic acid in the pathogenesis of Alzheimer's disease. *Advances in experimental medicine and biology* **527**, 167-176

134. Flanagan, E. M., Erickson, J. B., Viveros, O. H., Chang, S. Y., and Reinhard, J. F., Jr. (1995) Neurotoxin quinolinic acid is selectively elevated in spinal cords of rats with experimental allergic encephalomyelitis. *Journal of neurochemistry* **64**, 1192-1196

135. Aeinehband, S., Brenner, P., Ståhl, S., Bhat, M., Fidock, M. D., Khademi, M., Olsson, T., Engberg, G., Jokinen, J., Erhardt, S., and Piehl, F. (2016) Cerebrospinal fluid kynurenines in multiple sclerosis; relation to disease course and neurocognitive symptoms. *Brain Behav Immun* **51**, 47-55

136. Beal, M. F., Matson, W. R., Storey, E., Milbury, P., Ryan, E. A., Ogawa, T., and Bird, E. D. (1992) Kynurenic acid concentrations are reduced in Huntington's disease cerebral cortex. *Journal of the neurological sciences* **108**, 80-87

137. Wirthgen, E., Hoeflich, A., Rebl, A., and Günther, J. (2017) Kynurenic Acid: The Janus-Faced Role of an Immunomodulatory Tryptophan Metabolite and Its Link to Pathological Conditions. *Frontiers in immunology* **8**, 1957

138. Baran, H., Jellinger, K., and Deecke, L. (1999) Kynurenine metabolism in Alzheimer's disease. *Journal of neural transmission (Vienna, Austria : 1996)* **106**, 165-181

139. Baran, H., Cairns, N., Lubec, B., and Lubec, G. (1996) Increased kynurenic acid levels and decreased brain kynurenine aminotransferase I in patients with Down syndrome. *Life sciences* **58**, 1891-1899

140. Lewitt, P. A., Li, J., Lu, M., Beach, T. G., Adler, C. H., and Guo, L. (2013) 3-hydroxykynurenine and other Parkinson's disease biomarkers discovered by metabolomic

analysis. *Movement disorders : official journal of the Movement Disorder Society* **28**, 1653-1660

141. Okuda, S., Nishiyama, N., Saito, H., and Katsuki, H. (1996) Hydrogen peroxide-mediated neuronal cell death induced by an endogenous neurotoxin, 3-hydroxykynurenine. *Proc Natl Acad Sci U S A* **93**, 12553-12558

142. Guidetti, P., Bates, G. P., Graham, R. K., Hayden, M. R., Leavitt, B. R., MacDonald, M. E., Slow, E. J., Wheeler, V. C., Woodman, B., and Schwarcz, R. (2006) Elevated brain 3-hydroxykynurenine and quinolinate levels in Huntington disease mice. *Neurobiology of disease* **23**, 190-197

143. Thevandavakkam, M. A., Schwarcz, R., Muchowski, P. J., and Giorgini, F. (2010) Targeting kynurenine 3-monooxygenase (KMO): implications for therapy in Huntington's disease. *CNS & neurological disorders drug targets* **9**, 791-800

144. Mason, R. P., and Giorgini, F. (2011) Modeling Huntington disease in yeast: perspectives and future directions. *Prion* **5**, 269-276

145. Lindquist, C., Bjørndal, B., Lund, A., Slettom, G., Skorve, J., Nygård, O., Svardal, A., and Berge, R. K. (2020) Increased fatty acid oxidation and mitochondrial proliferation in liver are associated with increased plasma kynurenine metabolites and nicotinamide levels in normolipidemic and carnitine-depleted rats. *Biochimica et biophysica acta. Molecular and cell biology of lipids* **1865**, 158543

146. Wolowczuk, I., Hennart, B., Leloire, A., Bessede, A., Soichot, M., Taront, S., Caiazzo, R., Raverdy, V., Pigeyre, M., Guillemin, G. J., Allorge, D., Pattou, F., Froguel, P., and Poulain-Godefroy, O. (2012) Tryptophan metabolism activation by indoleamine 2,3-dioxygenase in adipose tissue of obese women: an attempt to maintain immune homeostasis and vascular tone. *American journal of physiology. Regulatory, integrative and comparative physiology* **303**, R135-143

147. Moffett, J. R., and Namboodiri, M. A. (2003) Tryptophan and the immune response. *Immunology and cell biology* **81**, 247-265

148. Metz, R., Duhadaway, J. B., Kamasani, U., Laury-Kleintop, L., Muller, A. J., and Prendergast, G. C. (2007) Novel tryptophan catabolic enzyme IDO2 is the preferred biochemical target of the antitumor indoleamine 2,3-dioxygenase inhibitory compound D-1-methyl-tryptophan. *Cancer research* **67**, 7082-7087

149. Prendergast, G. C., Metz, R., Muller, A. J., Merlo, L. M., and Mandik-Nayak, L. (2014) IDO2 in Immunomodulation and Autoimmune Disease. *Frontiers in immunology* **5**, 585

150. Opitz, C. A., Litzenburger, U. M., Opitz, U., Sahm, F., Ochs, K., Lutz, C., Wick, W., and Platten, M. (2011) The indoleamine-2,3-dioxygenase (IDO) inhibitor 1-methyl-D-tryptophan upregulates IDO1 in human cancer cells. *PloS one* **6**, e19823

151. Navas, L. E., and Carnero, A. (2021) NAD(+) metabolism, stemness, the immune response, and cancer. *Signal transduction and targeted therapy* **6**, 2

152. Brochez, L., Chevolet, I., and Kruse, V. (2017) The rationale of indoleamine 2,3-dioxygenase inhibition for cancer therapy. *European journal of cancer (Oxford, England : 1990)* **76**, 167-182

153. Löb, S., Königsrainer, A., Zieker, D., Brücher, B. L., Rammensee, H. G., Opelz, G., and Terness, P. (2009) IDO1 and IDO2 are expressed in human tumors: levo- but not dextro-1-methyl tryptophan inhibits tryptophan catabolism. *Cancer immunology, immunotherapy : CII* **58**, 153-157

154. Majumdar, T., Sharma, S., Kumar, M., Hussain, M. A., Chauhan, N., Kalia, I., Sahu, A. K., Rana, V. S., Bharti, R., Haldar, A. K., Singh, A. P., and Mazumder, S. (2019) Tryptophan-kynurenine pathway attenuates β-catenin-dependent pro-parasitic role of STING-TICAM2-IRF3-IDO1 signalosome in Toxoplasma gondii infection. *Cell death & disease* **10**, 161

155. Abo-Al-Ela, H. G. (2020) Toxoplasmosis and Psychiatric and Neurological Disorders: A Step toward Understanding Parasite Pathogenesis. *ACS chemical neuroscience* **11**, 2393-2406

156. Crozier-Reabe, K. R., Phillips, R. S., and Moran, G. R. (2008) Kynurenine 3-monooxygenase from Pseudomonas fluorescens: substrate-like inhibitors both stimulate flavin reduction and stabilize the flavin-peroxo intermediate yet result in the production of hydrogen peroxide. *Biochemistry* **47**, 12420-12433

157. Formisano, S., Hornig, M., Yaddanapudi, K., Vasishtha, M., Parsons, L. H., Briese, T., Lipkin, W. I., and Williams, B. L. (2017) Central Nervous System Infection with Borna Disease Virus Causes Kynurenine Pathway Dysregulation and Neurotoxic Quinolinic Acid Production. *Journal of virology* **91**

158. Thomas, T., Stefanoni, D., Reisz, J. A., Nemkov, T., Bertolone, L., Francis, R. O., Hudson, K. E., Zimring, J. C., Hansen, K. C., Hod, E. A., Spitalnik, S. L., and D'Alessandro, A. (2020) COVID-19 infection alters kynurenine and fatty acid metabolism, correlating with IL-6 levels and renal status. *JCI insight* **5**

159. Bipath, P., Levay, P. F., and Viljoen, M. (2015) The kynurenine pathway activities in a sub-Saharan HIV/AIDS population. *BMC infectious diseases* **15**, 346

160. Hayes, R. (1989) Surveillance for AIDS in Uganda. *World Health Organization AIDS technical bulletin* **2**, 85-86

161. Look, M. P., Altfeld, M., Kreuzer, K. A., Riezler, R., Stabler, S. P., Allen, R. H., Sauerbruch, T., and Rockstroh, J. K. (2000) Parallel decrease in neurotoxin quinolinic acid and soluble tumor necrosis factor receptor p75 in serum during highly active antiretroviral therapy of HIV type 1 disease. *AIDS research and human retroviruses* **16**, 1215-1221

162. McArthur, J. C., Steiner, J., Sacktor, N., and Nath, A. (2010) Human immunodeficiency virus-associated neurocognitive disorders: Mind the gap. *Annals of neurology* **67**, 699-714

163. Kardashian, A., Ma, Y., Yin, M. T., Scherzer, R., Nolan, O., Aweeka, F., Tien, P. C., and Price, J. C. (2019) High Kynurenine:Tryptophan Ratio Is Associated With Liver Fibrosis in HIV-Monoinfected and HIV/Hepatitis C Virus-Coinfected Women. *Open forum infectious diseases* **6**, ofz281

164. Jenabian, M. A., Mehraj, V., Costiniuk, C. T., Vyboh, K., Kema, I., Rollet, K., Paulino Ramirez, R., Klein, M. B., and Routy, J. P. (2016) Influence of Hepatitis C Virus

Sustained Virological Response on Immunosuppressive Tryptophan Catabolism in ART-Treated HIV/HCV Coinfected Patients. *Journal of acquired immune deficiency syndromes (1999)* **71**, 254-262

165. Larrea, E., Riezu-Boj, J. I., Gil-Guerrero, L., Casares, N., Aldabe, R., Sarobe, P., Civeira, M. P., Heeney, J. L., Rollier, C., Verstrepen, B., Wakita, T., Borrás-Cuesta, F., Lasarte, J. J., and Prieto, J. (2007) Upregulation of indoleamine 2,3-dioxygenase in hepatitis C virus infection. *Journal of virology* **81**, 3662-3666

166. Inoue, H., Matsushige, T., Ichiyama, T., Okuno, A., Takikawa, O., Tomonaga, S., Anlar, B., Yüksel, D., Otsuka, Y., Kohno, F., Hoshide, M., Ohga, S., and Hasegawa, S. (2020) Elevated quinolinic acid levels in cerebrospinal fluid in subacute sclerosing panencephalitis. *Journal of neuroimmunology* **339**, 577088

167. Lehrmann, E., Guidetti, P., Löve, A., Williamson, J., Bertram, E. H., and Schwarcz, R. (2008) Glial activation precedes seizures and hippocampal neurodegeneration in measles virus-infected mice. *Epilepsia* **49 Suppl 2**, 13-23

168. Choera, T., Zelante, T., Romani, L., and Keller, N. P. (2017) A Multifaceted Role of Tryptophan Metabolism and Indoleamine 2,3-Dioxygenase Activity in Aspergillus fumigatus-Host Interactions. *Frontiers in immunology* **8**, 1996

169. Zelante, T., Choera, T., Beauvais, A., Fallarino, F., Paolicelli, G., Pieraccini, G., Pieroni, M., Galosi, C., Beato, C., De Luca, A., Boscaro, F., Romoli, R., Liu, X., Warris, A., Verweij, P. E., Ballard, E., Borghi, M., Pariano, M., Costantino, G., Calvitti, M., Vacca, C., Oikonomou, V., Gargaro, M., Wong, A. Y. W., Boon, L., den Hartog, M., Spáčil, Z., Puccetti, P., Latgè, J. P., Keller, N. P., and Romani, L. (2021) Aspergillus fumigatus tryptophan metabolic route differently affects host immunity. *Cell Rep* **34**, 108673

170. Bedalov, A., Hirao, M., Posakony, J., Nelson, M., and Simon, J. A. (2003) NAD+-dependent deacetylase Hst1p controls biosynthesis and cellular NAD+ levels in Saccharomyces cerevisiae. *Mol Cell Biol* **23**, 7044-7054

171. Medvedik, O., Lamming, D. W., Kim, K. D., and Sinclair, D. A. (2007) MSN2 and MSN4 link calorie restriction and TOR to sirtuin-mediated lifespan extension in Saccharomyces cerevisiae. *PLoS Biol* **5**, e261

172. Anderson, R. M., Bitterman, K. J., Wood, J. G., Medvedik, O., and Sinclair, D. A. (2003) Nicotinamide and PNC1 govern lifespan extension by calorie restriction in Saccharomyces cerevisiae. *Nature* **423**, 181-185

173. Gallo, C. M., Smith, D. L., Jr., and Smith, J. S. (2004) Nicotinamide clearance by Pnc1 directly regulates Sir2-mediated silencing and longevity. *Mol Cell Biol* **24**, 1301-1312

174. Lu, S. P., Kato, M., and Lin, S. J. (2009) Assimilation of endogenous nicotinamide riboside is essential for calorie restriction-mediated life span extension in Saccharomyces cerevisiae. *J Biol Chem* **284**, 17110-17119

175. Bieganowski, P., Seidle, H. F., Wojcik, M., and Brenner, C. (2006) Synthetic Lethal and Biochemical Analyses of NAD and NADH Kinases in Saccharomyces cerevisiae Establish Separation of Cellular Functions. *Journal of Biological Chemistry* **281**, 22439-22445

176. Cankorur-Cetinkaya, A., Eraslan, S., and Kirdar, B. (2016) Transcriptomic response of yeast cells to ATX1 deletion under different copper levels. *BMC genomics* **17**, 489

177. Keller, G., Bird, A., and Winge, D. R. (2005) Independent metalloregulation of Ace1 and Mac1 in Saccharomyces cerevisiae. *Eukaryot Cell* **4**, 1863-1871

178. Yuan, D. S., Stearman, R., Dancis, A., Dunn, T., Beeler, T., and Klausner, R. D. (1995) The Menkes/Wilson disease gene homologue in yeast provides copper to a ceruloplasmin-like oxidase required for iron uptake. *Proc Natl Acad Sci U S A* **92**, 2632-2636

179. De Freitas, J., Wintz, H., Kim, J. H., Poynton, H., Fox, T., and Vulpe, C. (2003) Yeast, a model organism for iron and copper metabolism studies. *Biometals : an international journal on the role of metal ions in biology, biochemistry, and medicine* **16**, 185-197

180. Lin, S. J., Pufahl, R. A., Dancis, A., O'Halloran, T. V., and Culotta, V. C. (1997) A role for the Saccharomyces cerevisiae ATX1 gene in copper trafficking and iron transport. *J Biol Chem* **272**, 9215-9220

181. Zhang, Y., Colabroy, K. L., Begley, T. P., and Ealick, S. E. (2005) Structural studies on 3-hydroxyanthranilate-3,4-dioxygenase: the catalytic mechanism of a complex oxidation involved in NAD biosynthesis. *Biochemistry* **44**, 7632-7643

182. Stachowski, E. K., and Schwarcz, R. (2012) Regulation of quinolinic acid neosynthesis in mouse, rat and human brain by iron and iron chelators in vitro. *Journal of neural transmission (Vienna, Austria : 1996)* **119**, 123-131

183. Pláteník, J., Stopka, P., Vejrazka, M., and Stípek, S. (2001) Quinolinic acid-iron(ii) complexes: slow autoxidation, but enhanced hydroxyl radical production in the Fenton reaction. *Free radical research* **34**, 445-459

184. Pinson, B., Vaur, S., Sagot, I., Coulpier, F., Lemoine, S., and Daignan-Fornier, B. (2009) Metabolic intermediates selectively stimulate transcription factor interaction and modulate phosphate and purine pathways. *Genes Dev* **23**, 1399-1407

185. Perli, T., Wronska, A. K., Ortiz-Merino, R. A., Pronk, J. T., and Daran, J. M. (2020) Vitamin requirements and biosynthesis in Saccharomyces cerevisiae. *Yeast* **37**, 283-304

186. Nelp, M. T., Kates, P. A., Hunt, J. T., Newitt, J. A., Balog, A., Maley, D., Zhu, X., Abell, L., Allentoff, A., Borzilleri, R., Lewis, H. A., Lin, Z., Seitz, S. P., Yan, C., and Groves, J. T. (2018) Immune-modulating enzyme indoleamine 2,3-dioxygenase is effectively inhibited by targeting its apo-form. *Proc Natl Acad Sci U S A* **115**, 3249-3254

187. Donley, D. W., Realing, M., Gigley, J. P., and Fox, J. H. (2019) Iron activates microglia and directly stimulates indoleamine-2,3-dioxygenase activity in the N171-82Q mouse model of Huntington's disease. *bioRxiv*, 550905

188. Lee, Y. K., Lee, H. B., Shin, D. M., Kang, M. J., Yi, E. C., Noh, S., Lee, J., Lee, C., Min, C. K., and Choi, E. Y. (2014) Heme-binding-mediated negative regulation of the tryptophan metabolic enzyme indoleamine 2,3-dioxygenase 1 (IDO1) by IDO2. *Experimental & molecular medicine* **46**, e121

189. Cerejo, M., Andrade, G., Roca, C., Sousa, J., Rodrigues, C., Pinheiro, R., Chatterjee, S., Vieira, H., and Calado, P. (2012) A powerful yeast-based screening assay for the

identification of inhibitors of indoleamine 2,3-dioxygenase. *Journal of biomolecular screening* **17**, 1362-1371

190. Braun, R. J. (2012) Mitochondrion-mediated cell death: dissecting yeast apoptosis for a better understanding of neurodegeneration. *Front Oncol* **2**, 182

191. Giorgini, F., Guidetti, P., Nguyen, Q., Bennett, S. C., and Muchowski, P. J. (2005) A genomic screen in yeast implicates kynurenine 3-monooxygenase as a therapeutic target for Huntington disease. *Nat Genet* **37**, 526-531

192. Giorgini, F., Möller, T., Kwan, W., Zwilling, D., Wacker, J. L., Hong, S., Tsai, L. C., Cheah, C. S., Schwarcz, R., Guidetti, P., and Muchowski, P. J. (2008) Histone deacetylase inhibition modulates kynurenine pathway activation in yeast, microglia, and mice expressing a mutant huntingtin fragment. *J Biol Chem* **283**, 7390-7400

193. Zwilling, D., Huang, S. Y., Sathyasaikumar, K. V., Notarangelo, F. M., Guidetti, P., Wu, H. Q., Lee, J., Truong, J., Andrews-Zwilling, Y., Hsieh, E. W., Louie, J. Y., Wu, T., Scearce-Levie, K., Patrick, C., Adame, A., Giorgini, F., Moussaoui, S., Laue, G., Rassoulpour, A., Flik, G., Huang, Y., Muchowski, J. M., Masliah, E., Schwarcz, R., and Muchowski, P. J. (2011) Kynurenine 3-monooxygenase inhibition in blood ameliorates neurodegeneration. *Cell* **145**, 863-874

194. Gudipati, V., Koch, K., Lienhart, W. D., and Macheroux, P. (2014) The flavoproteome of the yeast Saccharomyces cerevisiae. *Biochim Biophys Acta* **1844**, 535-544

195. Giancaspero, T. A., Locato, V., and Barile, M. (2013) A regulatory role of NAD redox status on flavin cofactor homeostasis in S. cerevisiae mitochondria. *Oxidative medicine and cellular longevity* **2013**, 612784

196. di Salvo, M. L., Contestabile, R., and Safo, M. K. (2011) Vitamin B(6) salvage enzymes: mechanism, structure and regulation. *Biochim Biophys Acta* **1814**, 1597-1608

197. Ubbink, J. B., Bissbort, S., Vermaak, W. J., and Delport, R. (1990) Inhibition of pyridoxal kinase by methylxanthines. *Enzyme* **43**, 72-79

198. Lainé-Cessac, P., Cailleux, A., and Allain, P. (1997) Mechanisms of the inhibition of human erythrocyte pyridoxal kinase by drugs. *Biochemical pharmacology* **54**, 863-870

199. Lima, S., Khristoforov, R., Momany, C., and Phillips, R. S. (2007) Crystal structure of Homo sapiens kynureninase. *Biochemistry* **46**, 2735-2744

200. Rossi, F., Han, Q., Li, J., Li, J., and Rizzi, M. (2004) Crystal structure of human kynurenine aminotransferase I. *J Biol Chem* **279**, 50214-50220

201. Bernstein, B. E., Tong, J. K., and Schreiber, S. L. (2000) Genomewide studies of histone deacetylase function in yeast. *Proc Natl Acad Sci U S A* **97**, 13708-13713

202. Ivy, J. M., Klar, A. J., and Hicks, J. B. (1986) Cloning and characterization of four SIR genes of Saccharomyces cerevisiae. *Mol Cell Biol* **6**, 688-702

203. Rine, J., and Herskowitz, I. (1987) Four genes responsible for a position effect on expression from HML and HMR in Saccharomyces cerevisiae. *Genetics* **116**, 9-22

204. Fritze, C. E., Verschueren, K., Strich, R., and Easton Esposito, R. (1997) Direct evidence for SIR2 modulation of chromatin structure in yeast rDNA. *Embo j* **16**, 6495-6509

205. Aparicio, O. M., Billington, B. L., and Gottschling, D. E. (1991) Modifiers of position effect are shared between telomeric and silent mating-type loci in S. cerevisiae. *Cell* **66**, 1279-1287

206. Xu, F., Zhang, Q., Zhang, K., Xie, W., and Grunstein, M. (2007) Sir2 deacetylates histone H3 lysine 56 to regulate telomeric heterochromatin structure in yeast. *Mol Cell* **27**, 890-900

207. Bitterman, K. J., Anderson, R. M., Cohen, H. Y., Latorre-Esteves, M., and Sinclair, D. A. (2002) Inhibition of silencing and accelerated aging by nicotinamide, a putative negative regulator of yeast sir2 and human SIRT1. *J Biol Chem* **277**, 45099-45107

208. Schmidt, M. T., Smith, B. C., Jackson, M. D., and Denu, J. M. (2004) Coenzyme specificity of Sir2 protein deacetylases: implications for physiological regulation. *J Biol Chem* **279**, 40122-40129

209. Avalos, J. L., Bever, K. M., and Wolberger, C. (2005) Mechanism of Sirtuin Inhibition by Nicotinamide: Altering the NAD+ Cosubstrate Specificity of a Sir2 Enzyme. *Molecular Cell* **17**, 855-868

210. Sutton, A., Heller, R. C., Landry, J., Choy, J. S., Sirko, A., and Sternglanz, R. (2001) A novel form of transcriptional silencing by Sum1-1 requires Hst1 and the origin recognition complex. *Mol Cell Biol* **21**, 3514-3522

211. Brachmann, C. B., Sherman, J. M., Devine, S. E., Cameron, E. E., Pillus, L., and Boeke, J. D. (1995) The SIR2 gene family, conserved from bacteria to humans, functions in silencing, cell cycle progression, and chromosome stability. *Genes Dev* **9**, 2888-2902

212. Derbyshire, M. K., Weinstock, K. G., and Strathern, J. N. (1996) HST1, a new member of the SIR2 family of genes. *Yeast* **12**, 631-640

213. Kang, W. K., Devare, M., and Kim, J. Y. (2017) HST1 increases replicative lifespan of a sir2Delta mutant in the absence of PDE2 in Saccharomyces cerevisiae. *J Microbiol* **55**, 123-129

214. Xie, J., Pierce, M., Gailus-Durner, V., Wagner, M., Winter, E., and Vershon, A. K. (1999) Sum1 and Hst1 repress middle sporulation-specific gene expression during mitosis in Saccharomyces cerevisiae. *EMBO J* **18**, 6448-6454

215. McCord, R., Pierce, M., Xie, J., Wonkatal, S., Mickel, C., and Vershon, A. K. (2003) Rfm1, a novel tethering factor required to recruit the Hst1 histone deacetylase for repression of middle sporulation genes. *Mol Cell Biol* **23**, 2009-2016

216. Li, M., Valsakumar, V., Poorey, K., Bekiranov, S., and Smith, J. S. (2013) Genome-wide analysis of functional sirtuin chromatin targets in yeast. *Genome Biol* **14**, R48

217. Guillemette, B., Drogaris, P., Lin, H. H., Armstrong, H., Hiragami-Hamada, K., Imhof, A., Bonneil, E., Thibault, P., Verreault, A., and Festenstein, R. J. (2011) H3 lysine 4 is acetylated at active gene promoters and is regulated by H3 lysine 4 methylation. *PLoS Genet* **7**, e1001354

218. Weber, J. M., Irlbacher, H., and Ehrenhofer-Murray, A. E. (2008) Control of replication initiation by the Sum1/Rfm1/Hst1 histone deacetylase. *BMC Mol Biol* **9**, 100

219. Park, S. Y., and Kim, J. S. (2020) A short guide to histone deacetylases including recent progress on class II enzymes. *Experimental & molecular medicine* **52**, 204-212

220. Rundlett, S. E., Carmen, A. A., Kobayashi, R., Bavykin, S., Turner, B. M., and Grunstein, M. (1996) HDA1 and RPD3 are members of distinct yeast histone deacetylase complexes that regulate silencing and transcription. *Proc Natl Acad Sci U S A* **93**, 14503-14508

221. Kurdistani, S. K., Robyr, D., Tavazoie, S., and Grunstein, M. (2002) Genome-wide binding map of the histone deacetylase Rpd3 in yeast. *Nat Genet* **31**, 248-254

222. Carrozza, M. J., Florens, L., Swanson, S. K., Shia, W. J., Anderson, S., Yates, J., Washburn, M. P., and Workman, J. L. (2005) Stable incorporation of sequence specific repressors Ash1 and Ume6 into the Rpd3L complex. *Biochim Biophys Acta* **1731**, 77-87; discussion 75-76

223. Carrozza, M. J., Li, B., Florens, L., Suganuma, T., Swanson, S. K., Lee, K. K., Shia, W. J., Anderson, S., Yates, J., Washburn, M. P., and Workman, J. L. (2005) Histone H3 methylation by Set2 directs deacetylation of coding regions by Rpd3S to suppress spurious intragenic transcription. *Cell* **123**, 581-592

224. Grzenda, A., Lomberk, G., Zhang, J. S., and Urrutia, R. (2009) Sin3: master scaffold and transcriptional corepressor. *Biochim Biophys Acta* **1789**, 443-450

225. Sharma, V. M., Tomar, R. S., Dempsey, A. E., and Reese, J. C. (2007) Histone deacetylases RPD3 and HOS2 regulate the transcriptional activation of DNA damage-inducible genes. *Mol Cell Biol* **27**, 3199-3210

226. Knott, S. R., Viggiani, C. J., Tavaré, S., and Aparicio, O. M. (2009) Genome-wide replication profiles indicate an expansive role for Rpd3L in regulating replication initiation timing or efficiency, and reveal genomic loci of Rpd3 function in Saccharomyces cerevisiae. *Genes Dev* **23**, 1077-1090

227. Kadosh, D., and Struhl, K. (1997) Repression by Ume6 involves recruitment of a complex containing Sin3 corepressor and Rpd3 histone deacetylase to target promoters. *Cell* **89**, 365-371

228. Takahata, S., Yu, Y., and Stillman, D. J. (2011) Repressive chromatin affects factor binding at yeast HO (homothallic switching) promoter. *J Biol Chem* **286**, 34809-34819

229. Pinskaya, M., Gourvennec, S., and Morillon, A. (2009) H3 lysine 4 di- and tri-methylation deposited by cryptic transcription attenuates promoter activation. *Embo j* **28**, 1697-1707

230. Terzi, N., Churchman, L. S., Vasiljeva, L., Weissman, J., and Buratowski, S. (2011) H3K4 trimethylation by Set1 promotes efficient termination by the Nrd1-Nab3-Sen1 pathway. *Mol Cell Biol* **31**, 3569-3583

231. Lee, B. B., Choi, A., Kim, J. H., Jun, Y., Woo, H., Ha, S. D., Yoon, C. Y., Hwang, J. T., Steinmetz, L., Buratowski, S., Lee, S., Kim, H. Y., and Kim, T. (2018) Rpd3L HDAC links H3K4me3 to transcriptional repression memory. *Nucleic Acids Res* **46**, 8261-8274

232. Takahata, S., Yu, Y., and Stillman, D. J. (2009) The E2F functional analogue SBF recruits the Rpd3(L) HDAC, via Whi5 and Stb1, and the FACT chromatin reorganizer, to yeast G1 cyclin promoters. *Embo j* **28**, 3378-3389

233. Li, B., Gogol, M., Carey, M., Pattenden, S. G., Seidel, C., and Workman, J. L. (2007) Infrequently transcribed long genes depend on the Set2/Rpd3S pathway for accurate transcription. *Genes Dev* **21**, 1422-1430

234. Shahbazian, M. D., and Grunstein, M. (2007) Functions of Site-Specific Histone Acetylation and Deacetylation. *Annual Review of Biochemistry* **76**, 75-100

235. Delcuve, G. P., Khan, D. H., and Davie, J. R. (2012) Roles of histone deacetylases in epigenetic regulation: emerging paradigms from studies with inhibitors. *Clinical Epigenetics* **4**, 5

236. Sun, Z. W., and Hampsey, M. (1999) A general requirement for the Sin3-Rpd3 histone deacetylase complex in regulating silencing in Saccharomyces cerevisiae. *Genetics* **152**, 921-932

237. Loewith, R., Smith, J. S., Meijer, M., Williams, T. J., Bachman, N., Boeke, J. D., and Young, D. (2001) Pho23 is associated with the Rpd3 histone deacetylase and is required for its normal function in regulation of gene expression and silencing in Saccharomyces cerevisiae. *J Biol Chem* **276**, 24068-24074

238. Ruiz-Roig, C., Viéitez, C., Posas, F., and De Nadal, E. (2010) The Rpd3L HDAC complex is essential for the heat stress response in yeast. *Molecular Microbiology* **76**, 1049-1062

239. Yeheskely-Hayon, D., Minai, L., Golan, L., Dann, E. J., and Yelin, D. (2013) Optically Induced Cell Fusion Using Bispecific Nanoparticles. *Small* **9**, 3771-3777

240. Sertil, O., Vemula, A., Salmon, S. L., Morse, R. H., and Lowry, C. V. (2007) Direct role for the Rpd3 complex in transcriptional induction of the anaerobic DAN/TIR genes in yeast. *Mol Cell Biol* **27**, 2037-2047

241. Lardenois, A., Stuparevic, I., Liu, Y., Law, M. J., Becker, E., Smagulova, F., Waern, K., Guilleux, M. H., Horecka, J., Chu, A., Kervarrec, C., Strich, R., Snyder, M., Davis, R. W., Steinmetz, L. M., and Primig, M. (2015) The conserved histone deacetylase Rpd3 and its DNA binding subunit Ume6 control dynamic transcript architecture during mitotic growth and meiotic development. *Nucleic Acids Res* **43**, 115-128

242. Shanmugam, G., Rakshit, S., and Sarkar, K. (2022) HDAC inhibitors: Targets for tumor therapy, immune modulation and lung diseases. *Translational Oncology* **16**, 101312

243. Shukla, S., and Tekwani, B. L. (2020) Histone Deacetylases Inhibitors in Neurodegenerative Diseases, Neuroprotection and Neuronal Differentiation. *Frontiers in Pharmacology* **11**

244. Yoon, S., and Eom, G. H. (2016) HDAC and HDAC Inhibitor: From Cancer to Cardiovascular Diseases. *Chonnam Med J* **52**, 1-11

245. Tempel, W., Rabeh, W. M., Bogan, K. L., Belenky, P., Wojcik, M., Seidle, H. F., Nedyalkova, L., Yang, T., Sauve, A. A., Park, H. W., and Brenner, C. (2007)

Nicotinamide riboside kinase structures reveal new pathways to NAD+. *PLoS Biol* **5**, e263

246. Emanuelli, M., Amici, A., Carnevali, F., Pierella, F., Raffaelli, N., and Magni, G. (2003) Identification and characterization of a second NMN adenylyltransferase gene in Saccharomyces cerevisiae. *Protein expression and purification* **27**, 357-364

247. Suka, N., Suka, Y., Carmen, A. A., Wu, J., and Grunstein, M. (2001) Highly specific antibodies determine histone acetylation site usage in yeast heterochromatin and euchromatin. *Mol Cell* **8**, 473-479

248. Thurtle-Schmidt, D. M., Dodson, A. E., and Rine, J. (2016) Histone Deacetylases with Antagonistic Roles in Saccharomyces cerevisiae Heterochromatin Formation. *Genetics* **204**, 177-190

249. Amoiradaki, K., Bunting, K. R., Paine, K. M., Ayre, J. E., Hogg, K., Laidlaw, K. M. E., and MacDonald, C. (2021) The Rpd3-Complex Regulates Expression of Multiple Cell Surface Recycling Factors in Yeast. *Int J Mol Sci* **22**

250. Zhou, J., Zhou, B. O., Lenzmeier, B. A., and Zhou, J. Q. (2009) Histone deacetylase Rpd3 antagonizes Sir2-dependent silent chromatin propagation. *Nucleic Acids Res* **37**, 3699-3713

251. Peng, L., and Seto, E. (2011) Deacetylation of nonhistone proteins by HDACs and the implications in cancer. *Handb Exp Pharmacol* **206**, 39-56

252. Glozak, M. A., Sengupta, N., Zhang, X., and Seto, E. (2005) Acetylation and deacetylation of non-histone proteins. *Gene* **363**, 15-23

253. Oppikofer, M., Kueng, S., Martino, F., Soeroes, S., Hancock, S. M., Chin, J. W., Fischle, W., and Gasser, S. M. (2011) A dual role of H4K16 acetylation in the establishment of yeast silent chromatin. *EMBO J* **30**, 2610-2621

254. Zhao, C., Dong, H., Xu, Q., and Zhang, Y. (2020) Histone deacetylase (HDAC) inhibitors in cancer: a patent review (2017-present). *Expert Opin Ther Pat* **30**, 263-274

255. Hull, E. E., Montgomery, M. R., and Leyva, K. J. (2016) HDAC Inhibitors as Epigenetic Regulators of the Immune System: Impacts on Cancer Therapy and Inflammatory Diseases. *Biomed Res Int* **2016**, 8797206

256. Vaca, H. R., Celentano, A. M., Toscanini, M. A., Heimburg, T., Ghazy, E., Zeyen, P., Hauser, A. T., Oliveira, G., Elissondo, M. C., Jung, M., Sippl, W., Camicia, F., and Rosenzvit, M. C. (2021) The potential for histone deacetylase (HDAC) inhibitors as cestocidal drugs. *PLoS Negl Trop Dis* **15**, e0009226

257. Brachmann, C. B., Davies, A., Cost, G. J., Caputo, E., Li, J., Hieter, P., and Boeke, J. D. (1998) Designer deletion strains derived from Saccharomyces cerevisiae S288C: a useful set of strains and plasmids for PCR-mediated gene disruption and other applications. *Yeast* **14**, 115-132

258. Burke, D., Dawson, D., and Sterns, T. (2000) Methods in Yeast Genetics. Cold Spring Harbor Laboratory Press, Cold Spring Harbor, NY. pp 171-174

259. Lu, W., Su, X., Klein, M. S., Lewis, I. A., Fiehn, O., and Rabinowitz, J. D. (2017) Metabolite Measurement: Pitfalls to Avoid and Practices to Follow. *Annu Rev Biochem* **86**, 277-304

260. Fiehn, O. (2016) Metabolomics by Gas Chromatography-Mass Spectrometry: Combined Targeted and Untargeted Profiling. *Curr Protoc Mol Biol* **114**, 30 34 31-30 34 32

261. Kind, T., Wohlgemuth, G., Lee, D. Y., Lu, Y., Palazoglu, M., Shahbaz, S., and Fiehn, O. (2009) FiehnLib: mass spectral and retention index libraries for metabolomics based on quadrupole and time-of-flight gas chromatography/mass spectrometry. *Anal Chem* **81**, 10038-10048

262. Lai, Z., Tsugawa, H., Wohlgemuth, G., Mehta, S., Mueller, M., Zheng, Y., Ogiwara, A., Meissen, J., Showalter, M., Takeuchi, K., Kind, T., Beal, P., Arita, M., and Fiehn, O. (2018) Identifying metabolites by integrating metabolome databases with mass spectrometry cheminformatics. *Nat Methods* **15**, 53-56

263. Li, M., Petteys, B. J., McClure, J. M., Valsakumar, V., Bekiranov, S., Frank, E. L., and Smith, J. S. (2010) Thiamine biosynthesis in Saccharomyces cerevisiae is regulated by the NAD+-dependent histone deacetylase Hst1. *Mol Cell Biol* **30**, 3329-3341

264. Xie, N., Zhang, L., Gao, W., Huang, C., Huber, P. E., Zhou, X., Li, C., Shen, G., and Zou, B. (2020) NAD(+) metabolism: pathophysiologic mechanisms and therapeutic potential. *Signal transduction and targeted therapy* **5**, 227

265. Lautrup, S., Sinclair, D. A., Mattson, M. P., and Fang, E. F. (2019) NAD(+) in Brain Aging and Neurodegenerative Disorders. *Cell Metab* **30**, 630-655

266. Lin, Q., Zuo, W., Liu, Y., Wu, K., and Liu, Q. (2021) NAD(+) and cardiovascular diseases. *Clinica chimica acta; international journal of clinical chemistry* **515**, 104-110

267. Tummala, Krishna S., Gomes, Ana L., Yilmaz, M., Graña, O., Bakiri, L., Ruppen, I., Ximénez-Embún, P., Sheshappanavar, V., Rodriguez-Justo, M., Pisano, David G., Wagner, Erwin F., and Djouder, N. (2014) Inhibition of De Novo NAD+ Synthesis by Oncogenic URI Causes Liver Tumorigenesis through DNA Damage. *Cancer Cell* **26**, 826-839

268. Hong, S. M., Hwang, S. W., Wang, T., Park, C. W., Ryu, Y. M., Jung, J. H., Shin, J. H., Kim, S. Y., Lee, J. L., Kim, C. W., Yoon, G., Kim, K. H., Myung, S. J., and Choi, K. Y. (2019) Increased nicotinamide adenine dinucleotide pool promotes colon cancer progression by suppressing reactive oxygen species level. *Cancer Sci* **110**, 629-638

269. Gujar, A. D., Le, S., Mao, D. D., Dadey, D. Y. A., Turski, A., Sasaki, Y., Aum, D., Luo, J., Dahiya, S., Yuan, L., Rich, K. M., Milbrandt, J., Hallahan, D. E., Yano, H., Tran, D. D., and Kim, A. H. (2016) An NAD+-dependent transcriptional program governs self-renewal and radiation resistance in glioblastoma. *Proceedings of the National Academy of Sciences* **113**, E8247-E8256

270. Jahan, F., and Bagchi, R. A. (2021) Enhancing NAD(+) Metabolome in Cardiovascular Diseases: Promises and Considerations. *Front Cardiovasc Med* **8**, 716989

271. Hou, Y., Wei, Y., Lautrup, S., Yang, B., Wang, Y., Cordonnier, S., Mattson, M. P., Croteau, D. L., and Bohr, V. A. (2021) NAD(+) supplementation reduces

neuroinflammation and cell senescence in a transgenic mouse model of Alzheimer's disease via cGAS-STING. *Proc Natl Acad Sci U S A* **118**

272. Zhen, X., Zhang, S., Xie, F., Zhou, M., Hu, Z., Zhu, F., and Nie, J. (2021) Nicotinamide Supplementation Attenuates Renal Interstitial Fibrosis via Boosting the Activity of Sirtuins. *Kidney Diseases* **7**, 186-199

273. Som, I., Mitsch, R. N., Urbanowski, J. L., and Rolfes, R. J. (2005) DNA-bound Bas1 recruits Pho2 to activate ADE genes in Saccharomyces cerevisiae. *Eukaryot Cell* **4**, 1725-1735

274. O'Neill, E. M., Kaffman, A., Jolly, E. R., and O'Shea, E. K. (1996) Regulation of PHO4 nuclear localization by the PHO80-PHO85 cyclin-CDK complex. *Science* **271**, 209-212

275. Kaffman, A., Rank, N. M., and O'Shea, E. K. (1998) Phosphorylation regulates association of the transcription factor Pho4 with its import receptor Pse1/Kap121. *Genes Dev* **12**, 2673-2683

276. Vidal, M., and Gaber, R. F. (1991) RPD3 encodes a second factor required to achieve maximum positive and negative transcriptional states in Saccharomyces cerevisiae. *Mol Cell Biol* **11**, 6317-6327

277. Wongwisansri, S., and Laybourn, P. J. (2005) Disruption of histone deacetylase gene RPD3 accelerates PHO5 activation kinetics through inappropriate Pho84p recycling. *Eukaryot Cell* **4**, 1387-1395

278. Korber, P., and Barbaric, S. (2014) The yeast PHO5 promoter: from single locus to systems biology of a paradigm for gene regulation through chromatin. *Nucleic Acids Res* **42**, 10888-10902

279. Reinke, H., Gregory, P. D., and Hörz, W. (2001) A transient histone hyperacetylation signal marks nucleosomes for remodeling at the PHO8 promoter in vivo. *Mol Cell* **7**, 529-538

280. Wang, S. S., Zhou, B. O., and Zhou, J. Q. (2011) Histone H3 lysine 4 hypermethylation prevents aberrant nucleosome remodeling at the PHO5 promoter. *Mol Cell Biol* **31**, 3171-3181

281. Boer, V. M., Crutchfield, C. A., Bradley, P. H., Botstein, D., and Rabinowitz, J. D. (2010) Growth-limiting intracellular metabolites in yeast growing under diverse nutrient limitations. *Mol Biol Cell* **21**, 198-211

282. Gauthier, S., Coulpier, F., Jourdren, L., Merle, M., Beck, S., Konrad, M., Daignan-Fornier, B., and Pinson, B. (2008) Co-regulation of yeast purine and phosphate pathways in response to adenylic nucleotide variations. *Mol Microbiol* **68**, 1583-1594

283. Takaine, M., Imamura, H., and Yoshida, S. (2022) High and stable ATP levels prevent aberrant intracellular protein aggregation in yeast. *Elife* **11**

284. Bun-Ya, M., Nishimura, M., Harashima, S., and Oshima, Y. (1991) The PHO84 gene of Saccharomyces cerevisiae encodes an inorganic phosphate transporter. *Mol Cell Biol* **11**, 3229-3238

285. Auesukaree, C., Homma, T., Tochio, H., Shirakawa, M., Kaneko, Y., and Harashima, S. (2004) Intracellular phosphate serves as a signal for the regulation of the PHO pathway in Saccharomyces cerevisiae. *J Biol Chem* **279**, 17289-17294

286. Vogel, K., Horz, W., and Hinnen, A. (1989) The two positively acting regulatory proteins PHO2 and PHO4 physically interact with PHO5 upstream activation regions. *Mol Cell Biol* **9**, 2050-2057

287. Munsterkotter, M., Barbaric, S., and Horz, W. (2000) Transcriptional regulation of the yeast PHO8 promoter in comparison to the coregulated PHO5 promoter. *J Biol Chem* **275**, 22678-22685

288. Ceschin, J., Saint-Marc, C., Laporte, J., Labriet, A., Philippe, C., Moenner, M., Daignan-Fornier, B., and Pinson, B. (2014) Identification of yeast and human 5-aminoimidazole-4-carboxamide-1-beta-d-ribofuranoside (AICAr) transporters. *J Biol Chem* **289**, 16844-16854

289. Ueda, Y., and Oshima, Y. (1975) A constitutive mutation, phoT, of the repressible acid phosphatase synthesis with inability to transport inorganic phosphate in Saccharomyces cerevisiae. *Mol Gen Genet* **136**, 255-259

290. Toh-e, A., Ueda, Y., Kakimoto, S. I., and Oshima, Y. (1973) Isolation and characterization of acid phosphatase mutants in Saccharomyces cerevisiae. *J Bacteriol* **113**, 727-738

291. Noda, T., and Klionsky, D. J. (2008) The quantitative Pho8Δ60 assay of nonspecific autophagy. *Methods Enzymol* **451**, 33-42

292. Ozdemir, A., Spicuglia, S., Lasonder, E., Vermeulen, M., Campsteijn, C., Stunnenberg, H. G., and Logie, C. (2005) Characterization of Lysine 56 of Histone H3 as an Acetylation Site in Saccharomyces cerevisiae*. *Journal of Biological Chemistry* **280**, 25949-25952

293. Wang, X., and Hayes, J. J. (2008) Acetylation mimics within individual core histone tail domains indicate distinct roles in regulating the stability of higher-order chromatin structure. *Mol Cell Biol* **28**, 227-236

294. Cruz, C., Della Rosa, M., Krueger, C., Gao, Q., Horkai, D., King, M., Field, L., and Houseley, J. (2018) Tri-methylation of histone H3 lysine 4 facilitates gene expression in ageing cells. *Elife* **7**